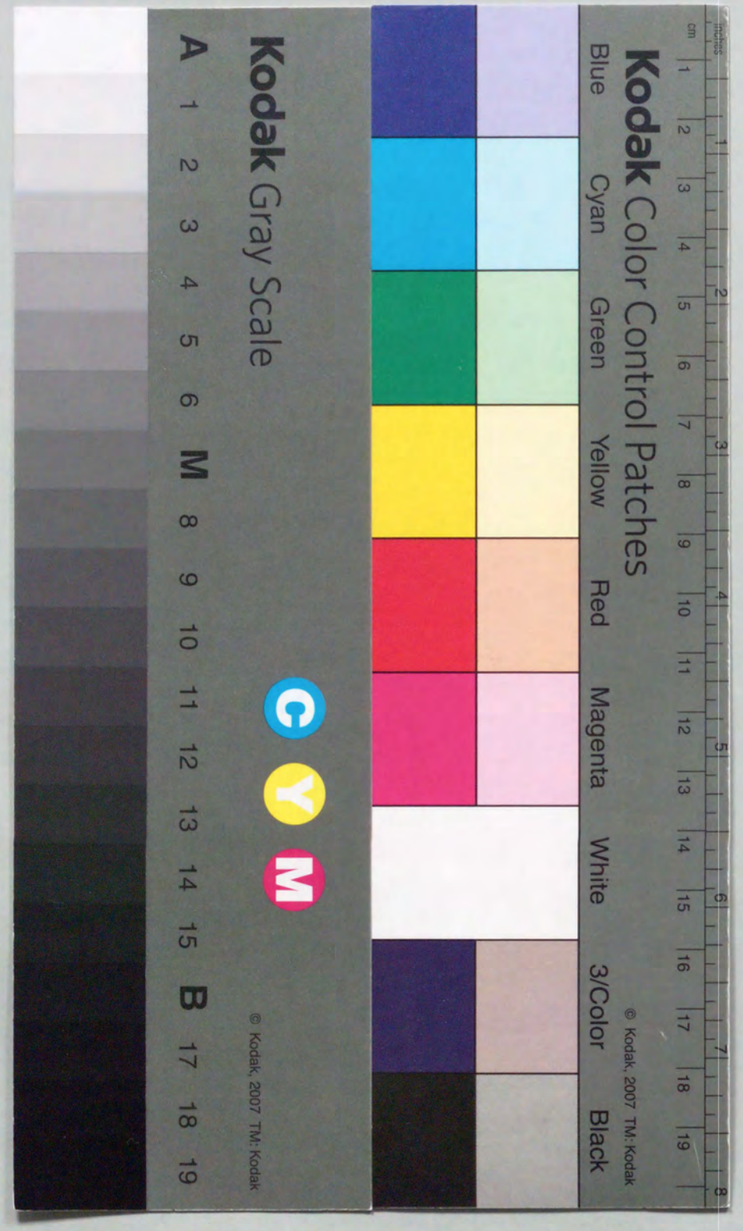

Mössbauer Spectroscopic Study of Uranium Intermetallic Compounds

(UFe_2, U_6Fe, UGe_2, UPd_2Al_3 and URu_2Si_2)

Satoshi TSUTSUI

OSAKA UNIVERSITY

Graduate School of Engineering Science
Department of Physical Science
Division of Materials Physics
Toyonaka Osaka

January 1999

Mössbauer Spectroscopic Study of Uranium Intermetallic Compounds

(UFe_2, U_6Fe, UGe_2, UPd_2Al_3 and URu_2Si_2)

Satoshi TSUTSUI

OSAKA UNIVERSITY

Graduate School of Engineering Science
Department of Physical Science
Division of Materials Physics
Toyonaka Osaka

January 1999

Abstract

Physical properties of uranium compounds depend on the characteristics of the 5*f*-electrons of uranium atoms. The nature of the 5*f*-electrons in actinide compounds is described by the characteristic properties of 3*d*- and 4*f*-electrons. Namely, the 5*f*-electrons in the actinide compounds behave like itinerant 3*d*-electron and/or localized 4*f*-electrons.

The Mössbauer spectroscopy is one of the useful tools to investigate the local electronic states in various compounds. Since the Mössbauer effects can be observed in some isotopes of the light actinide elements, the Mössbauer measurements of actinide isotopes enable us to investigate the local electronic states of the 5*f*-electrons of actinide atoms directly. For the actinide intermetallic compounds, the ^{237}Np Mössbauer spectroscopic studies of the neptunium intermetallic compounds had been extensively performed between 1960's and 1970's. However, the Mössbauer studies of uranium isotopes for the uranium intermetallic compounds have never been performed, although the uranium intermetallics have various interesting physical properties, for example, their anisotropic superconductivity.

In this work, the ^{238}U and the ^{57}Fe Mössbauer measurements of the uranium intermetallics have been performed in order to investigate the physical properties of the uranium intermetallics, mainly to investigate their magnetic properties.

Firstly, the g-factor of the first excited state in the ^{238}U Mössbauer transition has been determined as $0.254 \pm 0.015\ \mu_N$ by using ^{238}U Mössbauer and ^{235}NMR measurements of UO_2. Nuclear g-factor is an important coupling constant on the discussion of the physical properties of uranium compounds.

In U-Fe intermetallics, the isomer shift values obtained by ^{57}Fe Mössbauer spectroscopy reveal the strong hybridization between 3*d*-electrons of iron atoms and 5*f*-elecrons of uranium atoms. The hyperfine coupling constant of ^{57}Fe in UFe_2 also indicates the hybridization between 3*d*- and 5*f*-electrons. The results from the ^{238}U Mössbauer spectroscopy of UFe_2 suggest that the spin and the orbital moments of uranium atoms in UFe_2 do not cancel out each other and the magnetic moments do not exist at uranium atoms.

In UGe_2, the magnitude of the hyperfine magnetic field at 5.3 K is 240 ± 10 T. The hyperfine coupling constant does not depend on the temperature.

For the heavy fermion superconductors of UPd_2Al_3 and URu_2Si_2, the broadening of Mössbauer absorption spectra due to the paramagnetic relaxation is observed at the temperature where the magnitude of each magnetic susceptibility has the maximum value. Above these temperatures, the metamagnetic transitions of both compounds are reported to disappear. These phenomena are thought to be related to the appearance of the heavy fermion which plays an important role in their superconductivity.

The hyperfine coupling constants of ^{238}U nucleus obtained in this work are obtained as 140 - 160 T / μ_B in UO_2, UGe_2 and UPd_2Al_3.

Contents

Chapter 1. Introduction

1. 1. General Introduction

The Mössbauer spectroscopy has been applied to the various fields in physics, chemistry, biology, solid state physics and material science, after R. L. Mössbauer accomplished the first successful observation of the recoil-free nuclear gamma-ray resonance [1.1.1]. This phenomenon was named as the Mössbauer effect from his first observation. The Mössbauer spectroscopy by using various isotopes such as ^{57}Fe, ^{119}Sn, ^{151}Eu and so on, is applied to investigate the physical properties of various materials. The Mössbauer effect can be observed in 88 nuclei of about 40 elements. For the uranium isotopes as an actinide element, the Mössbauer effect has been observed for ^{234}U, ^{236}U and ^{238}U nuclei. The Mössbauer spectroscopy enables us to investigate the local electronic state of the Mössbauer probe atom through the hyperfine interactions. The Mössbauer effect of the uranium isotopes was investigated for several uranium compounds like oxides, hydride and so on at the period between 1960 and 1970's [1.1.2-6]. However, the ^{238}U Mössbauer studies of uranium intermetallic compounds have never been performed except for UFe_2, whereas the ^{237}Np Mössbauer studies of neptunium intermetallic compounds which are typical actinide intermetallics have been progressively performed in that period. The facility and the space where these experiments are permitted to perform are restricted by law since the sources and the samples used in these works are nuclear fuel materials. Moreover, there is a fatal reason, that is, the source used in the Mössbauer measurements requires the highly purified isotopes as written below.

The nuclear methods through the hyperfine interactions for the elements with *f*-electrons have never been performed in the cerium and the uranium intermetallic compounds some of which have interesting physical properties like a typical behavior as a heavy fermion system and a coexistence or competition of the magnetic ordering and superconductivity. There are no suitable isotopes for cerium to observe the Mössbauer effect and nuclear magnetic resonance (NMR), since the nuclear spin of the ground state of ^{140}Ce is zero. On the other hand, in uranium compounds, both NMR and Mössbauer measurements can be performed. Since the natural abundance of ^{235}U which is the only one suitable isotope to observe the NMR is as small as 0.72 %, it is difficult to perform the ^{235}U NMR study for the uranium compounds and the reports of

the study are quite less [1.1.7-8]. In the ^{238}U Mössbauer spectroscopy, the probe isotope is ^{238}U whose natural abundance is 99.275 % and the largest in all of the uranium isotopes. Natural uranium and depleted uranium are easier to treat than the uranium enriched with ^{235}U, so-called uranium for the nuclear fuel. Samples made from natural or depleted uranium can be used for the ^{238}U Mössbauer spectroscopy. The motivation of this study is to investigate the local electronic states of uranium intermetallic compounds, mainly their magnetic properties using the ^{238}U and the ^{57}Fe Mössbauer spectroscopy.

In Chapter 1, we show the fundamental physical properties of uranium intermetallic compounds and the Mössbauer measurements of actinide compounds which are previously reported, in Chapter 2, the principles of the Mössbauer effect and the details of hyperfine interactions and in Chapter 3, Mössbauer spectroscopic results. Since the g-factor of the excited state of the ^{238}U Mössbauer transition has not yet been determined, the g-factor was determined by the combination of the ^{238}U Mössbauer spectroscopy and the ^{235}U NMR of UO_2. The magnetic properties of U-Fe intermetallics are discussed mainly with the ^{57}Fe Mössbauer spectroscopy. The magnetic properties of the itinerant ferromagnet UGe_2 and the heavy fermion superconductors of UPd_2Al_3 and URu_2Si_2 are investigated with the ^{238}U Mössbauer spectroscopy. The conclusion of present study is described in Chapter 4.

References

[1.1.1] R. L. Mössbauer, Z. Physik., **151**, 124 (1958).

[1.1.2] S. L. Ruby, G. M. Kalvius, B. D. Dunlap, G. K.Shenoy D. Cohen, M. D. Bodsky and D. J. Lam, Phys. Rev., **184**, 374 (1969).

[1.1.3] R. D. Meeker, G. M. Kalvius, B. D. Dunlap, S. L. Ruby and D. Cohen, Nucl. Phys., **A224**, 429 (1974).

[1.1.4] J. A. Monard, P. G. Huray and J. O. Thomson, Phys. Rev., **B9**, 2838 (1974).

[1.1.5] G. K. Shenoy, M. Kuznietz, B. D. Dunlap and G. K. Kalvius, Phys. Letters, **42**, 61 (1972).

[1.1.6] G. K. Shenoy, G. M. Kalvius, S. L. Ruby, B. D. Dunlap, M. Kuznietz and F. P. Kampos, Intern. J. Magnetism, **1**, 23, (1970).

[1.1.7] H. Le Bail, C. Chachaty, P. Rigny and R. Bougon, J. Physique Lett., **44**, 1017 (1983).

[1.1.8] I. Ursu, D. E. Demco, M. Bogdan, P. Filoti and A. Darabont, J. Physique Lett., **46**, 1017 (1983).

1. 2. Characteristic Properties of Uranium Compounds [1.2.1-2]

Generally, the physical properties of uranium compounds depend on the characteristics of the 5*f*-electrons. The 5*f*-electrons in actinide compounds have a nature characterized by both specific properties of 3*d*- and 4*f*-electrons. The feature of 3*d* transition metals and compounds are generally itinerant electronic systems, whereas that of 4*f* transition metals and compounds is of a localized electronic system. The electron configuration of uranium atoms is $[Rn](5f)^3(6d)^1(7s)^2$. Generally speaking, actinide atoms could take higher valence state than lanthanide atoms which can take only the divalent and trivalent. Uranium atoms can take the valence state up to hexavalent, that is, UO_3, UF_6 and so on in the uranium compounds. These facts show the wave function of 5*f*-electrons has larger probability in distant region from the nucleus than that of 4*f*-electrons. Therefore, it implies that the 5*f*-electrons could contribute to the chemical bond with the neighbor atoms. The effect of the *f-p* and *f-d* hybridization exists in 5*f*-electron systems so that the 5*f*-electrons in the light actinide compounds tends to be itinerant and those of the heavy actinide compounds to be localized. Namely, as the electronic properties, some actinide compounds show itinerant behavior and some are localized behavior.

The relationships of the distance of the nearest neighbor uranium atoms to the existence of the magnetic order and the magnetic ordering temperature are given by a Hill's plot [1.2.3]. According to the Hill's plot, when the distance between uranium atoms is over 0.35 nm, the magnetic order exists. When the distance is less than 0.35 nm, the wave functions of 5*f* electrons are adequately overlapped and 5*f*-electrons are delocalized and itinerant. However, when the *f-p* and/or *f-d* hybridization with the electrons at the ligands causes the delocalization of 5*f*-electron, the formation of the broad 5*f* bands occurs and the 5*f* levels approach to the Fermi level. In spite of the large distance over 0.35 nm between the nearest neighbor uranium atoms, these hybridization effects enable 5*f*-electrons to be itinerant. The Hill's plot is the experiential index to understand the properties of 5*f*-electrons in uranium compounds, but the localization and delocalization of 5*f*-electrons cannot necessarily be determined by the distance between uranium atoms. Since the nature of 5*f*-electrons depends on the various factor such as the distance between the nearest neighbor uranium atoms, the

hybridization with the electrons at ligands and so on, the variety of the physical properties of uranium compounds is caused by that of 5*f*-electrons.

Electronic properties of some uranium compounds show the typical behavior as a heavy fermion system and the characteristic superconductivity which has been observed in cerium compounds. UPd_2Al_3 and URu_2Si_2 whose ^{238}U Mössbauer effects have been measured in this work, are also heavy fermion superconductors. Some uranium compounds show the similar physical properties as those observed in cerium compounds, whereas some experimental results from a neutron scattering experiments, were reported to be different from those of cerium compounds.

Recently, the purified samples of the uranium compounds reveal interesting electronic properties as a heavy fermion system, which shows a coexistence of the magnetic ordered state and the anisotropic superconducting state. In UPt_3, superconductivity with odd parity has been firstly observed by NMR [1.2.4]. In UPd_2Al_3, a magnetic reflection in the elastic neutron scattering has an anomaly at the transition temperature of superconductivity, T_C and a excitation peak in the inelastic neutron scattering has been observed below T_C. These results show the interplay between its magnetic properties and superconductivity [1.2.5-9].

References

[1.2.1] ed. A. J. Freeman and G. H. Lander, *Handbook on the Physics and Chemistry of the Actinides*, vol. 2, North-Holland, 1985.

[1.2.2] K. Ueda and Y. Ōnuki, *Omoidenshikei-no-Butsuri* (*Physics of Heavy Electron Systems*), Shoukabou,1998.

[1.2.3] H. H. Hill, Nucl. Metall. **17**, 2 (1970).

[1.2.4] H. Tou, Y. Kitaoka, K. Asayama, N. Kimura, Y. Ōnuki, E. Yamamoto and K. Maezawa, Phys. Rev. Lett. **77**, 1374 (1996).

[1.2.5] N. Sato, N. Aso, B. Roessli, G. H. Lander, T. Komatsubara, Y. Endo and O. Sakai, J. Alloys Compd., **271-273**, 4336 (1998).

[1.2.6] Y. Koike, N. Metoki, Y. Haga, Y. Morii and Y. Ōnuki, Physica **B241-243**, 823 (1997).

[1.2.7] N. Metoki, Y. Haga, Y. Koike and Y. Ōnuki, Physica **B241-243**, 845 (1997).

[1.2.8] N. Metoki, Y. Haga, Y. Koike and Y. Ōnuki, Phys. Rev. Lett., **80**, 5417 (1998).

[1.2.9] N. Metoki, Y. Haga, Y. Koike, N. Aso and Y. Ōnuki, J. Magn. Magn. Mater., **177-181**, 449 (1998).

1. 3. Previous Mössbauer Spectroscopic Studies of Uranium Isotopes

The Mössbauer spectroscopy of uranium isotopes has been performed in even-even uranium isotopes, ^{234}U, ^{236}U and ^{238}U. The sources of these Mössbauer measurements are also even-even plutonium isotopes, ^{238}Pu, ^{240}Pu and ^{242}Pu, respectively. The decay schemes of these isotopes are shown in Fig. 1.3.1. When all of the parent isotopes experience alpha-decay, the first excited state ($I = 2^+$) of each isotope is populated by 25 % of all transitions. The gamma-rays emitted by the transitions between the first excited state ($I = 2^+$) and the ground state ($I = 0^+$) are the Mössbauer gamma-rays of uranium isotopes. The energies of the Mössbauer gamma-rays from these uranium isotopes are around 45 keV.

The spectra obtained are very simple in shape because the ground state of all uranium isotopes is $I = 0^+$. The hyperfine interactions of even-even uranium isotopes are mentioned in detail at Section 2. 2. In all of the Mössbauer spectra obtained from these uranium isotopes, the isomer shift value which depends on the valence states of the uranium atoms cannot be observed because its magnitude is nearly zero or less than the experimental error [1.3.1]. This fact is caused by the very small difference in the nuclear radius between the ground and the excited state. This is one of the characteristic nature of the ^{238}U isotopes. Moreover, although it is reported that the magnetic splitting is observed in UO_2 [1.3.1], the magnitude of the hyperfine field cannot be determined because of unknown g-factor of the first excited state ($I = 2^+$) of the even-even uranium isotopes.

Table 1.3.1 shows the nuclear data of the Mössbauer transition for the actinide elements, ^{57}Fe, ^{119}Sn, ^{151}Eu and ^{197}Au nucleus [1.3.2-5]. The g-factors of even-even uranium isotopes are the theoretical values reported by Nilsson et al.[1.3.4]. As shown in Table 1.3.1, the life-time of the excited state of every even-even uranium isotopes is shorter than those of the other Mössbauer isotopes. The short life-time of the excited state implies that the spectra obtained are intrinsically broad because the life-time and full-width at half maximum (FWHM) of the spectrum have the uncertainty relationships between the time and the energy. The natural line-width of the ^{238}U Mössbauer spectrum obtained from this uncertainty principle is 27 mm s^{-1}. This line-width is much broader than the Mössbauer spectrum of the other isotopes, for example, 0.192

mm s^{-1} for ^{57}Fe and 1.87 mm s^{-1} for ^{197}Au.

In the case of the ^{238}U Mössbauer effect, theoretical g-factor of the excited state is 0.25 μ_N which is a nearly same value as the other isotopes. On the other hand, the magnitudes of their quadrupole moments are 10 times larger than those of the other isotopes, for example, + 0.2 barn for ^{57}Fe and - 0.08 barn for ^{119}Sn. Although the natural line-width of the ^{238}U Mössbauer spectrum is broader than the other isotopes, its hyperfine interactions can thus be discussed from the split and/or broadening of the spectrum.

The typical quadrupole split patterns show in Fig. 1.3.2. Figure 1.3.2 shows even-even uranium Mössbauer spectra of $UO_2(NO_3)_2 \cdot 6H_2O$. These spectra seem to be asymmetric spectra with two peaks. The sign of the quadrupole moment is minus in each even-even uranium isotopes as shown in Table 1.3.1. The transition probabilities from the excited states, $M = \pm 2, \pm 1$ and 0, to the ground state are 2:2:1, respectively. The spectra shown in Fig. 1.3.3 are fitted by the theoretical lines whose intensities are 2:2:1, respectively, as velocity increases. Since the sign of the quadrupole moments of every even-even uranium isotopes is minus, these results show the sign of the electric field gradient is minus. These results indicate that the excited state of each uranium nuclei split three levels. As shown in Table 1.3.1, the magnitude of the quadrupole moments of every even-even uranium nuclei are nearly equal. Since the every nucleus experienced the equal electric field gradient in $UO_2(NO_3)_2 \cdot 6H_2O$, the shapes of the quadrupole split spectra obtained from each isotope are almost identical.

A typical magnetically split pattern is shown in Fig. 1.3.3. Figure 1.3.3 shows the ^{238}U Mössbauer spectra of UO_2 at 77 K and 4.2 K [1.3.1]. Since the Néel temperature of UO_2 is 30.8 K, the spectrum at 4.2 K can be analyzed as a magnetic pattern. The details of the results obtained in this work are discussed in Section 3.1.

Although the Mössbauer spectroscopy is one of the useful tools with which the physical properties of uranium compounds can be investigated through the hyperfine interactions at uranium nucleus, this measurement has never been performed up to now. In the case of ^{234}U and ^{236}U Mössbauer spectroscopy, the natural abundance of these isotopes is too small to perform the experiments. For the ^{238}U Mössbauer spectroscopy, the natural abundance of its isotope is 99.275 % which is large enough to perform the experiments, but it is necessary to use the extremely purified $^{242}PuO_2$ source.

The source for the ^{238}U Mössbauer measurements requires a high purity of ^{242}Pu. Isotopes separated generally with the mass separator. ^{242}Pu cannot be separated from ^{241}Pu perfectly. Moreover, the life-time of ^{241}Pu and that of ^{241}Am which is the daughter nucleus of ^{241}Pu are much shorter than that of ^{242}Pu. As shown in Fig. 1.3.1, ^{242}Pu decays to ^{238}U in the half-life of 3.76×10^5 years with alpha-decay and emits the ^{238}U Mössbauer gamma-ray. On the other hand, ^{241}Pu decays to ^{241}Am in the half-life of 14.4 years with beta-decay, and ^{241}Am decays to ^{237}Np in the half-life of 433 years with alpha-decay, as shown in Fig. 1.3.4. In the decay from ^{241}Am to ^{237}Np, about 80 % of the transition emits the gamma-ray whose energy is 59.536 keV. The internal conversion coefficients of ^{238}U and ^{237}Np are 625 and 1, respectively. Therefore, the existence of the small amounts of ^{241}Pu isotope disturbs the detection of the ^{238}U Mössbauer gamma-ray. This fact requires the highly purified $^{242}PuO_2$ source.

Figure 1.3.5. shows the gamma-ray energy spectrum of even-even plutonium (^{238}Pu, ^{240}Pu and ^{242}Pu) reported previously [1.3.6]. These are the sources for ^{234}U, ^{236}U and ^{238}U Mössbauer measurements, respectively. Since the half-life of ^{242}Pu is longer than those of ^{238}Pu and ^{240}Pu, this spectrum shows the Mössbauer gamma-ray for ^{238}U is difficult to detect. In order to take off these difficulties, Ruby et al. reported that the chemical separation of ^{241}Am from the source was performed every three months in order to detect the Mössbauer gamma-ray, which is essential to measure the Mössbauer spectra [1.3.1].

Although the ^{238}U Mössbauer study were performed and reported previously by Ruby et al.[1.3.1], they investigated UO_2, $UO_2(NO_3)_2 \cdot 6H_2O$ and compounds as listed in Table 1.3.2. However, we want to emphasize that the ^{238}U Mössbauer studies of its intermetallic compounds which we described in this work have never been performed except for UFe_2.

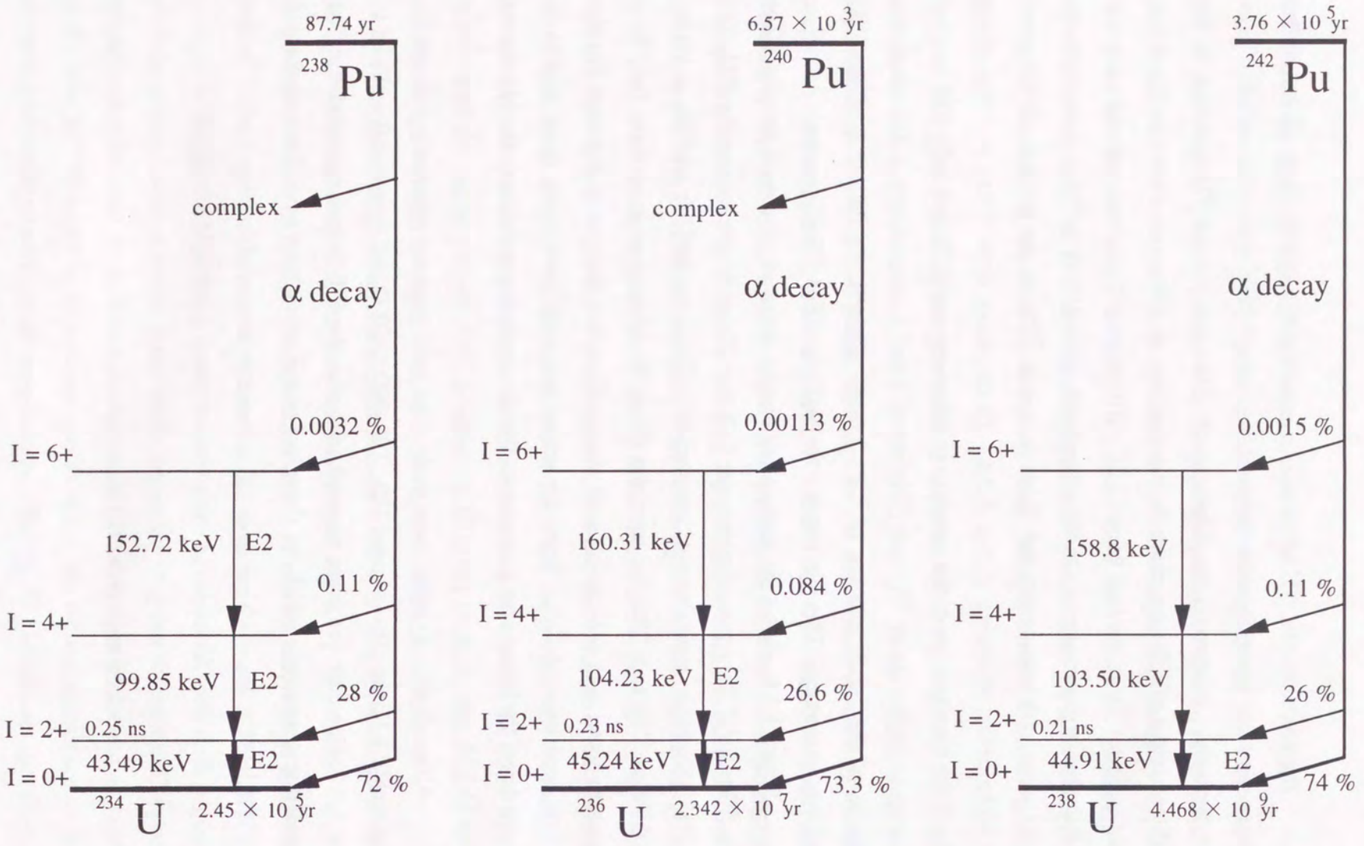

Fig. 1.3.1. Decay scheme of the even-even plutonium isotopes to the even-even uranium isotopes.

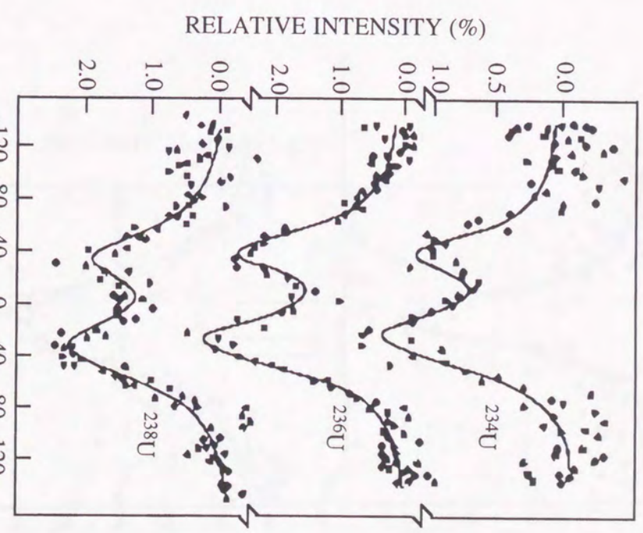

Fig. 1.3.2. Mössbauer spectra of the even-even uranium isotopes in $UO_2(NO_3)_2 \cdot 6H_2O$ after R. D. Meeker et al. in 1974 [1.3.6].

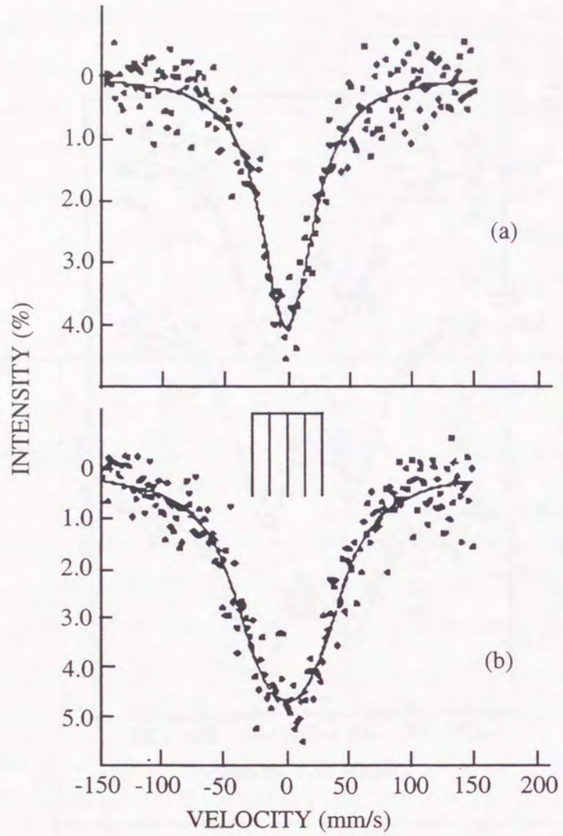

Fig. 1.3.3. ^{238}U Mössbauer spectra of UO_2 at (a) 77 K and (b) 4.2 K after S. L. Ruby et al in 1969 [1.3.1].

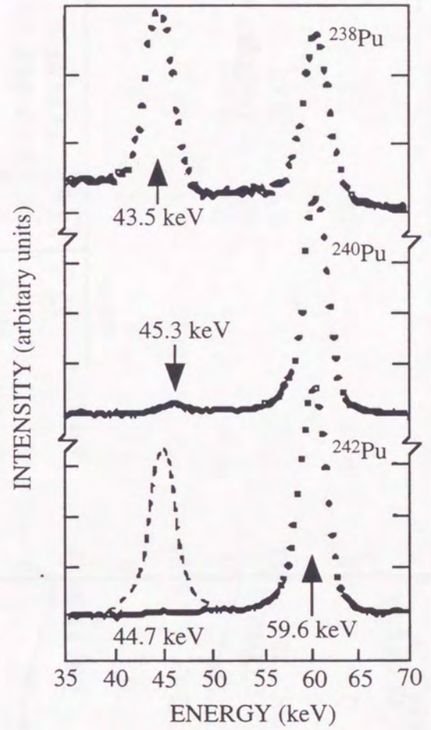

Fig. 1.3.4. Energy spectrum of the Mössbauer gamma-ray source for every even-even uranium isotopes reported by R. D. Meeker et al. in 1974 [1.3.6]. The peaks at 59.6 keV is the one of the gamma-ray from ^{241}Am in which the source include as impurity. The dash line shows the effect of the chemical separation of the souce from ^{241}Am.

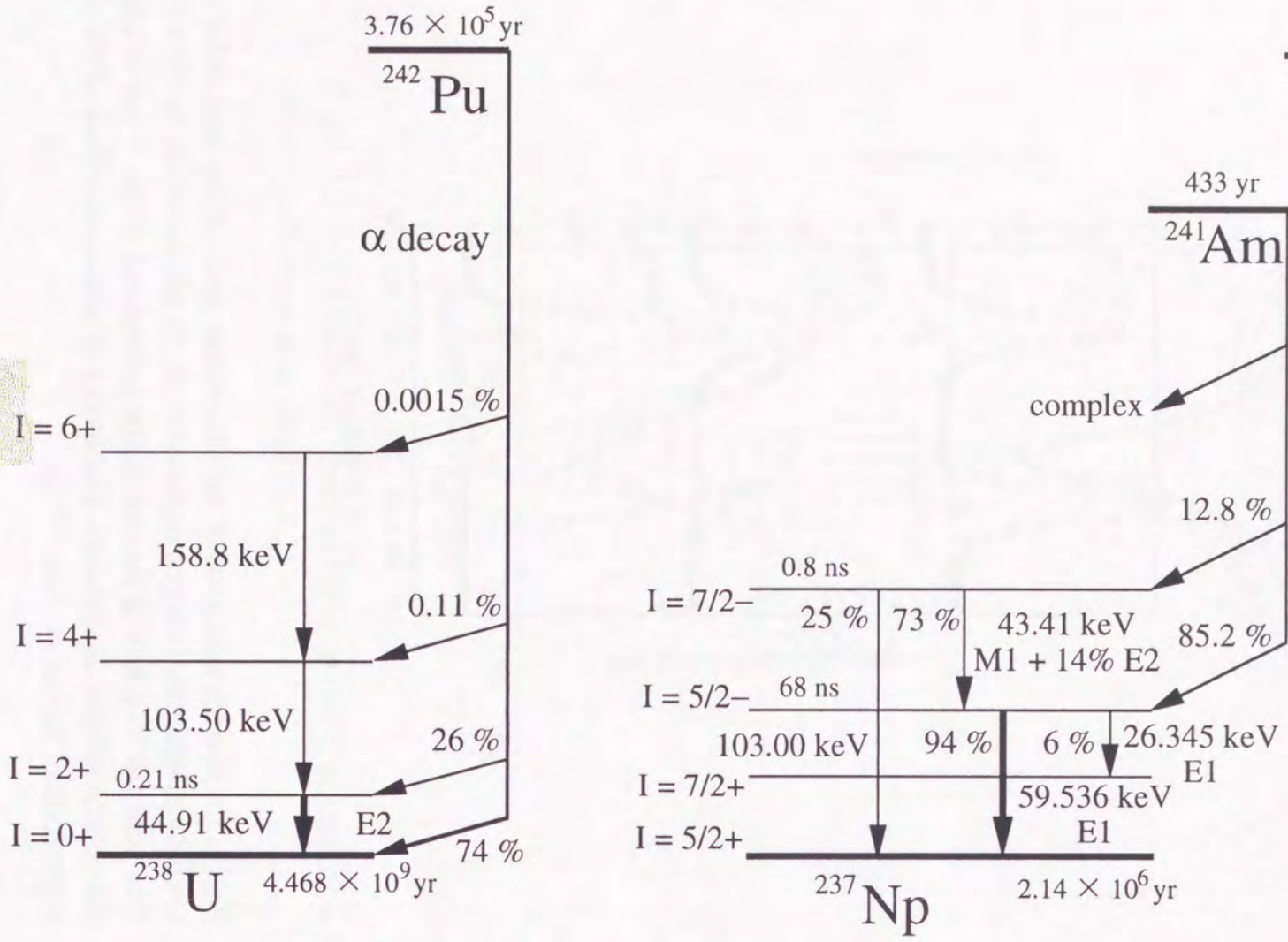

Fig. 1.3.5. Decay scheme for ^{242}Pu and ^{241}Pu.

Table 1. Nuclear data for Mössbauer Transition.

Parameter	^{231}Pa	^{234}U	^{236}U	^{238}U	^{237}Np	^{239}Pu	^{243}Am	^{57}Fe	^{119}Sn	^{151}Eu	^{197}Au
E_γ	84.21	43.49	45.24	44.91	59.536	57.273	84.0	14.412	23.875	21.55	77.34
I_e	3/2-	2+	2+	2+	5/2+	5/2+	5/2-	3/2-	3/2+	7/2+	1/2+
I_g	5/2+	0+	0+	0+	5/2-	1/2+	5/2+	1/2+	1/2+	5/2+	3/2+
μ_e [μ_N]	4.5	0.5	0.5	0.5	+1.34	-	2.86	-0.1547	+0.67	+2.587	+0.419
μ_g [μ_N]	2.0	0	0	0	+2.5	0.2	1.6	+0.0902	-1.041	+3.465	+0.419
Q_e [barn]	0.69	-3.0	-3.0	-3.2	4.1	-	+4.9	0.2	-0.08	+1.51	0
Q_g [barn]	-1.7	0	0	0	4.1	-	4.9	0	0	+1.16	+0.56
$t_{1/2}$ [ns]	44	0.25	0.23	0.21	68	0.10	2.3	99.3	18.3	8.8	1.892
Γ [mm s^{-1}]	0.08	24	26	27	0.07	47.9	1.4	0.192	0.626	1.44	1.87
α_T	-	780±55	607±29	625	1.06	-	0.2	8.17	5.12	29	4
σ_0 [10^{-18} cm^2]	-	0.008	0.01	0.01	0.33	-	0.29	2.57	1.40	0.23	0.041
t_S	25.5 h	86 yr	6.58×10^3 yr	3.79×10^5 yr	458 yr	2.33 d	4.98 h	270 d	250 d	87 yr	18 h

E_γ : γ-ray energy ; I_g : the ground state nuclear spin ; I_e : the excited state nuclear spin ; μ_g : the ground state nuclear magnetic moment ; μ_e : the excited state nuclear magnetic moment ; Q_g : the ground state nuclear quadrupole moment ; Q_e : the excited state nuclear quadrupole moment ; $t_{1/2}$: the half life of the excited state ; Γ : natural linewidth ; α_T : total internal conversion coefficient ; σ_0 : resonant absorption cross-section ; t_S : the half life of the source

Table 1.3.2. ^{238}U Mössbauer parameter of uranium compounds [1.3.1].

Compounds	Temperature K	Background Counts	Relative Absorption %	FWHM mm / s	Magnetic Splitting mm / s	$e^2qQ/4$ mm / s	Isomer Shift mm / s
UO_2	78	61000	4.0±0.2	48±23	-	-	2±3
	4.2	60000	7.0±0.2	45±1	58±4.0	-	1±1
UF_4	4.2	86000	4.6±0.2	45±4	80±4	-	1±1
UC	4.2	78000	3.3±0.1	55±3	-	-	0.5±1.0
$UO_2(NO_3)_2 \cdot 6H_2O$	4.2	55000	4.3±0.2	47±2	-	-42±2	3±1
$UO_2(NO_3)_2$ in H_2O	4.2	88000	2.5±0.2	50±6	-	-47±3	-3±2
UO_3	4.2	128000	3.0±0.2	60±6	-	40±2	-2±2
α-U	78	74000	2.7±0.2	48	-	-19±2	1±1
	4.2	68000	5.1±0.2	48	-	-21±1	1±1
UFe_2	4.2	137000	2.0±0.1	48	16±12	-	2±2

References

[1.3.1] S. L. Ruby, G. M. Kalvius, B. D. Dunlap, G. K. Shenoy, D. Cohen, M. D. Bodsky and D. J. Lam, Phys. Rev., **184**, 374 (1969).

[1.3.2] N. N. Greenwood and T. C. Gibb, *Mössbauer Spectroscopy*, Chapman and Hall Ltd., 1971.

[1.3.3] Edited by G. J. Long, *Mössbauer Spectroscopy Applied to Inorganic Chemistry*, vol. 2, Plenum Press.

[1.3.4] S. G. Nilsson and O. Prior, Kgl. Danske Videnskab, Selskab, Mat.-Fys. Medd., **32**, No. 16 (1961).

[1.3.5] ed. A. J. Freeman and G. H Lander, *Handbook on the Physics and Chemistry of the Actinides*, vol. 2, North-Holland.

[1.3.6] R. D. Meeker, G. M. Kalvius, B. D. Dunlap, S. L. Ruby and D. Cohen, Nucl. Phys., **A224**, 429 (1974).

Chapter 2. Mössbauer Spectroscopy

2. 1. Principle of the Mössbauer Effect [2.1-4]

2. 1. 1. Mössbauer Effect

The resonant absorption by the transition between the electronic states of atoms is proved by R. W. Wood [2.5]. Since the life-time in the excited state is generally short, the photon energy emitted from the atom by the de-excitation to the ground state is equal to the energy difference between the excited and ground state.

W. Kurn suggested that the energy levels and resonant absorption of nuclear exist such atom and molecule systems [2.6]. However, the energy differences between nuclear levels are about 1000 times larger than those of the atom and molecule systems, and their resonant absorptions have never been able to observed because the free atom experiences the recoil in the emission and absorption process by the gamma-ray.

When the gamma-ray is emitted from the nucleus, the conservation law of the energy gives the following relation,

$$E = E_\gamma + E_R, \tag{2.1.1}$$

where E is the difference of the energy between two levels in a gamma transition, E_γ the energy of the emitted gamma-ray, E_R is the recoil energy in the emission process of the gamma-ray. The conservation law of the momentum in this gamma transition gives

$$0 = \frac{E_\gamma}{c} - p, \tag{2.1.2}$$

where p is the momentum of emitted or absorbed atoms, c the velocity of light. The recoil energy E_R is written using p by

$$E_R = \frac{p^2}{2M} = \frac{(E_\gamma / c)^2}{2M}, \tag{2.1.3}$$

Where M is the mass of the emitting nucleus. From Eq. (2.1.1), the observed energy of the emitted gamma-ray is smaller than the transition energy by the recoil energy, E_R. In the absorption process of the gamma-ray, the absorbed nucleus recoils towards incident direction of the gamma-ray. Therefore, the loss of the emission and absorption energy of the gamma-ray is just $2E_R$.

Since the recoil energy of nuclear gamma-ray is very large in its emission and absorption processes, it is larger than the width of the gamma-ray. The energy of the Mössbauer gamma-ray, for example, is 14.4 keV in ^{57}Fe Mössbauer transition. Its

recoil energy is

$$E_R = 1.94 \times 10^{-3}\ \text{eV}. \tag{2.1.4}$$

On the other hand, the natural line width of its gamma-ray Γ is given by the principle of uncertainty,

$$\Gamma\tau = \hbar, \tag{2.1.5}$$

where τ is the life-time of the excited state, $\hbar$ Planck constant. Since the life time of the first excited state in ^{57}Fe isotope is 99.3 nsec,

$$\Gamma = 6.74 \times 10^{-9}\ \text{eV}. \tag{2.1.6}$$

In the case of the atoms and molecules, the loss due to the recoil energy is much smaller than the line-width and the resonant absorption can be realized.

R. L. Mössbauer studied the scattering of 129 keV gamma-ray of ^{191}Ir, and observed an increase of the scattering probability as the temperature of the scatterer decreases. This phenomenon was not predicted from the classical theory [2.7], but is easily explained by Einstein model of the solid. Einstein model to explain the specific heat of the solid permits the change of the solid states whose quantum number is different by one or more than one. This change is the integral multiples of the energy of lattice vibration as the emission and absorption. Considering the case of the excitation of the phonon in the emission process of the gamma-ray, f is defined as the probability of the emission of the gamma-ray without the excitation of the phonon. The recoil energy of ^{57}Fe Mössbauer transition is 10^{-3} eV, comparable to the energy of the phonon. Therefore, neglecting the transition with the two or more than two quantum number change, the relation between the recoil energy E_R and the probability f is given by

$$E_R = (1-f)\hbar\omega. \tag{2.1.7}$$

This probability f is called the recoil-free fraction. Zero phonon absorption and scattering of gamma-ray is called Mössbauer effect, and the recoil-free fraction f indicates the probability of Mössbauer effect.

2.1.2. Recoil-free fraction

Since Mössbauer effect is the nuclear gamma-ray resonance without the excitation of phonon, the probability of this effect depends on three things, which are

the recoil energy of a free atom, the properties of the lattice and the temperature. Therefore, recoil-free fraction, f, is greater, the smaller the probability of excitation of phonon, that is, the smaller Mössbauer gamma-ray energy, the firmer the binding of atoms in the lattice and the lower the temperature is.

The probability, W, of gamma-ray emission without the excitation of the phonon from a nucleus in a solid can be written as follows. The probability W is written by

$$W = const\langle i|H|f\rangle, \tag{2.1.8}$$

where $|i\rangle$ is the initial state, $|f\rangle$ the final state of the system and H the interaction Hamiltonian operator and depends on the positional coordinates of the atom and the momentum and spins of the particles within nucleus. The forces acting within the nucleus are extremely short range, whereas those holding the lattice together are much long range. Since the nuclear decay and the vibrational state are independent of each other, the matrix element can be reduced to the one term for the transition from initial vibration state L_i to the final state L_f of the lattice, and can be rewritten by

$$f = const \times \left|\left\langle L_i \left| e^{ik\cdot x} \right| L_f \right\rangle\right|^2, \tag{2.1.9}$$

where $\boldsymbol{k}$ is the wave vector for the emitted gamma-ray and $\boldsymbol{x}$ the coordinate vector of the center of mass of the decaying nucleus. Since the lattice modes are unchanged for zero phonon emission, the recoil-free fraction is rewritten by

$$f = const \times \left|\left\langle L_i \left| e^{ik\cdot x} \right| L_i \right\rangle\right|^2. \tag{2.1.10}$$

Since $|L_i\rangle$ is a normalized function,

$$f = e^{-k^2x^2}. \tag{2.1.11}$$

The Debye model leads to

$$k^2x^2 = \frac{\hbar}{2M}\int_0^{\omega_D} \frac{N(\omega)}{\omega} \coth\left(\frac{\hbar\omega}{2k_BT}\right) d\omega, \tag{2.1.12}$$

where $N(\omega) = const \times \omega^2$, ω_D cutoff frequency, M the mass of nucleus and k_B the Boltzman constant. Therefore, the recoil-free fraction is written by

$$f = \exp\left[\frac{-6E_R}{k\theta_D}\left\{\frac{1}{4}+\left(\frac{T}{\theta_D}\right)^2\int_0^{\frac{\theta_D}{T}}\frac{xdx}{e^x-1}\right\}\right], \tag{2.1.13}$$

by using Debye model, where E_R is the recoil energy, and θ_D the Debye temperature.

2.1.3. Mössbauer Spectrum

In the Mössbauer spectroscopy, the energy of the gamma-ray is modulated by Doppler effect and the transmission of the gamma-ray versus the Doppler velocity is a Mössbauer spectrum. The energy change, ΔE, due to the first order Doppler effect is given by

$$\Delta E = \frac{v}{c}E_\gamma, \tag{2.1.14}$$

where v is the Doppler velocity.

A Mössbauer spectrum is determined by the line-width of the emitted gamma-ray and the scattering cross section of the absorber. The energy distribution of the gamma-ray emitted from the source is given by

$$S(E) = \frac{f_S\Gamma_S}{2\pi}\frac{1}{(E-E_0)+(\Gamma_S/2)^2}, \tag{2.1.15}$$

and the scattering cross section of the absorber is given by

$$\sigma(E) = \frac{t_{eff}(\Gamma_A/2)^2}{(E-E_0)+(\Gamma_A/2)^2}, \tag{2.1.16}$$

where E_γ is the energy of the gamma-ray emitted form the source, Γ_S the line-width of the gamma-ray emitted from the source, E_0 the energy of the gamma-ray absorbed by the absorber, Γ_A the line-width of the absorption resonance, t_{eff} ($=f_a n_a a_a \sigma_0 t_a$) the effective thickness of the absorber, f_a the recoil-free fraction of the absorber, n_a the number of atoms of the element concerned per cm^3 in the absorber, a_a the fractional abundance of the resonant isotope, σ_0 the cross section of the Mössbauer resonance, t_a the thickness of the absorber. Generally, the resonant absorption spectrum is expressed by

$$p(v) = N_0 + \int_{-\infty}^{+\infty} S(E-v)\exp\left[-\sigma(E)\right]dE, \tag{2.1.17}$$

where $p(v)$ is the count rate as a function of Doppler velocity, v, and N_0 background. When the contribution of the self-absorption in the source is small and the absorber is

an ideally thin foil, the Eq. (2.1.17) can be rewritten by

$$A = \int_{-\infty}^{+\infty}\{N_0 - p(v)\}dv \approx A' f_S \times f_A. \tag{2.1.18}$$

In a thin foil approximation, the resonance line is written by the combolution of two Lorentz function. The resonance line is the Lorentz function whose line-width is equal to the summation of the line-widths of source and absorber. On the other hand, when experimental condition is not treated as a thin foil approximation and/or the obtained spectra consist of the superposed lines, the line-shape $p(v)$ is treated as the function of Eq. (2.1.17) in spectrum analyses without thin foil approximation.

2.1.4. Internal Conversion Process

As written above, the Mössbauer effect is the resonance emission and absorption of the nuclear gamma-ray. However, the de-excitation processes in the Mössbauer effect are as follows: The first one is the case where the gamma-ray is re-emitted. The second one is the case where the characteristic X-ray of a probe atom without the emission of the resonance gamma-ray is emitted. The third one is the case where the bound electron of a probe atom substituted for the resonance gamma-ray is emitted. The second and third processes are called the internal conversion process. How to observe the Mössbauer effect are the detection of the emitted gamma-ray, the emitted characteristic X-ray and the emitted inner-shell electrons.

The conventional way of the Mössbauer spectroscopy is the transmission geometry how the gamma-ray through a sample is detected. In the case of measurements of too thick the bulk or single crystal for the Mössbauer gamma-ray to transmit, the measurements by using the internal conversion process is more useful way than those in the transmission geometry.

2. 2. Hyperfine interactions [2.1-4]

2. 2. 1. Isomer shift

The nucleus is surrounded by electronic charge with which it interacts electrostatically. The energy of interaction can be computed classically by considering a uniformly charged spherical nucleus imbedded in its *s*-electron charge cloud. Since there exists the Coulomic interaction between the electron and nucleus, a change in the *s*-electron density might arise from a change in valence will result as a shift of the nuclear levels. This energy shift corresponds to the monopole term of the hyperfine interaction. This is written by

$$\delta E = \frac{2\pi}{5} Ze^2 |\psi(0)|^2 R^2 , \qquad (2.2.1)$$

where Z is the number of atomic number, e the charge of the electron, $|\psi(0)|^2$ the density of electron at the nucleus and R the radius of the nucleus. If two nuclei, one in source and the other in absorber, are at the same electronic state, their values of $|\psi(0)|^2$ are same. That means Mössbauer resonance is observed at zero Doppler velocity. In general, however, the chemical states are different between source and absorber so that the density of *s*-electrons in source is different from that in absorber. Therefore, the difference of the chemical state is observed as the difference of the nuclear energy level. In the Mössbauer spectrum, this effect is observed as the shift of the spectrum. Such a energy shift due to the chemical state is called as an isomer shift, δ. Isomer shift, δ, is written by

$$\delta = \frac{4\pi}{3} Ze^2 R^2 \left(\frac{\delta R}{R}\right)\left\{|\psi_A(0)|^2 - |\psi_S(0)|^2\right\} , \qquad (2.2.2)$$

by using Eq. (2.2.1). Isomer shift depends on two factors. One is the difference between the radius of the ground state and the excited state. Another is the electronic charge density at the nucleus, which is basically an atomic or chemical parameter, since it is affected by the valence state of the atom. In the case of the application of the Mössbauer spectroscopy to the material physics, the nuclear parameter is thought to be constant. The isomer shift value is thus the important parameter from which the valence state of the probe atom can be known.

2. 2. 2. Second Ordered Doppler Shift

The existence of a relativistic temperature-dependent contribution to the isomer shift was pointed out by Pound and Rebka [2.8] and by Josephson [2.9]. The emitting or absorbing atom is vibrating on its lattice site in the crystal. The frequency of oscillation about the mean position is of the order of 10^{12} per second, so that the time averaged displacement during the Mössbauer event is zero. However, there is a term in the Doppler shift which depends on v^2, so that the mean value $\langle v^2 \rangle$ is not zero.

The relativistic equation for the Doppler effect on an emitting photon gives the observed frequency ν' for the velocity, v, in the direction from source to observer as

$$\nu' = \nu\left(1 - \frac{v}{c}\right)\left(1 - \frac{v^2}{c^2}\right)^{-\frac{1}{2}} \approx \nu\left(1 - \frac{v}{c} + \frac{v^2}{2c^2}\right) \qquad (2.2.3)$$

where ν is the frequency for a stationary system. The first-order term in velocity is a function of the velocity of the atom vibrating on its lattice site to the direction of the gamma-ray and will average to zero over the lifetime of the state. The second-order term with v^2 will not average to zero and is therefore independent to the direction of gamma-ray radiation. This term is usually referred to as a second-order Doppler shift and expressed as

$$\nu' = \nu\left(1 + \frac{\langle v^2 \rangle}{2c^2}\right) . \qquad (2.2.4)$$

Accordingly, there is a shift in the Mössbauer resonance line given by

$$\frac{\delta E_\gamma}{E_\gamma} = \frac{\delta \nu}{\nu} = -\frac{\langle v^2 \rangle}{2c^2} . \qquad (2.2.5)$$

It is instructive to consider the description of $\langle v^2 \rangle$ in terms of the lattice dynamics of the solid. The following treatment is a simplification of that by Hazony [2.10]. Using a harmonic approximation, the average energy associated with each atom is

$$\frac{1}{2} M \langle v^2 \rangle = 3\left(n_j + \frac{1}{2}\right)\hbar\omega_j , \qquad (2.2.6)$$

where $n_j = 1/[\exp(\hbar\omega_j / k_B T) - 1]$ and ω_j is the oscillation frequency. We wish to sum over all possible frequencies and modes of vibration, so that

$$\frac{\delta\nu}{\nu} = -\frac{3}{2Mc^2}\sum_j A_j^2 \hbar\omega_j \left(\frac{1}{2} + n_j\right), \tag{2.2.7}$$

where the A_j^2 terms are weighting factors such that $\sum_j A_j^2 = 1$. M is the atomic mass of the Mössbauer nucleus. From the view point of intercomparison of isomer shifts, it is useful to consider the general equation as $T \to 0$. There is a zero-point motion term by

$$\frac{\delta\nu}{\nu} = -\frac{3}{4Mc^2}\sum_j A_j^2 \hbar\omega_j . \tag{2.2.8}$$

The magnitude of the zero-point motion will be dependent on the exact mode of vibration in the crystal, so that $\delta\nu/\nu$ will not generally be the same in all compounds.

Since the mean square of the velocity <v^2> of nucleus, which results from thermal vibration of the lattice, depends on the temperature, the second order Doppler shift depends on the temperature. According to the Debye model of solid, the second order Doppler shift $\Delta_S^D(T)$ in the velocity unit, is written as follows,

$$\Delta_S^D(T) = \frac{9k_B\theta_D}{16Mc} + \frac{9k_B\theta_D}{2Mc}\left(\frac{T}{\theta_D}\right)^3 \int_0^{\frac{\theta_D}{T}} \frac{x^3 dx}{e^x - 1}. \tag{2.2.9}$$

The shift $\delta(T)$ observed in the spectrum contains both isomer shift $\Delta_S^{I.S}(T)$ and second ordered Doppler shift $\Delta_S^D(T)$ of the source and the absorber, so that $\delta(T)$ is represented as follows,

$$\delta(T) = \left\{\Delta_A^{I.S}(T) - \Delta_A^D\right\} - \left\{\Delta_S^{I.S}(T) - \Delta_S^D(T)\right\}. \tag{2.2.10}$$

When the source or absorber is kept at a temperature, information about the lattice vibration, for example θ_D, can be obtained from temperature dependence of the shift of the spectrum.

2. 2. 3. Electric Quadrupole Interaction

When the nuclear spin I is 0 or 1/2, the nuclear charge is spherical symmetric and has zero quadrupole moment. When $I > 1$, on the other hand, the charge distribution of the nucleus is distorted from spherical symmetry, and the nucleus has non-zero quadrupole moment. The magnitude of the charge deformation of a nucleus is described as the nuclear quadrupole moment Q, given by

$$eQ = \int \rho r^2 (3\cos^2\theta - 1) d\tau , \tag{2.2.11}$$

where e is the charge of the proton, r is the charge density in a volume element $d\tau$, which is at distance r from the center of the nucleus and making an induced angle θ to the nuclear spin quantization axis. The sign of Q depends on the shape of the deformation. A negative quadrupole moment indicates that the nucleus is oblate or flattened along the spin axis, whereas for a positive moment it is prorate or elongated.

In a chemically bonded atom, the electronic charge distribution is usually not spherically symmetric. The electric field gradient at the nucleus is defined as a tensor $E_{ij} = -V_{ij} = \left(-\partial^2 V / \partial x_i \partial x_j\right)$ (x_i, x_j = x, y, z), where V is the electrostatic potential. It is customary to define the coordinate axis for the system and $V_{zz} = eq$ is the maximum value of the field gradient. The orientation of the nuclear quantized axis with respect to the principal axis, z, is quantized. There is an interaction energy between Q and eq which is different for each possible orientation of the nucleus.

The Laplace equation requires that the electric field gradient is traceless tensor, so that

$$V_{xx} + V_{yy} + V_{zz} = 0. \tag{2.2.12}$$

Consequently, only two independent parameters are needed to specify the electric field gradient completely, and the two which are usually chosen are V_{zz} and an asymmetry parameter η defined as

$$\eta = \frac{V_{xx} - V_{yy}}{V_{zz}}. \tag{2.2.13}$$

Using the relationships of $|V_{zz}| > |V_{yy}| \geq |V_{xx}|$ ensures that $0 \leq \eta \leq 1$.

The Hamiltonian of the quadrupole interaction can be written as

$$H_{Quad} = \frac{eQ}{2I(2I-1)}\left(V_{zz}\hat{I}_z^2 + V_{xx}\hat{I}_x^2 + V_{yy}\hat{I}_y^2\right), \tag{2.2.14}$$

where I is the nuclear spin and $\hat{I}_z$, $\hat{I}_x$ and $\hat{I}_y$ are the nuclear spin operator. Using Eq. (2.2.13), the Hamiltonian becomes

$$H_{Quad} = \frac{e^2qQ}{2I(2I-1)}\left[3\hat{I}_z^2 - I(I+1) + \eta\left(\hat{I}_x^2 - \hat{I}_y^2\right)\right] \tag{2.2.15}$$

or

$$H_{Quad} = \frac{e^2 qQ}{2I(2I-1)}\left[3\hat{I}_z^2 - I(I+1) + \eta\left(\hat{I}_+^2 + \hat{I}_-^2\right)\right] \tag{2.2.16}$$

where I_- and I_+ are shift operator.

The numerical value of the principal component of the electric field gradient ($V_{zz} = -E_{zz}$) due to an electronic wave function is given by

$$V_{zz} = eq = -e\left\langle \psi \left| \frac{3\cos^2\theta - 1}{r^3} \right| \psi \right\rangle \tag{2.2.17}$$

and

$$\eta q = \left\langle \psi \left| \frac{3\sin^2\theta\cos 2\phi}{r^3} \right| \psi \right\rangle. \tag{2.2.18}$$

A table of the appropriate values for hydrogen-like wave functions is given in Table 2.2.1. The $\langle r^{-3} \rangle$ value is the expectation value of $1/r^3$ for the appropriate hydrogen-like wave function, ψ. In the case of the rare earth and actinide elements, the electric field gradient will mainly be caused by the electronic orbital of the probe atoms themselves.

The lattice term q_{latt} can be similarly evaluated as the sum of contributions from individual changes Z_i and can be written

$$q_{latt} = \sum_i \frac{Z_i}{r_i^3}(3\cos^2\theta_i - 1) \tag{2.2.19}$$

Generally the valence term is a major contribution to the electric field gradient unless the ion has the high intrinsic symmetry of an S-state ion such as high-spin Fe^{3+}. In the latter case, the lattice term will be dominant.

2. 2. 4. Magnetic Hyperfine Interaction

The important part of the hyperfine interaction is the magnetic hyperfine interaction. This arises from the interaction between the nuclear magnetic moment and the magnetic field at nucleus due to the electrons of the probe atom itself. The Hamiltonian of this interaction is

$$H_{Mag} = -\mu \cdot H = -g\mu_N I \cdot H \tag{2.2.20}$$

and the energy levels which are obtained are

$$E_M = -\frac{\mu_N HM}{I} = -g\mu_N HM\,, \tag{2.2.21}$$

where μ_N is the nuclear magneton and g the g-factor. According to Eq. (2.2.21), every level is split with equally spaced energy.

In nuclear magnetic resonance (NMR) measurements, direct observations are made of transition adjacent magnetic sublevels of the ground states since its transition permits the only magnetic quantum number changes by 1 (ΔM = ±1). In the Mössbauer effect, however, gamma-ray transitions are observed between two nucleus levels, which in generally both exhibit magnetic hyperfine structures. The gamma-ray corresponds to a transition from a particular magnetic sublevel of an excited state to a sublevel of the ground state. The selection rule depends on the multipolarity of the radiation.

Generally, a gamma transition between two nuclear levels of spin I_1 an I_2 must conserve the z-component of the angular momentum. The angular momentum, L, carried off by the gamma-ray must satisfy

$$|I_1 - I_2| \le L \le |I_1 + I_2| \tag{2.2.22}$$

However, L cannot be zero. For a given L, transitions between sublevels are limited to those with $|\Delta M| \le L$. In the presence of magnetic hyperfine structure, the individual transitions between magnetic sublevels may be resolved. These probabilities are given by the square of Clebsch-Gordon coefficients, $(I_1 I_2 M_1 M_2 | I_1 I_2 L M_1 - M_2)^2$.

This magnetic interaction is caused by various sources. These are the Fermi contact interaction, the orbital current, the dipole interaction, the applied external field, and the Lorentz and demagnetizing field due to the applied field. The Fermi contact interaction is the most contributed one to the hyperfine magnetic field in all the sources of hyperfine magnetic interaction in the case of ^{57}Fe. As written below, the Fermi contact interaction is acting between the *s*-electrons at nucleus and the nuclear magnetic dipole moment. In the case of the trivalent iron, the hyperfine magnetic field is taken into account of this interaction because the quenching of the orbital angular momentum by the crystalline electric fields causes the other contribution to the magnetic fields is almost equal to zero. In the other cases, however, the contribution of the hyperfine field by the orbital current should be taken into account. The contribution of the

hyperfine field to each source is explained as follows.

The Fermi contact interaction is written by

$$H_{FC} = \frac{8}{3}\pi\mu_B g\sum_n\left[\rho_{ns}^{\uparrow}(0)-\rho_{ns}^{\downarrow}(0)\right], \qquad (2.2.23)$$

where $\rho_{ns}^{\uparrow}(0)$ and $\rho_{ns}^{\downarrow}(0)$ are the contact density of *s*-electrons of the *n*-th shell having spin up and spin down, μ_B is Bohr magneton, *g* is Lande's g-factor. Its actual origin may be from intrinsic inpairing of the actual *s*-electrons, or indirectly as a result of polarization effects on filled *s*-orbitals. These can occur if the atom has unpaired electrons in *d*- or *f*-electrons. Since the interaction between an unpaired *d*- or *f*-electron and *s*-electrons with parallel spin is different from that with antiparallel spin, there is a slight imbalance of spin density at the nucleus. In the case of metals, direct conduction-electron polarization as well as indirect core-polarization effects might be important.

In non-relativistic theory, H_{orb} produced by the total angular momentum, $\boldsymbol{J}$, of open-shell electrons is given by

$$H_{orb} = a_{hf}\left\langle J\|N\|J\right\rangle\left\langle r^{-3}\right\rangle m_J. \qquad (2.2.24)$$

Here a_{hf} is a hyperfine coupling constant per atomic units, $\left\langle J\|N\|J\right\rangle$ a reduced matrix element, $N=\sum\left\{\boldsymbol{l}_i-\boldsymbol{s}_i+3(\boldsymbol{r}_i\cdot\boldsymbol{s}_i)\boldsymbol{r}_i/\boldsymbol{r}_i^2\right\}$, $\boldsymbol{l}_i$ angular momentum, $\boldsymbol{s}_i$ spin momentum, m_J the azimuthal number connected with J_z, $\left\langle r^{-3}\right\rangle$ the expectation value of $1/r^3$ for the wave functions of the open shell electrons [2.11]. The contribution of the orbital current to the hyperfine field is thought to be nearly proportional to the magnetic moment in the case of the lanthanide elements and neptunium of actinide.

2. 2. 5. Combined Magnetic Hyperfine Interaction and Quadrupole Interaction

When the combined magnetic and quadrupole interactions are observed in the Mössbauer spectrum, the observed spectrum is a little bit complicated. When the hyperfine magnetic field is sufficiently large, the axially symmetric field gradient causes shifts of the magnetically split absorption lines. In this case, every energy level is a pure state. The quadrupole interaction is treated as the perturbation to the hyperfine magnetic interaction.

When the quadrupole interaction is comparable or large enough to magnetic interaction, every nuclear energy level is no more pure state. In this case, the quadrupole interaction cannot be treated as the perturbation to the hyperfine magnetic interaction. The spectrum-analysis in this case is more complicated than in the former case.

2. 2. 6. Mössbauer Effect and Hyperfine Structure of ^{57}Fe

The decay scheme of ^{57}Co is shown in Fig. 2.2.1. ^{57}Fe Mössbauer effect is observed in the transition from I = 3/2 to I = 1/2 and from 5/2 to 1/2. In the transition from I = 3/2 to 1/2, its Mössbauer effect can be observed even at room temperature because the transition energy of 14.4 keV is rather than small the recoil-free fraction is expected to be large. On the other hand, its Mössbauer effect in the transition from 5/2 to 1/2 can be observed only at very low temperature because the recoil energy of 133 keV gamma-ray is large. The conventional ^{57}Fe Mössbauer spectroscopy uses 14.4 keV gamma-ray. Typical energy spectrum of the popular gamma-ray source of ^{57}Co in Rh is shown in Fig. 2.2.2.

The typical level schemes and spectra are shown in Fig. 2.2.3. The transition probability between ^{57}Fe Mössbauer levels is shown in Table 2.2.2. In its powder pattern, the spectra when ^{57}Fe nuclei experience only the magnetic field are symmetric sextet, and the spectra when ^{57}Fe nuclei experience only the electric field gradient are symmetric doublet.

2. 2. 7. Mössbauer Effect and Hyperfine Structure of ^{238}U

The decay scheme of ^{242}Pu is shown in Fig. 2.2.4. ^{238}U Mössbauer effect is observed in the transition from $I = 2^+$ to $I = 0^+$. The energy spectrum of the source used for ^{238}U Mössbauer spectroscopy is shown in Fig. 2.2.5. The source which contains 99.99 % ^{242}Pu has been used in this work. The $^{242}PuO_2$ source in the present work does not need to perform the chemical separation from ^{241}Am, or the observation of ^{238}U Mössbauer gamma-ray is not disturbed from the gamma-ray of ^{241}Am.

The typical level schemes and spectra are shown in Fig. 2.2.6. The transition probability of ^{238}U Mössbauer levels is shown in Table 2.2.3. The spectra when ^{238}U nuclei experience only the magnetic field are symmetric ones like that of UO_2 at 4.2 K

reported by Ruby et al.[2.12]. The spectra when ^{238}U nuclei experience only the electric field gradient are asymmetric ones like that of $UO_2(NO_3)_2 \cdot 6H_2O$ at 4.2 K reported by Ruby et al. Since the *g*-factor of the first excited state in even-even uranium isotopes has not yet been determined except for the theoretical value [2.13], the hyperfine magnetic field have not been able to be determined directly by the Mössbauer measurement of uranium isotopes. No isomer shift of the Mössbauer spectroscopy of even-even uranium isotopes can be observed because the difference of the nuclear radius between the ground state and first excited state is too small to observe the shift in the resonance absorption line.

Table 2.2.1. Magtitude of q and η for various atomic orbitals

Orbital	q	η
p_z	$-\frac{4}{5}\langle r^{-3}\rangle$	0
p_x	$+\frac{2}{5}\langle r^{-3}\rangle$	-3
p_y	$+\frac{2}{5}\langle r^{-3}\rangle$	$+3$
d_{z^2}	$-\frac{4}{7}\langle r^{-3}\rangle$	0
$d_{x^2-y^2}$	$+\frac{4}{7}\langle r^{-3}\rangle$	0
d_{xy}	$+\frac{4}{7}\langle r^{-3}\rangle$	0
d_{xz}	$-\frac{2}{7}\langle r^{-3}\rangle$	$+3$
d_{yz}	$-\frac{2}{7}\langle r^{-3}\rangle$	-3
f_{z^3}	$+\frac{8}{15}\langle r^{-3}\rangle$	0
f_{xz^2}	$-\frac{1}{10}\langle r^{-3}\rangle$	-2
f_{yz^2}	$-\frac{1}{10}\langle r^{-3}\rangle$	$+2$
$f_{z(x^2-y^2)}$	0	0
$f_{z(x^2-y^2)}$	0	0
$f_{x(x^2-3y^2)}$	$-\frac{1}{6}\langle r^{-3}\rangle$	0
$f_{y(3x^2-y^2)}$	$-\frac{1}{6}\langle r^{-3}\rangle$	0

Table. 2.2.2. Relative intensity and angular dependence of ^{57}Fe Mössbauer transitions for the powdered thin specimens. θ is the angle between the magnetic axis or the principle axis of the electric field gradient and the propagation direction of the gamma-ray.

Transition	Relative Intensity in Powder Pattern	Angular Dependence
	Magnetic Spectra	
$+\frac{3}{2}\rightarrow+\frac{1}{2}$	1	$1+\cos^2\theta$
$+\frac{1}{2}\rightarrow+\frac{1}{2}$	$\frac{2}{3}$	$2\sin^2\theta$
$-\frac{1}{2}\rightarrow+\frac{1}{2}$	$\frac{1}{3}$	$1+\cos^2\theta$
$-\frac{3}{2}\rightarrow+\frac{1}{2}$	0	0
$+\frac{3}{2}\rightarrow-\frac{1}{2}$	0	0
$+\frac{1}{2}\rightarrow-\frac{1}{2}$	$\frac{1}{3}$	$1+\cos^2\theta$
$-\frac{1}{2}\rightarrow-\frac{1}{2}$	$\frac{2}{3}$	$2\sin^2\theta$
$-\frac{3}{2}\rightarrow-\frac{1}{2}$	1	$1+\cos^2\theta$
	Quadrupole Spectra	
$\pm\frac{1}{2}\rightarrow\pm\frac{1}{2}$	1	$2+3\sin^2\theta$
$\pm\frac{3}{2}\rightarrow\pm\frac{1}{2}$	1	$3(1+\cos^2\theta)$

Table. 2.2.3. Relative intensity and angular dependence of ^{238}U Mössbauer transitions for the powdered thin specimens. θ is the angle between the magnetic axis or the principle axis of the electric field gradient and the propagation direction of the gamma-ray.

Transition	Relative Intensity in Powder Pattern	Angular Dependence
	Magnetic Spectra	
$+2\rightarrow0$	1	$\sin^2\theta+\frac{\sin^2 2\theta}{4}$
$+1\rightarrow0$	1	$\cos^2\theta+\cos^2 2\theta$
$0\rightarrow0$	1	$\frac{3}{2}\sin^2 2\theta$
$-1\rightarrow0$	1	$\cos^2\theta+\cos^2 2\theta$
$-2\rightarrow0$	1	$\sin^2\theta+\frac{\sin^2 2\theta}{4}$
	Quadrupole Spectra	
$\pm2\rightarrow0$	2	$\sin^2\theta+\frac{\sin^2 2\theta}{4}$
$\pm1\rightarrow0$	2	$\cos^2\theta+\cos^2 2\theta$
$0\rightarrow0$	1	$\frac{3}{2}\sin^2 2\theta$

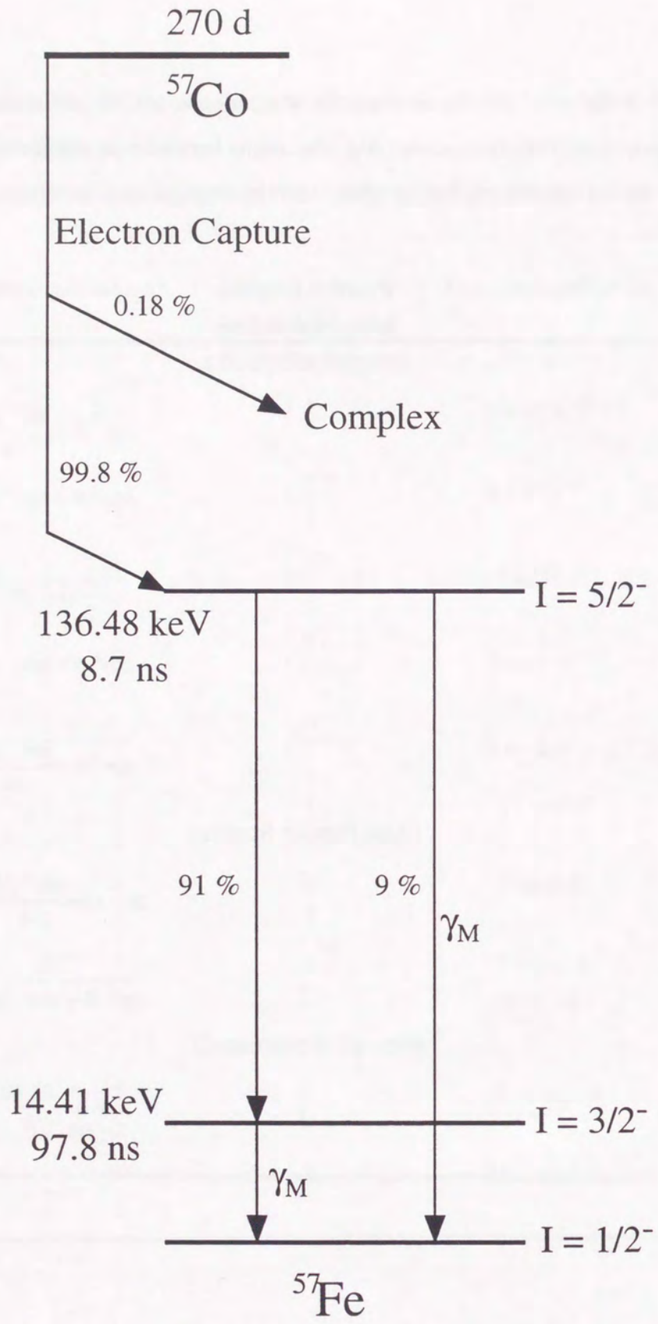

Fig. 2.2.1. Decay scheme of ^{57}Co.

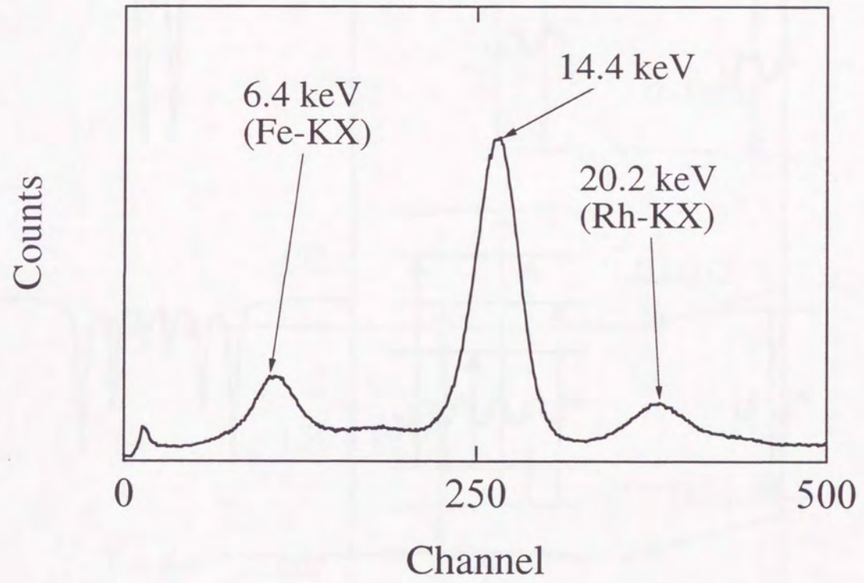

Fig. 2.2.2. Energy spectrum of ^{57}Fe Mössbauer source, ^{57}Co in Rh, which is measured by using a Xe gas filled proportional counter.

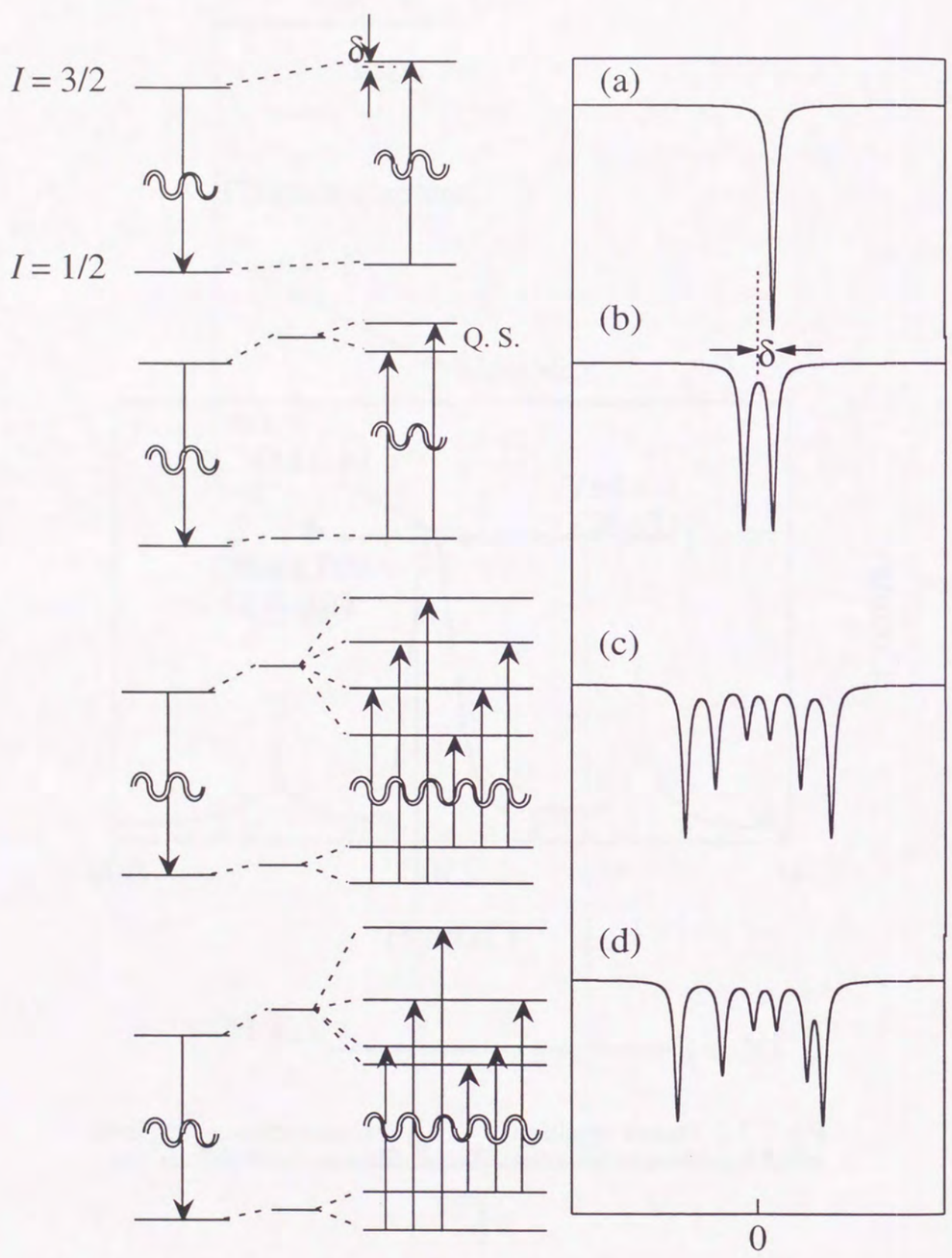

Fig. 2.2.3. Schmatic drawing of the hyperfine structure and corresponding spectrum of ^{57}Fe. (a) Electric monopole interaction. (b) Electric quadrupole interaction. (c) Magnetic dipole interaction. (d) Magnetic dipole interaction with weak electric quadrupole interaction.

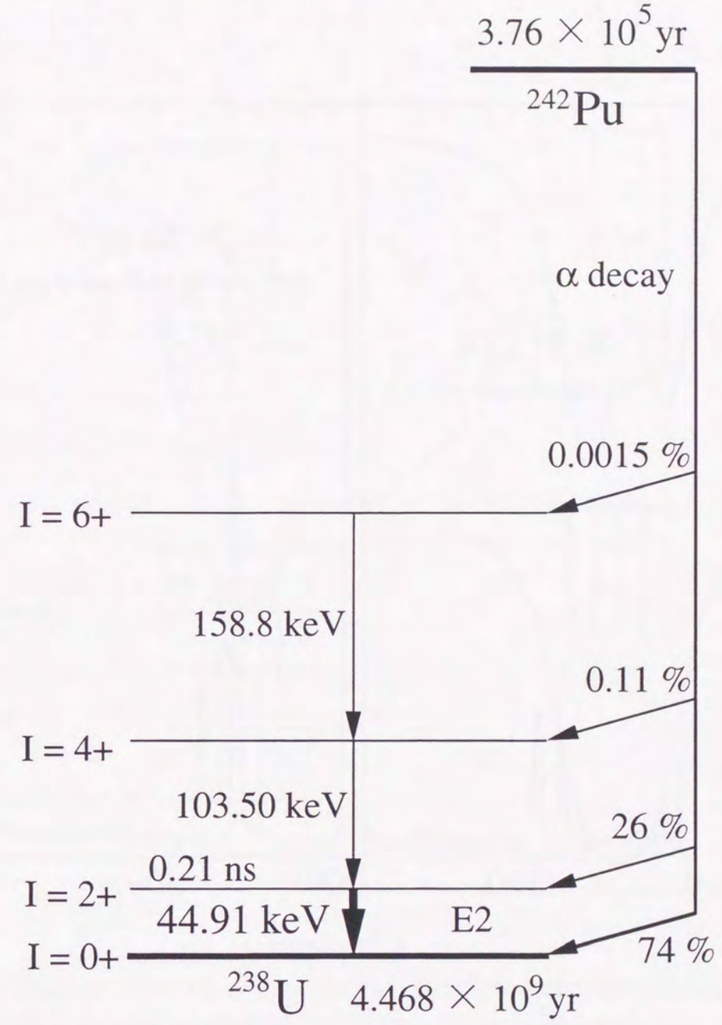

Fig. 2.2.4. Decay scheme of ^{242}Pu.

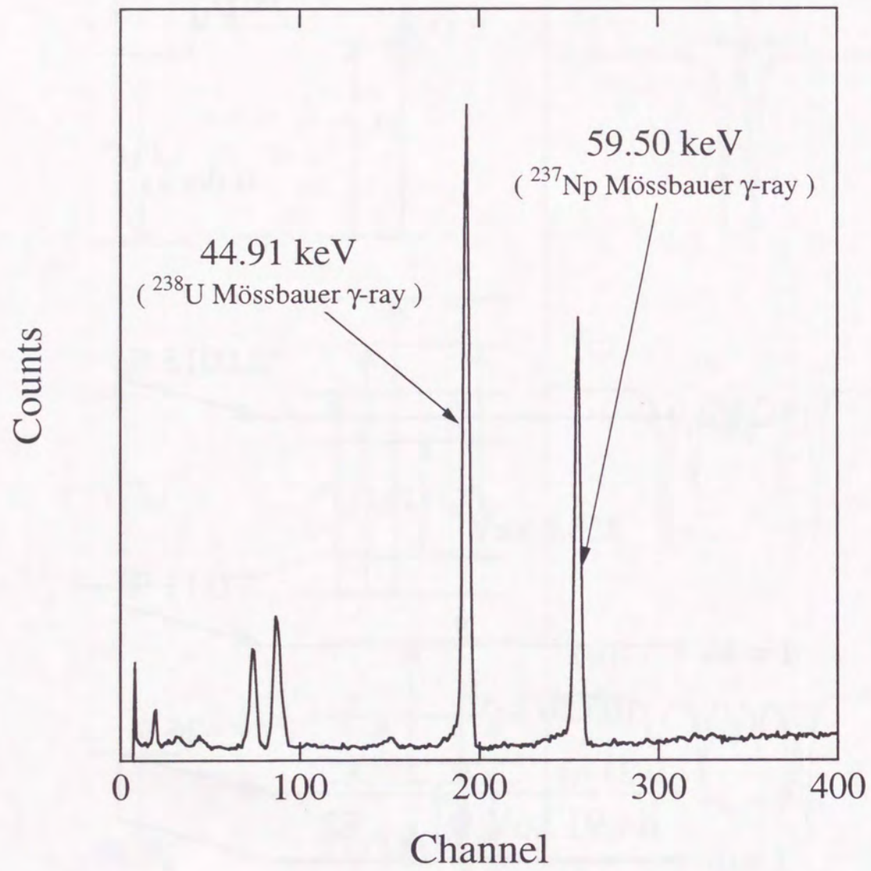

Fig. 2.2.5. Energy spectrum of $^{242}PuO_2$ Mössbauer source, which was measured by using a pure Ge solid state detector.

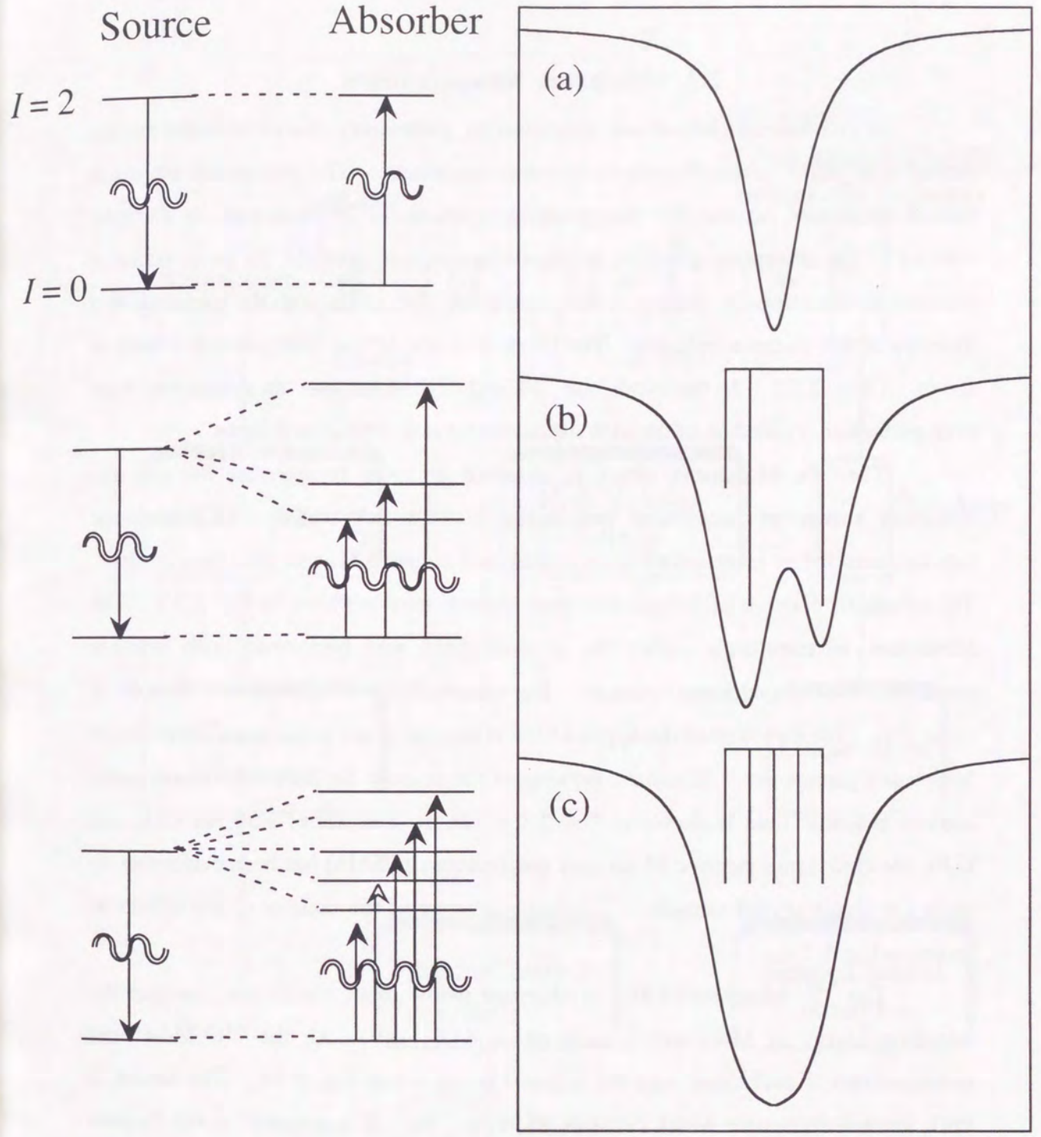

Fig. 2.2.6. Schematic drawing of the hyperfine structure and corresponding spectrum of ^{238}U. (a) No hyperfine interaction. (b) Electric quadrupole interaction. (c) Magnetic dipole interaction.

2.3. Mössbauer Measurements

In conventional Mössbauer spectroscopy, gamma-ray source is mount on the driving unit which is usually electro-magnetic transducer. The gamma-ray source is moved oscillatory, so that the energy of the gamma-ray is modulated by Doppler velocity. The absorption spectrum of the specimen which contains the probe nuclei is obtained by detecting the number of the gamma-ray photons through the specimen as a function of the Doppler velocity. The block diagram of the measurement system is shown in Fig. 2.3.1. In this work, the ^{57}Fe and ^{238}U Mössbauer measurements have been performed. Procedure of the each measurement is described as follows.

The ^{57}Fe Mössbauer effect is observed at room temperature because the transition energy of Mössbauer gamma-ray is 14.4 keV. The ^{57}Fe Mössbauer measurement below room temperature is achieved by using He gas flow type cryostat. The schematic drawing of the gas-flow type cryostat used is shown in Fig. 2.3.2. The Mössbauer measurements under the external field was performed with cryostat containing a superconducting solenoid. The magnitude of the applied external field is up to 7 T. The direction of the applied field is parallel to the propagation direction of Mössbauer gamma-ray. Schematic drawing of the cryostat for the measurement under applied magnetic field is shown in Fig. 2.3.3. In the Mössbauer study of UFe_2 and U_6Fe, the conversion electron Mössbauer spectroscopy (CEMS) has been performed by using the single crystal samples. Schematic drawing of the counter of the CEMS as shown in Fig. 2.3.4.

The ^{238}U Mössbauer effect is observed below room temperature because the transition energy of Mössbauer gamma-ray is 44.91 keV. All the ^{238}U Mössbauer measurements is performed with the cryostat as shown in Fig. 2.3.5. The source is PuO_2 gamma-ray source which contains 99.99 % ^{242}Pu. It is prepared at the Russian Federal Nuclear Center in All-Russian Research Institute of Experimental Physics. The schematic drawing of the source used is shown in Fig. 2.3.6. Since the activity of $^{242}PuO_2$ is 72.6 MBq and rather weak for the Mössbauer gamma-ray source, a specially designed sample holder shown in Fig. 2.2.7 was used in order to eliminate the electronic absorption of the Mössbauer gamma-ray.

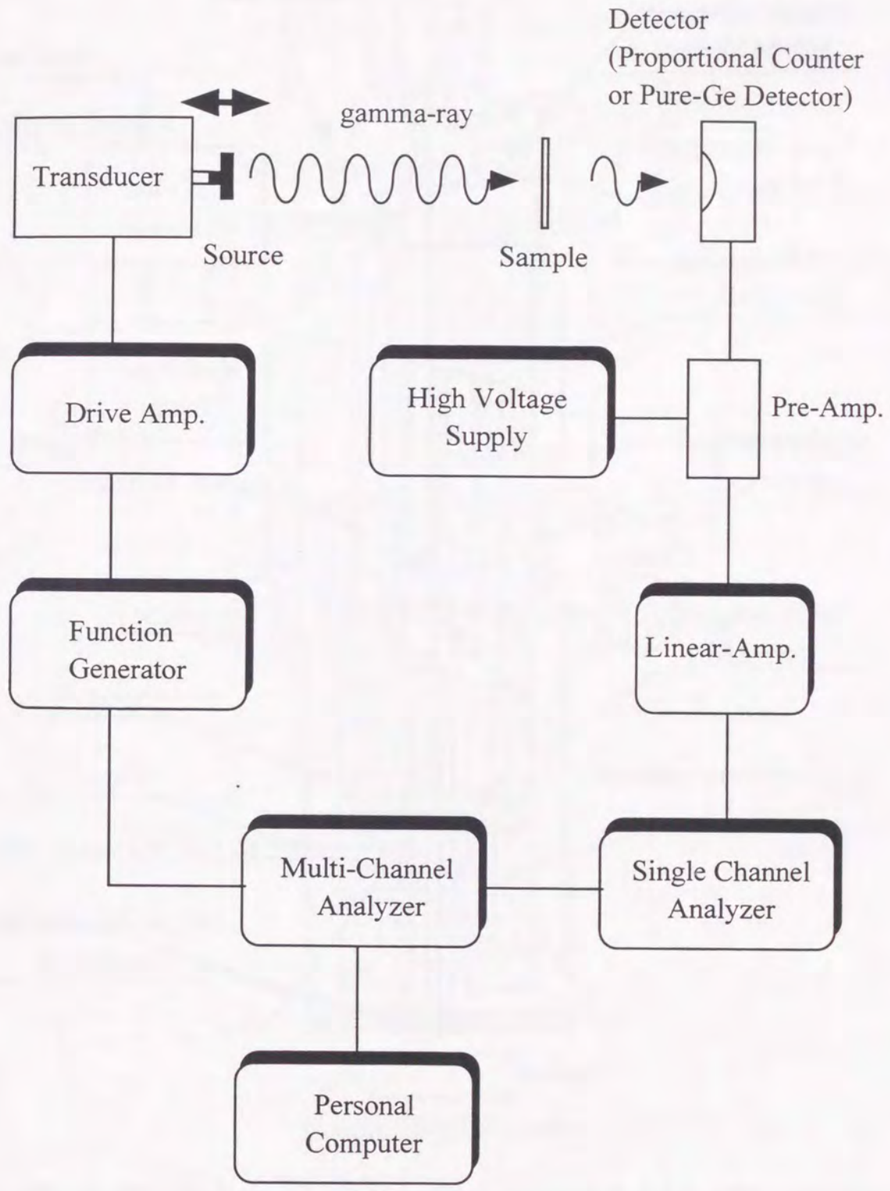

Fig. 2.3.1. Schematic drawing of the Mössbauer Measurements.

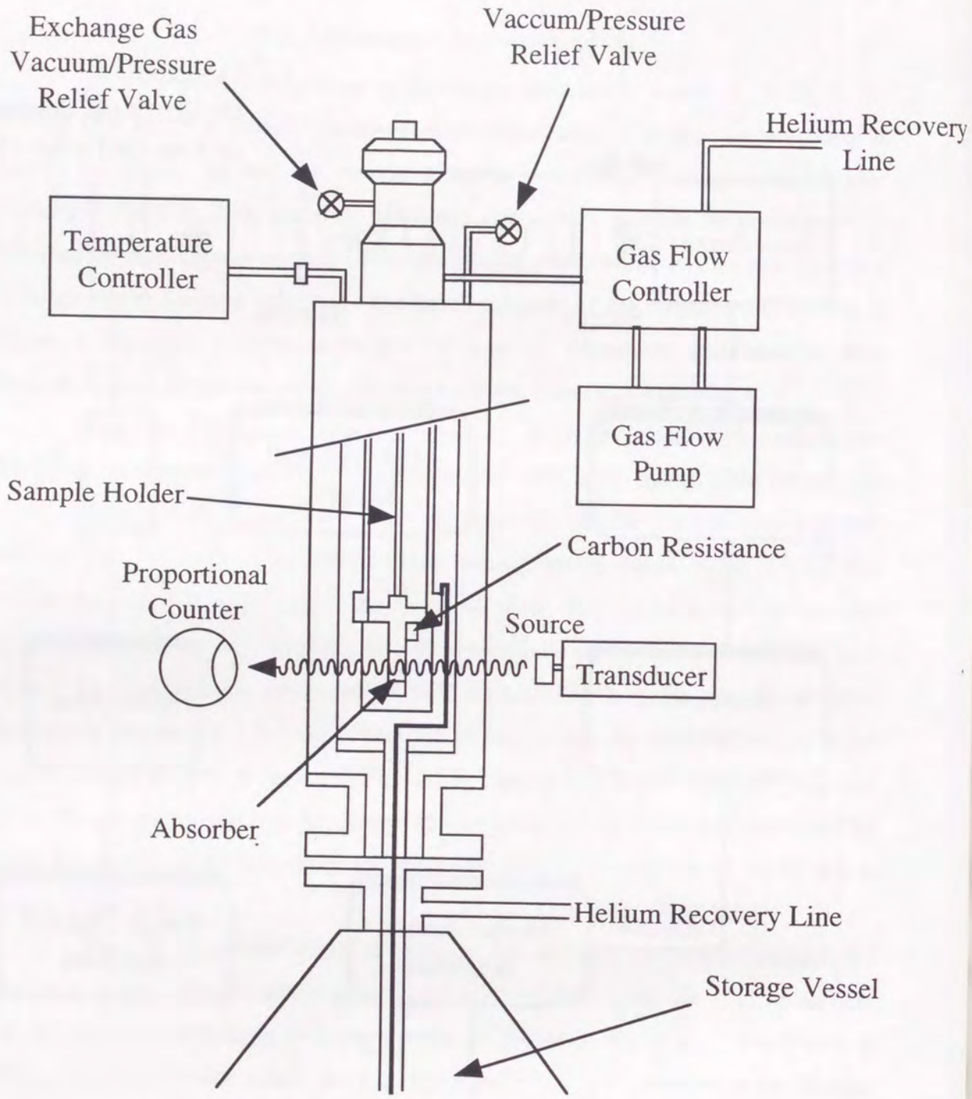

Fig. 2.3.2. Schematic drawing of the He gas flow type cryostat (Oxford Instruments Limited, CF500).

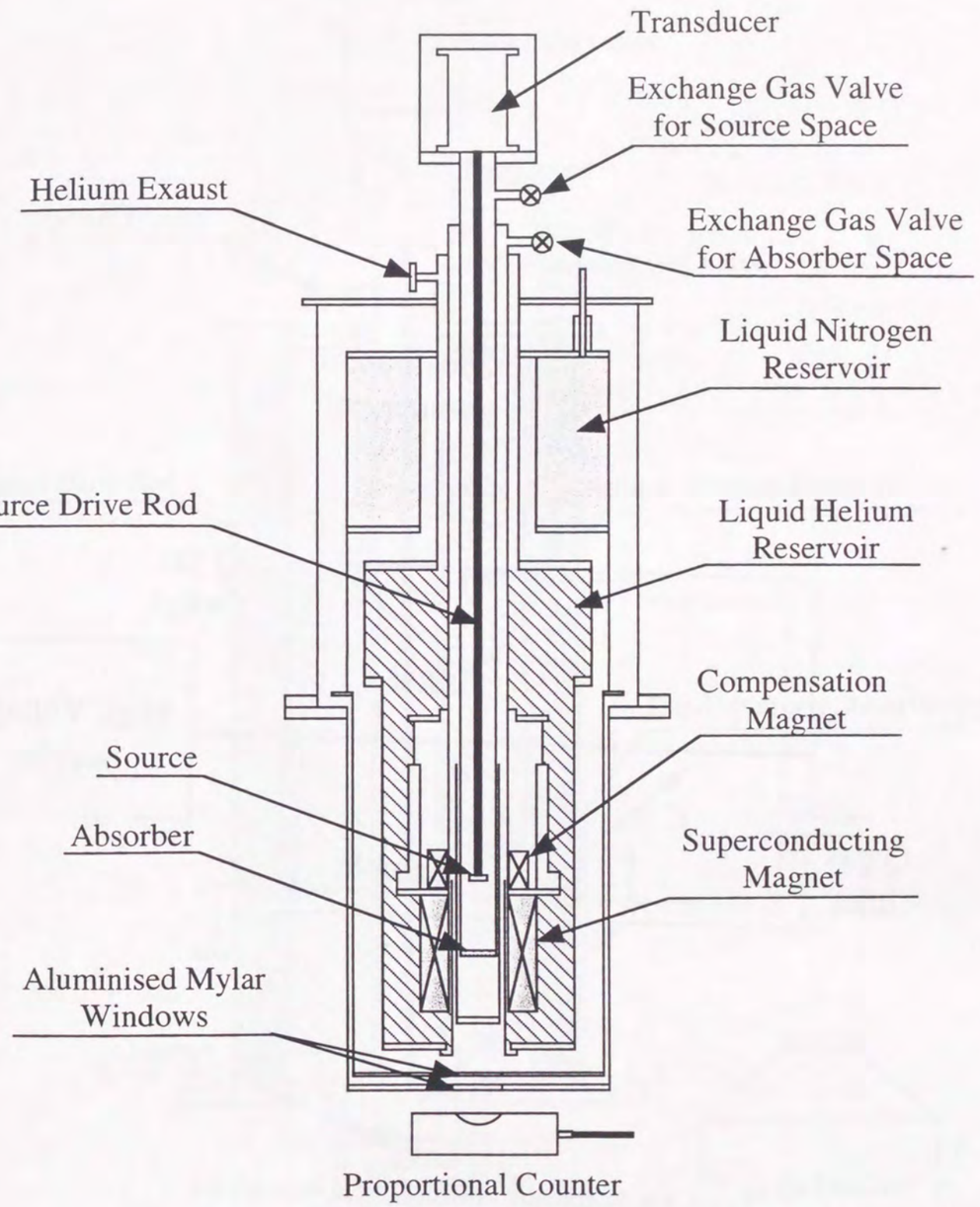

Fig. 2.3.3. Schematic drawing of the cryostat with superconducting magnet (Oxford Instruments Limited, ITC-4).

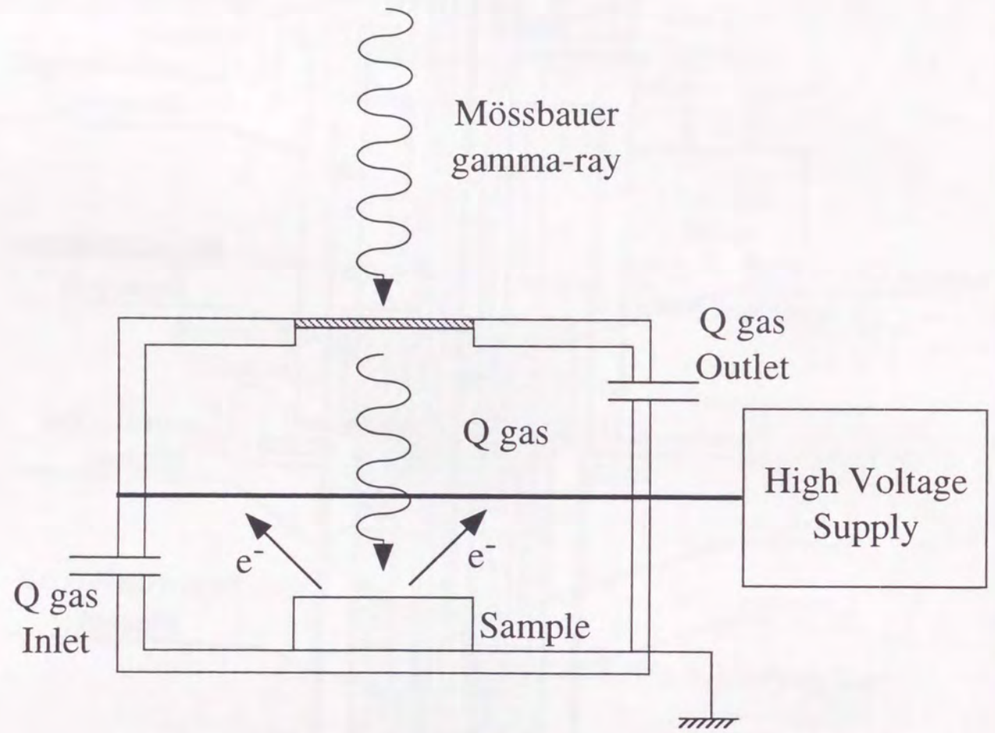

Fig. 2.3.4. Schematic drawing of the detector for the conversion electron Mössbauer spectroscopy (CEMS).

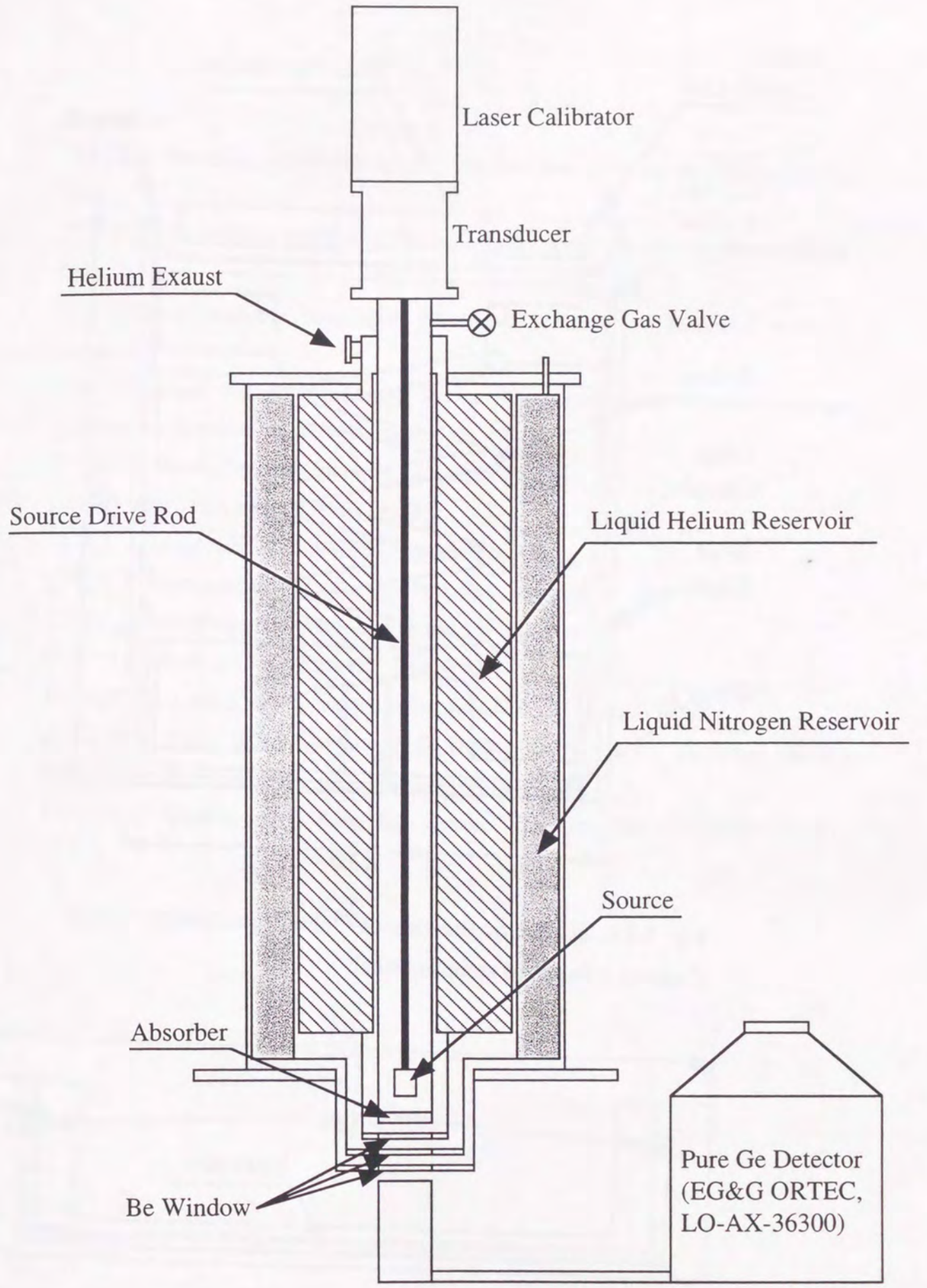

Fig. 2.3.5. Schematic drawing of the cryostat for ^{238}U Mössbauer spectroscopy (Taiyo Toyo Sanso co Ltd,TEC-337).

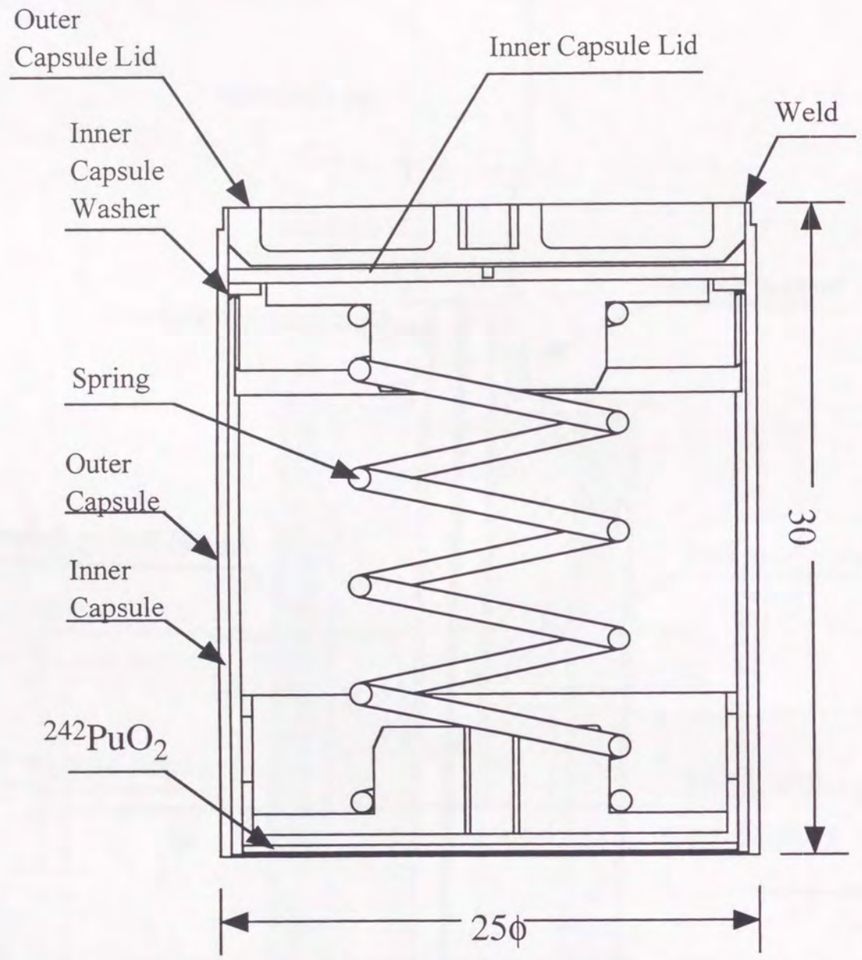

Fig. 2.3.6. Schematic drawing of $^{242}PuO_2$ gamma-ray source. Capsule is made of stainless steel.

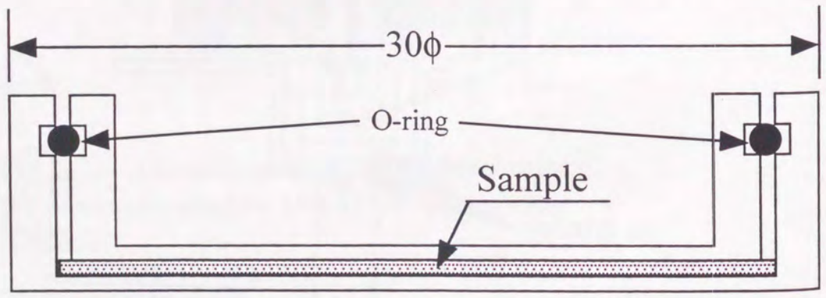

Fig. 2.3.7. Schematic drawing of the sample holder of the ^{238}U Mössbauer spectroscopy made of aluminum.

References

[2.1] G. K. Wertheim, *Mossbauer Effect, Principles and Applications*, Academic Press, 1964.

[2.2] N. N. Greenwood and T. C. Gibb, *Mossbauer Spectroscopy*, Chapman and Hall, 1971.

[2.3] H. Sano, *Mossbauer Bunkougaku (Mossbauer Spectroscopy)*, Kodansha, 1972. (in Japanese)

[2.4] G. Schatz and A. Weidinger, *Nuclear Condensed Matter Physics, Nuclear Methods and Applications*, John Wiley & Sons, 1996.

[2.5] R.W. Wood, *Physical Optics*, Macmilan, 1934.

[2.6] W. Kurn, Phil. Mag., **8**, 625 (1929).

[2.7] R. L. Mössbauer, Z. Phisik, **151**,124 (1958).

[2.8] P. V. Pound and G. A. Rebka, Jr., Phys. Rev. Lett. **4**, 274 (1960).

[2.9] B. D. Josephson, Phys. Rev. Lett. **4**, 341 (1960).

[2.10] Y. Hazony, J. Chem. Phys. **45**, 2664 (1960).

[2.11] R. Elliot and K. W. H. Stevens, Proc. Roy. Soc., **A218**, 553 (1953).

[2.12] S. L. Ruby, G. M. Kalvius, B. D. Dunlap, G. K. Shenoy, D. Cohen, M. B. Brodsky and D. J. Lam, Phys. Rev. **184**, 374 (1969).

[2.13] S. G. Nilssons and O. Prior, Kgl. Danske Vielenskab, Mat.-Fys. Medd., **32**, 49 (1961).

Chapter 3. Results and Discussion

3.1. Determination of the g-factor in the First Excited State of ^{238}U

3.1.1. Introduction

In previous works, ^{238}U Mössbauer spectroscopy applied to several magnetic materials [3.1.1]. However, since the g-factor of the first excited state of the ^{238}U nucleus is unknown except for the theoretical value [3.1.2], the magnitude of the hyperfine magnetic field is determined in every magnetic material. The only energy of the magnetic Zeeman splitting had been obtained by the spectrum analysis precisely. On the other hand, the magnitude of the hyperfine magnetic field at uranium nuclei is directly determined using ^{235}U NMR because the gamma-value is already known, 0.784 MHz / T [3.1.3]. Since the existence of the hyperfine magnetic field at uranium nuclei of UO_2 have already been known in its antiferromagnetic state [3.1.1]. In this work, the g-factor of the first excited state of ^{238}U nuclei tried to be determined using the combination of ^{238}U Mössbauer and ^{235}U NMR measurements of UO_2 in the antiferromagnetic state.

The physical properties of UO_2 have been investigated very well. UO_2 has an antiferromagnetic material and ceramic nuclear fuel. Its Néel temperature and effective moment is 30.8 K and 3.1 μ_B / U, respectively, determined by the magnetic susceptibility measurement. Its saturated moment is 1.78 μ_B / U determined by the neutron scattering [3.1.4]. Its crystal field was also observed by neutron scattering [3.1.5]. Its ground state reveals Γ_5 triplet, using several experimental results [3.1.6]. However, its magnetic properties including its antiferromagnetic transition was not understood clearly. Its phase transition is the first-order transition [3.1.4]. It is believed the first-order transition results from the competition between the exchange interaction and the Jahn-Teller distortion [3.1.7]. If so, the ground state of UO_2 is considered to be the coexistence and/or competition of the antiferromagnetic ordering and quadrupole ordering [3.1.7-9]. This phenomenon has not been explained clearly in the view point of experiments. ^{238}U Mössbauer measurement was performed only at 77 K which is the temperature range of its paramagnetic state and 4.2 K which is of its antiferromagnetic state [3.1.1]. ^{235}U NMR measurement have never been performed as long as I know. Fortunately, the ^{235}U NMR signals of UO_2 have been firstly observed in the antiferromagnetic state. In order to determine the g-factor of the first excited

state of ^{238}U nuclei, ^{238}U Mössbauer and ^{235}U NMR measurements of antiferromagnetic UO_2 have been thus performed in its antiferromagnetic state.

3.1.2. Experimental Procedure

Two samples were prepared. One is for ^{238}U Mössbauer spectroscopy, and another for ^{235}U NMR spectroscopy. As written above, the probe isotope of ^{238}U Mössbauer measurement includes 99.275 %, whereas that of ^{235}U NMR measurement includes 0.72 %. Therefore, the sample for the Mössbauer measurement made from the oxide of natural uranium, and that for the NMR measurement from the uranium oxide enriched to 93.01 % with ^{235}U. Both samples prepared by sintering uranium oxide for 10 hours at 1273 K under an atmosphere of hydrogen gas. The lattice parameter of UO_{2-x} depends on the oxygen content and the detail relationships between them have been established [3.1.10]. Using the previously reported table, the stoichiometry of the specimen was confirmed by the lattice parameter obtained from X-ray diffraction pattern [3.1.10-12].

^{238}U Mössbauer spectra were measured between 5.4 K and 280 K using transmission geometry. The gamma-ray source used is $^{242}PuO_2$ which includes 99.99 % ^{242}Pu. Doppler velocity calibrated with a laser calibrator. Zero isomer shift was adopted as ^{238}U in PuO_2. ^{235}U NMR spectrum was measured using pulsed NMR method at 1.5 K.

3.1.3. Results and Discussion

A ^{235}U NMR spin-echo spectrum of UO_2 at 1.5 K was observed [3.1.13]. Seven resonance lines were obtained. The results obtained show that the magnitude of the hyperfine magnetic field of ^{235}U nuclei is 252.3 ± 0.5 T, and that quadrupole splitting is $\left|e^2qQ\left(3\cos^2\theta-1\right)/h\right|$ = 392 ± 11 MHz [3.1.13]. The magnitudes of the nuclear quadrupole moments of ^{235}U and ^{238}U isotopes are $Q(^{235}U)$ = 4.1 barn in the ground state and $Q_{ex}(^{238}U)$ = -3.2 barn in the first excited state ($I = 2^+$), respectively [3.1.14]. The quadrupole splitting observed for ^{235}U NMR spectrum corresponds to $\left|e^2qQ\left(3\cos^2\theta-1\right)\right|$ = 1.70 ± 0.04 mm s^{-1} for the ^{238}U Mössbauer spectrum. Since the natural line width of ^{238}U Mössbauer spectra is 27 mm s^{-1}, as calculated from the short

life time 0.21 ns of the first excited state ($I = 2^+$), the quadrupole splitting of ^{238}U in UO_2 is, unfortunately, too small to distinguish it from the line-width.

^{238}U Mössbauer spectra of UO_2 at various temperatures are shown in Fig. 3.1.1. The full width at half maximum (FWHM) increased appreciably with decreasing temperature. The obvious line broadening was observed at 25 K and 5.4 K below the Néel temperature, T_N = 30.8 K [3.1. 14]. The spectra at 25 K and 5.4 K were analyzed as a superposition of magnetically split 5 lines. The nuclear spin of ^{238}U is $I = 0^+$ in the ground state, and $I = 2^+$ in the first excited state. In order to determine the magnitude of nuclear Zeeman splitting, we used two different methods in spectrum-analysis. Method I is to analyze the spectrum by a least-square-fit with non-constrained FWHM. Method II is a least-square-fit using a constrained FWHM. FWHM depends on the temperature because of the temperature dependence of the recoil-free fraction of UO_2 and $^{242}PuO_2$.

The Mössbauer parameters obtained by Method I are as follows: The magnetic splitting and FWHM are equal to 62.7 ± 2.1 mm s^{-1} and 38.3 ± 6.6 mm s^{-1} respectively at 5.4 K. The temperature dependence of FWHM had the maximum near the Néel temperature as shown in Fig. 3.1.2. The absorption area in the ^{238}U Mössbauer spectra of UO_2, which is proportional to the recoil-free fraction, does not change appreciably below about 50 K, as also shown in Fig. 3.1.2. FWHM of the spectrum is represented as a function of the effective thickness of the specimen, which includes the recoil-free fraction of sources and absorbers and increases with decreasing temperature. When FWHM is narrower than that obtained at higher temperatures where the effective thickness is smaller, the results obtained by the analysis of superposed spectra show, in general, the overestimated quadrupole and magnetic splitting [3.1.15].

In the spectrum-analysis using Method II, we considered the temperature dependence of FWHM and recoil-free fraction. Temperature dependence of the absorption areas is related to the product of the recoil-free fractions of UO_2 and PuO_2. FWHM of the spectrum, which is also related to the recoil-free fraction [3.1.16], could not change appreciably below 50 K and the values of FWHM between 35 K and 5.4 K should be equal to the value observed at 50 K. From the reason mentioned above, the spectra in the antiferromagnetic state at 25 K and 5.4 K were analyzed using the FWHM value at 50 K, 46.5 ± 1.57 mm s^{-1}. The results from Method II are as follows: The

magnitude of the magnetic splitting and FWHM are 59.1 ± 3.9 mm s^{-1} and 46.5 ± 1.57 mm s^{-1} at 5.4 K, respectively. From the relationships between FWHM and absorption area, the results from Method II is better than those from Method I.

In this study, both of the source and the absorber specimen are at the same temperature, and the temperature difference between them is less than 1 K as an experimental error. Generally, the resonant absorption is expressed by

$$p(v) = N_0 + \int_{-\infty}^{\infty} S(E - v)\exp[-\sigma(E)]dE, \qquad (3.1.1)$$

where $p(v)$ is counts rate as a function of Doppler velocity, v, N_0 background, $S(E)$ the distribution of gamma-ray energy from a source, $\sigma(E)$ the resonant absorption cross-section of an absorber. In thin foil approximation, the absorption area is given by

$$A = \int_{-\infty}^{\infty} \{N_0 - p(v)\}dv \approx A' f_S \times f_A, \qquad (3.1.2)$$

where f_S and f_A are the recoil-free franction of source and absorber. The recoil-free fraction f is a probability of the zero-phonon emission and absorption of gamma-ray in the lattice and is given by

$$f = \left|\left\langle \omega_q \left| e^{ik\cdot x} \right| \omega_q \right\rangle\right|^2$$

$$\approx \exp\left[-\frac{6E_R}{k\theta_D}\left\{\frac{1}{4} + \left(\frac{T}{\theta_D}\right)^2 \int_0^{\theta_D} \frac{x}{e^x - 1}\right\}\right]. \qquad (3.1.3)$$

The 2nd formula is expressed with the Debye model. ω_q is the phonon spectrum of the lattice, $\boldsymbol{k}$ wave vector of the gamma-ray, $\boldsymbol{u}$ is a displacement of the nucleus from its equilibrium position, E_R the recoil energy and θ_D the Debye temperature of source or absorber. The Debye temperature of UO_2 was reported to be 182 K using the specific heat measurement [3.1.7]. We adopted this value to determine the Debye temperature of ^{238}U in PuO_2. The temperature dependence of the absorption area in a combination between UO_2 and $^{242}PuO_2$ is shown as the line calculated using the Debye temperature 182 K for UO_2 and 250 K for PuO_2, which is obtained by the least-square-fit in the temperature range above 50 K. Below 50 K, the absorption area approaches to a nearly constant value. These results suggest that the Debye temperature of uranium atoms in PuO_2 is about 250 K. Recoil-free fractions of UO_2 and/or PuO_2 do not change below 50 K and suggest the slight change in the phonon spectrum might be induced by

the antiferromagnetic ordering of UO_2. From the consideration of the recoil-free fraction with the Debye model, we adopt the results of the spectrum-analysis using Method II rather than Method I.

The hyperfine magnetic fields obtained by ^{235}U NMR and ^{238}U Mössbauer effect were at the different temperatures, 1.5 K and 5.4 K, respectively. Since the magnitude of the magnetic moments of uranium atoms in UO_2 saturates at low temperature like 5.4 K [3.1.4]. The magnitude of the hyperfine magnetic field obtained by the ^{235}U NMR spin-echo spectrum at 1.5 K should be the same as that obtained by the ^{238}U Mössbauer effect at 5.4 K within the experimental error. We determine the g-factor of the excited state in the ^{238}U Mössbauer transition using the results from Mössbauer effect and NMR measurements.

The energy of the hyperfine magnetic interaction is equal to $4g_{ex}\mu_N H$, where μ_N is the nuclear magneton ($e\hbar/2m_p$), H is the hyperfine magnetic field at ^{238}U nucleus. The energy of ^{238}U Mössbauer gamma-ray is 44.91 keV [3.1.14]. The nuclear Zeeman splitting is equal to (8.85 ± 0.58) × 10^{-6} eV. Therefore the g-factor of the excited state in the ^{238}U Mössbauer transition is 0.254 ± 0.015. This is almost equal to the theoretical value, 0.25 within the experimental error [3.1.2]. From present investigation, the conversion factor, 4.27 ± 0.28 T / mm s^{-1}, has been obtained.

The anomaly of the temperature dependence of the recoil-free fraction below 50 K was observed as written above. The observed recoil-free fraction is smaller that the calculated value in this temperature range as shown in Fig. 3.1.2. This result means the recoil-free fraction decreases below 50 K. As written below, the anomaly cannot be observed in the other compounds, UGe_2, UPd_2Al_3 and URu_2Si_2, whose Mössbauer effect is measured in this work. Therefore, it is suggested this anomaly is caused by the anomaly of UO_2 rather than that of PuO_2.

Generally, when a quadrupole ordering exists at a finite temperature, the softening of the elastic constant is observed at this temperature. Since the elastic constant is relate to the recoil-free fraction, the softening of the elastic constant must be the decrease of the recoil-free fraction. For the antiferromagnetic ordering of UO_2, it has been proposed to be the coexistence and/or competition with the quadrupole ordering [3.1.7-9]. The result obtained Indicates that the elastic constant at uranium

atoms in UO_2 is softened around 50 K. This result suggests UO_2 undergoes the quadrupole ordering around 50 K. This is suggested that UO_2 does not undergo both of the antiferromagnetic transition and the quadrupole ordering at Néel temperature.

3.1.4. Conclusion

The combination of ^{238}U Mössbauer and ^{235}U NMR measurements of antiferromagnetic UO_2 has been performed in the magnetic ordered state. The g-factor of the excited state of ^{238}U Mössbauer transition is 0.254 ± 0.015. From the obtained g-factor, the conversion factor becomes 4.27 ± 0.28 T / mm s^{-1}.

In consideration for the obtained results of ^{238}U Mössbauer measurement, the observed anomaly of the recoil-free fraction is thought to be due to the anomaly of the phonon spectra in UO_2. This result suggests that UO_2 does not the antiferromagnetic and the quadrupole orderings at Néel temperature, but that it experiences the quadrupole ordering at higher temperature than the antiferromagnetic ordering.

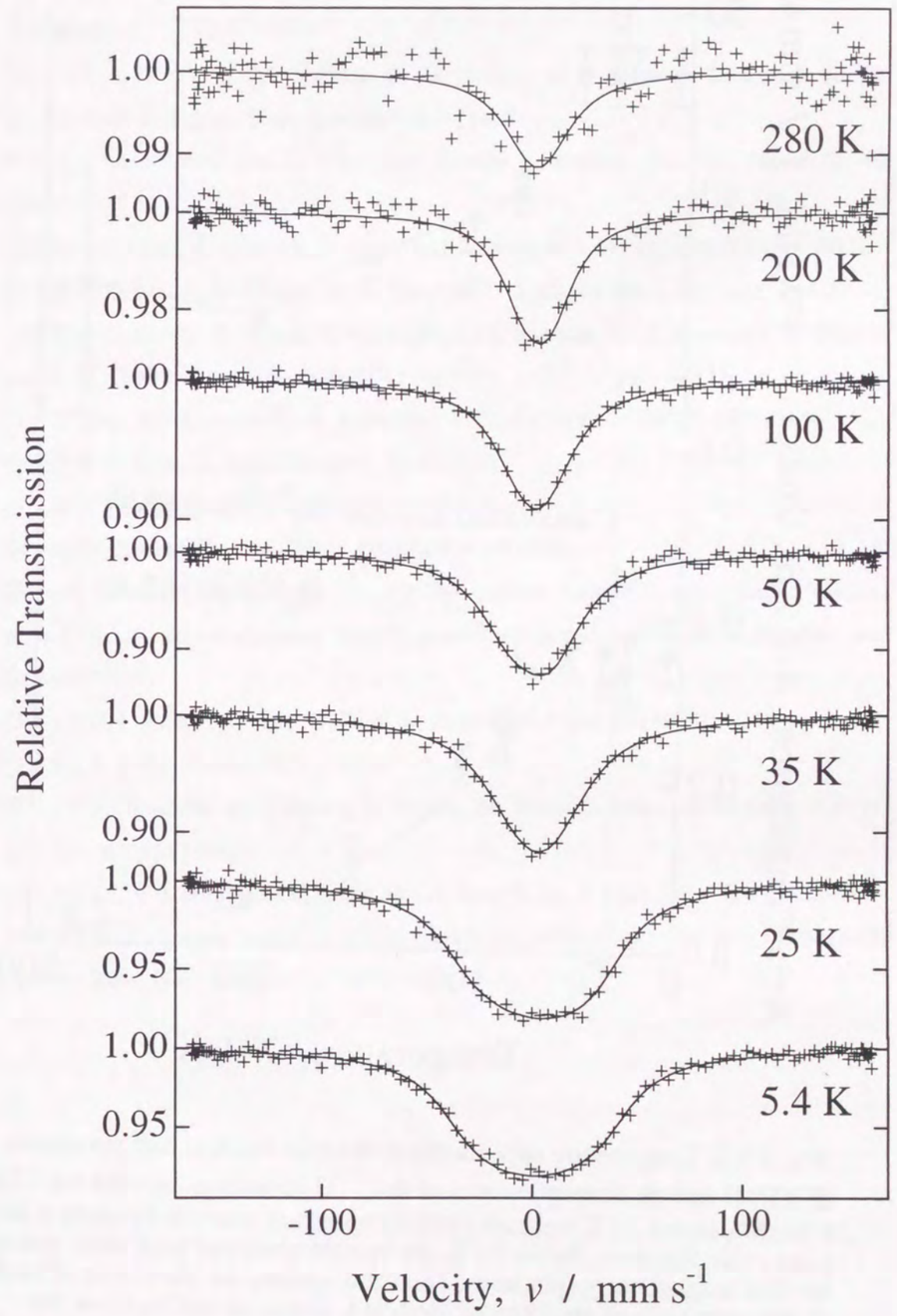

Fig. 3.1.1. ^{238}U Mössbauer spectra of UO_2 at various temperatures.

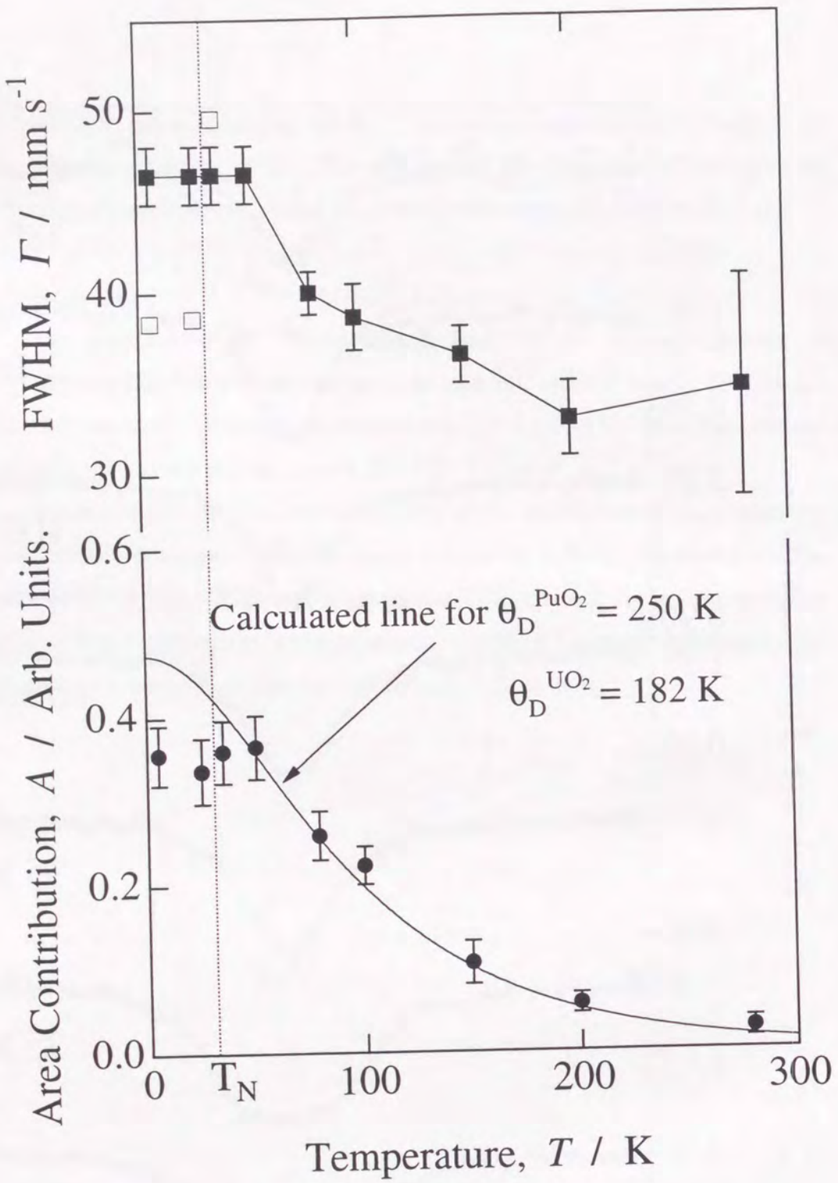

Fig. 3.1.2. Temperature dependence of the full-width at half maximum (FWHM) and the absorption area of the ^{238}U Mössbauer spectra for UO_2. FWHM's above 35 K were obtained by spectrum analysis by using a single Lorentzian function. Below 25 K, the spectra observed were analyzed by the five magnetically split lines: The solid squares are the results of Method II, the open squares are those of Method I. The solid circles show the temperature dependence of the absorption area. The solid line is theoretical curve obtained by using the Debye model in which the Debye temperatures of UO_2 and PuO_2 were 182 K and 250 K, respectively.

References

[3.1.1] S. L. Ruby, G. M. Kalvius, B. D. Dunlap, G. K. Shenoy, D. Cohen, M. B. Brodsky and D. J. Lam, Phys. Rev. **184**, 374 (1969).

[3.1.2] S. G. Nilssons and O. Prior, Kgl. Danske Vielenskab, Mat.-Fys. Medd. **32**, 49 (1961).

[3.1.3] H. Le Bail, C. Chachty, P. Rigny and R. Bougon, J. Physique **44**, L1017 (1983).

[3.1.4] B. C. Frazer, G. Shirane, D. E. Cox, and C. E. Olsen, Phys. Rev. **140**, A1448.

[3.1.5] G. Amoretti, A. Blaise, R. Caciuffo, J. M. Fournier, M. T. Huchings, R. Osborn and A. D. Taylor, Phys. Rev. **B40**, 1865 (1989).

[3.1.6] H. U. Rahman and W. A. Runciman, J. Phys. Chem. Solids 27, 1833 (1966).

[3.1.7] S. J. Allen, Jr, Phys. Rev. **166**, 166 (1968).

[3.1.8] S. J. Allen, Jr, Phys. Rev. **167**, 167 (1968).

[3.1.9] G. Solt and P. Erdos, Phys. Rev. **B22**, 4718 (1980).

[3.1.10] Technical Report Series No. 39, International Atomic Energy Agency, Vienna, p. 6 (1965), "*Thermodynamic and Transport Properties of Uranium Dioxide and Related Phases*".

[3.1.11] C. L. Duke and W. L. Talbort, Jr, Phys. Rev. **173** 1125 (1968).

[3.1.12] P. Perio, Thesis, Paris (1965).

[3.1.13] K. Ikushima, H. Yasuoka, S. Tsutsui, M. Saeki, S. Nasu and M. Date, J. Phys. Soc. Jpn. **67**, 65 (1998).

[3.1.14] Ed. V. S. Shirley, *Table of Isotopes*, John Wiley & Sons, Inc., New York, 1996.

[3.1.15] G. K. Shenoy and S. L. Ruby, *Mössbauer Methodology*, Ed. I. J. Gruverman, Prenum Press, New York, 1974, Vol. 9, p. 227.

3. 2. U-Fe Intermetallic compounds

3. 2. 1. Introduction

In U-Fe system, only two intermetallic compounds have been formed in UFe_2 and U_6Fe. UFe_2 is the ferromagnetic compound whose Curie temperature is 167 K [3.2.1.1] and Laves phase whose crystal structure is C-15 ($MgCu_2$) type one. The Curie temperature of UFe_2 is sensitive to its stoichiometry [3.2.1.1-2]. On the other hand, U_6Fe is Pauli paramagnetic compounds and superconductor whose transition temperature is 3.96 K. U_6Fe is difficult to obtain the single phase sample because the metallic uranium and UFe_2 is easy to include as the main impurities [3.2.1.3].

In both of UFe_2 and U_6Fe, the ^{57}Fe Mössbauer measurements have been performed in previous works [3.2.1.4-7]. In UFe_2, the ^{238}U Mössbauer measurement was performed by Ruby et al.[3.2.1.8]. As for the ^{57}Fe Mössbauer spectroscopy of UFe_2 and U_6Fe, temperature dependence of the Mössbauer parameter was discussed. In UFe_2, temperature dependence of the absorption area has the anomaly at Curie temperature. According to results of McGuire et al., this is caused by the magnetoristriction [3.2.1.5]. In U_6Fe, the second order Doppler shift, absorption area and quadrupole splitting have anomalies around 100 K. This was reported to be caused by the change of the phonon system around this temperature [3.2.1.6].

However, since single crystal samples were difficult to be obtained in those compounds, especially U_6Fe [3.2.1.3], the conversion electron Mössbauer spectroscopy (CEMS). The Mössbauer measurement under the applied magnetic field of those compounds has never been performed, either. Since UFe_2 has the magnetic ordering below 167 K, the sign of the electric field gradient and the anisotropy parameter are determined by the spectra in the ferromagnetic ordered state, but the different magnitude of the hyperfine magnetic field in the crystalographically same site are observed in the previous works. Since U_6Fe is a Pauli paramagnetic compound, those are determined with the conventional Mössbauer measurement using the powdered sample.

In this work, the conventional ^{57}Fe Mössbauer measurements of U-Fe intermetallic compounds and the ^{238}U Mössbauer spectroscopy of UFe_2 has been performed. Moreover, the conversion electron Mössbauer spectroscopy and the ^{57}Fe Mössbauer measurements in the applied field have also been performed.

References

[3.2.1.1] A. T. Aldred, J. Magn. Magn. Mater., **10**, 42 (1979).

[3.2.1.2] Yu. Popov, R. Z. Levitin, M. Zeleny and A. V. Andreev, Sov. Phys. JETP, **51**, 1223 (1980)

[3.2.1.3] E. Yamamoto, M. Hedo, Y. Inada, T. Ishida, Y. Haga and Y. Ōnuki, J. Phys. Soc. Jpn., **65**, 1034 (1996).

[3.2.1.4] J. Gal, A. Hadari, E. R. Bauminger, I. Nowik, S. Ofer and M. Perkel, Phys. Lett., **A31**, 511 (1970).

[3.2.1.5] T. K. McGuire and R. H. Herber, Solid State Commun., **48**, 393 (1983).

[3.2.1.6] S. Blow, J. Phys. Chem. Solids, **30**, 1549 (1969).

[3.2.1.7] C. W. Kimball, P. P. Vaishnava, A. E. Dwight, J. D. Jorgensen and F. Y. Fradin, Phys. Rev., **B32**, 4419 (1985).

[3.2.1.8] S. L. Ruby, G. M. Kalvius, B. D. Dunlap, G. K. Shenoy, D. Cohen, M. D. Bodsky and D. J. Lam, Phys. Rev., **184**, 374 (1969).

3. 2. 2. ^{57}Fe and ^{238}U Mössbauer Spectroscopy of UFe_2

3. 2. 2. 1. Introduction

The several Laves phases ($AnFe_2$), UFe_2, $NpFe_2$, $AmFe_2$ and $PuFe_2$, which contain actinide elements (An) and iron, are known. It was reported the Curie temperature of UFe_2 is between 150 K and 200 K [3.2.2.1-7]. Its crystal structure is C-15 type ($MgCu_2$) structure as shown in Fig. 3.2.2.1. On the other hand, the Curie temperature of the other actinide-iron Laves phase compounds are above room temperature. As for the Curie temperature of UFe_2, it was reported to depend exactly on the stoichiometry between U and Fe [3.2.2.6-7]. UFe_2 has a lower magnetic transition temperature and smaller magnetic moment at actinide ion site than the other actinide-iron Laves phase compounds. The magnetization of UFe_2 has smaller anisotropy than the other Laves phase compounds [3.2.2.5, 3.2.2.8-12]. The saturated magnetic moments at iron site are 0.6 μ_B, while the magnetic moment of the uranium site is almost zero [3.2.2.13]. As for the magnetic moment at uranium site of UFe_2, neutron scattering and magnetic Compton scattering studies was suggested that the spin and the orbital moment are coupled antiparallelly and the net magnetic moment was canceled out to zero [3.2.2.13-14].

The Laves phase compounds which contain iron and rare earth elements have the very high Curie temperatures above the room temperature [3.2.2.15-21]. They have the bigger magnetic moments at both iron and rare earth sites than in UFe_2. In these Laves phase compounds except for UFe_2, 4*f*- or 5*f*- electrons are thought to be comparably localized at rare earth or actinide sites [3.2.2.22]. The highly anisotropic magnetization of these compounds is thought to be caused by the localized 4*f*-electrons or nearly localized 5*f*-electrons. In UFe_2, its magnetic moments at uranium atoms are thought to be related to the character of 5*f*-electrons at uranium atoms. The distance between uranium atoms is 0.3056 nm and shorter than the Hill's limit of 0.35 nm [3.2.2.23]. This fact might suggest that the uranium atoms in UFe_2 have no magnetic moment.

In order to investigate the physical properties of UFe_2, the Mössbauer spectroscopy fortunately applies to both elements of ^{238}U and ^{57}Fe those are constituent elements of UFe_2. The Curie temperature of UFe_2 is reported to be between 150 K and

200 K and the ^{238}U Mössbauer gamma-ray energy of 44.91 keV is higher than that of ^{57}Fe Mossbauer gamma-ray energy, ^{238}U Mössbauer effect is difficult to observe in its paramagnetic state. The ^{238}U Mössbauer spectroscopy enables us to give the local electronic state at uranium atoms in the ferromagnetic state through the observed hyperfine magnetic field. Whereas, since the energy of the ^{57}Fe Mössbauer gamma-ray is 14.4 keV, the ^{57}Fe Mössbauer effect can be observed even in its paramagnetic state and gives the local electronic state in both of paramagnetic and ferromagnetic states. In this work, the ^{57}Fe and the ^{238}U Mössbauer measurements of UFe_2 has been performed in order to investigate the physical properties, mainly the magnetic properties.

3. 2. 2. 2. Experimental Procedure

Both of the ^{57}Fe and the ^{238}U Mössbauer measurements have been performed by means of the transmission geometry. The samples used in the transmission geometry are highly purified polycrystalline powders and the specimens for the conversion electron Mössbauer spectroscopy were bulk single crystals having a specific plane surfaces. Since UFe_2 is easy to be oxidized, the measured sample is the polycrystalline one whose ingot was powdered in argon gas atmosphere. The sample for the conversion electron Mössbauer spectroscopy was the single crystal cut perpendicular to the easy axis of the magnetization, <111>.

The ^{57}Fe Mössbauer measurement have been performed at the temperature range between 298 K and 4.2 K. The ^{238}U Mössbauer measurements have been performed at 200 K, 82 K and 5.2 K. The ^{57}Fe conversion electron Mössbauer measurements have been performed at room temperature. The Curie temperature was determined using a Mössbauer thermal scan method. The used sources are ^{57}Co in Rh for the the ^{57}Fe Mössbauer measurement and PuO_2 which contains 99.99 % ^{242}Pu for the ^{238}U Mössbauer measurement, respectively. The velocity calibration of the ^{57}Fe Mössbauer spectroscopy was referred to the α-Fe spectrum at room temperature. The Doppler velocity of the ^{238}U Mössbauer spectroscopy was calibrated by using a laser calibrator and its zero isomer shift value was adopted to the isomer shift value of ^{238}U in PuO_2.

3. 2. 2. 3. Results and Discussion

Figure 3.2.2.2 shows the ^{57}Fe Mössbauer spectra of UFe_2 at various temperatures. The spectra above 170 K are symmetric doublet, while those below 160 K are asymmetric. The spectra below 100 K seem to consist of the superposed four resonance lines. Since the Curie temperature is between 150 K and 200 K, the observed asymmetric patterns is thought to be related to the appearance of the hyperfine field due to the magnetic ordering.

The isomer shift value at room temperature is - 0.21 mm s^{-1}. The isomer shift values give us the density of *s*-electrons at probe nucleus. Since the nuclear radius of the excited state is smaller than that of the ground state, this result shows the density of electrons at ^{57}Fe nucleus is larger than metallic iron. In consideration for the neutrality of the charge at iron atoms, the larger density of *s*-electrons at ^{57}Fe nucleus is caused by the wide-spread wave function of 3*d*-electrons of iron atoms in UFe_2. Therefore, the results obtained suggest that the 3*d*-electrons of iron atoms are hybridized with 5*f*-electrons of uranium atoms.

As written above, spectra change from a symmetric doublet pattern to an asymmetric pattern between 160 K and 170 K, When the spectra change with an increase or a decrease of the temperature, the count rate is expected to change at a velocity range around the isomer shift value. In this case, since UFe_2 is a ferromagnetic compound, it is expected the magnetic pattern is observed below Curie temperature and that the paramagnetic pattern is observed above this temperature. The magnetic pattern is generally a wide-spread spectrum so that the relative absorption near the isomer shift value decreases with a decrease of the temperature. Therefore, the temperature at which the slope change of the count rate at a certain Doppler velocity versus temperature occurred is determined as the Curie temperature.

The temperature dependence of the count rate at 0 mm s^{-1} is shown as Fig. 3.2.2.3. In both the processes of temperature increasing and decreasing, the slope change of the count rate occurred at 167.50 K and 167.04 K, respectively. At this temperature, the presence of the anomaly due to the phase transition was observed in the electrical resistivity measurement. This temperature is fairly agreed to the reported Curie temperature of $UFe_{2.00}$ [3.2.2.6]. These results show the Curie temperature is 167 K.

Temperature dependence of the isomer shift and quadrupole splitting above the Curie temperature is shown in Fig. 3.2.2.4. The magnitude of the quadrupole splitting at room temperature is 0.45 mm s^{-1}. The quadrupole splitting does not almost change or slightly decreases above Curie temperature. On the other hand, the isomer shift increases above Curie temperature as temperature decreasing. This phenomenon corresponds to the temperature dependence caused by the second order Doppler shift.

Below the Curie temperature, the hyperfine magnetic field originated from the magnetic ordering of UFe_2 is observed. Generally, the ^{57}Fe Mössbauer spectrum with the hyperfine magnetic field is a sextet Lorentzian. The typical magnetic pattern such as α-FeOOH at 77 K is analyzed with the combined hyperfine magnetic and quadrupole pattern treated as the perturbation of the quarupole interaction to the hyperfine magnetic interaction. Since the saturated magnetic moment is 0.6 μ_B / Fe, the hyperfine magnetic field observed in the ferromagnetic ordered state is thought to be too small to treat the quadrupole interaction as the perturbation [3.2.2.13]. The spectra obtained below the Curie temperature were not analyzed with the usual least-square fitting using a sextet Lorentzian function in which the quadrupole splitting was treated as the perturbation to the magnetic splitting. In the spectrum-analysis below the Curie temperature, the comparison of the calculated spectra to the spectra obtained has been substituted for the conventional least-square fitting.

Figure 3.2.2.5 shows the arrangement of the iron atoms around a probe iron atom in UFe_2. The magnetization easy axis of UFe_2 is <111> and the principal axis of the electric field gradient expected from the atomic arrangements as shown in Fig. 3.2.2.5 is [111] directions. The angle between the magnetization easy axis and the principal axis of the electric field gradient is 0 or 109.47 degree. The site of ion atoms are called as Fe(1) and Fe(2), respectively, as shown in Fig. 3.2.2.5. The ratio of Fe(1) to Fe(2) is 1 : 3. Figure 3.2.2.6 shows the obtained Mössbauer spectra and the calculated spectra with the above consideration. The calculated spectra are compared with the experimental results. The ^{57}Fe Mössbauer parameters obtained at 4.2 K are shown in Table 1. The hyperfine magnetic field at Fe(1) and Fe(2) are 3.1 T and 4.1 T, respectively, although those locate at the same site crystallographycally. These results agreed well to the results obtained from the previous works [3.2.2.24-25].

Temperature dependence of the averaged hyperfine field in UFe_2 is shown in

Fig. 3.2.2.7. It is similar to that of its magnetization [3.2.2.6]. The hyperfine coupling constants are 5.3 T / μ_B at Fe(1) and 6.9 T / μ_B at Fe(2). These values are smaller than the coupling constant of α-Fe, 15.5 T / μ_B. In the case of ^{57}Fe Mössbauer spectroscopy, the origin of the hyperfine field is caused mainly by Fermi contact interaction represented by

$$H_{FC} = \frac{8}{3}\pi\mu_B g \sum_n \left[\rho_{ns}^{\uparrow}(0) - \rho_{ns}^{\downarrow}(0)\right]. \qquad (3.2.2.1)$$

The small hyperfine coupling constant was obtained and its reason might be due to the hybridization of the 3*d* electrons of iron atoms with the 5*f* electrons of uranium.

Temperature dependence of the resonant absorption area is shown in Fig. 3.2.2.8. As shown in Eq. (2.1.18) of previous section, the resonance absorption area is represented by

$$A = \int_{-\infty}^{+\infty}\{N_0 - p(v)\}dv = A' f_S \times f_A, \qquad (3.2.2.2)$$

where N_0 is background, and f_S and f_A are the recoil-free fractions of the source and absorber. Since the temperature of the source used in this work is room temperature, the recoil-free fraction of source is constant. The resonant absorption strength is, thus, proportionate to the recoil-free fraction of UFe_2. Generally, the recoil-free fraction increases continuously as a decrease of the temperature. The temperature dependence of f in UFe_2 has an anomaly near the Curie temperature. This phenomenon was reported already in the previous works [3.2.2.24]. Since the Mössbauer effect is the nuclear gamma-ray resonance without the excitation of phonon, the anomaly of the recoil-free fraction which corresponds to the probability of the Mössbauer effect indicates the change of the lattice system. This anomaly was reported to be caused by the magnetostriction [3.2.2.24] or the change of the phonon spectrum [3.2.2.13]. Temperature dependence of the resonant absorption area below the Curie temperature was fitted by the theoretical curve obtained by using the Debye model in which Debye temperature of UFe_2 was 300 K. Resonant absorption area above Curie temperature was fitted by a theoretical curve obtained by using the Debye model in which the Debye temperature was 250 K. The difference of the Debye temperatures between the ferromagnetic and the paramagnetic states might be due to the elastic constant enhancement which appeared below Curie temperature. These results show the elastic

constant enhancement caused by the magnetoristriction, as reported by McGuire et al [3.2.2.13].

On the other hand, the enhancement of the absorption area just at the Curie temperature cannot be explained with the only difference of the Debye temperature. If the only Debye temperature changes at Curie temperature, the estimated values at 0 K of the theoretical curves are nearly equal because of the Debye temperature of 250 K and 300 K in the paramagnetic and ferromagnetic states, respectively. However, the estimated values at 0 K are very different between theoretical curves with which the temperature dependence of the absorption areas in the paramagnetic and ferromagnetic states, as shown in Fig. 3.2.2.8. This result suggests the phonon spectrum changes at Curie temperature. It corresponds to the results from neutron scattering experiments [3.2.2.13]. Therefore, these results show the enhancement by the magnetoristriction as well as the change of the phonon spectra.

In this work, the ^{238}U Mössbauer spectroscopy has also been performed for UFe_2. Figure 3.2.2.9 shows ^{238}U Mössbauer spectra of UFe_2 at 82 K and 5.5 K. The observation of the ^{238}U Mössbauer effect has been tried at 200 K, above the Curie temperature of 167 K. However, since its recoil-free fraction at this temperature is very small, its spectrum at 200 K could not be obtained. The ^{238}U Mössbauer spectrum has been successfully observed at room temperature for UO_2 whose Debye temperature is 187 K. Therefore, the Debye temperature of UFe_2 might be lower than 187 K. The magnitude of the full width at half maximum (FWHM) at 82 K and 5.5 K were 31.8 $\pm$ 3.4 mm s^{-1} and 43.8 $\pm$ 2.5 mm s^{-1}, respectively. The results obtained at 5.5 K agreed with the previous works by Ruby et al. within the experimental error [3.2.2.25]. The value of the FWHM at 82 K was nearly equal to the natural line-width of ^{238}U Mössbauer transition, 27 mm s^{-1}.

Paolasini et al. proposed that UFe_2 has a magnetic moment at uranium atoms, but that it is extremely small, comparable to the other actinide-iron Laves phase compounds, because spin and orbital moments canceled out with each other [3.2.2.13]. Lawson et al. also suggested with their magnetic Compton scattering experiment that, since the spin and orbital moments were coupled antiparallel, the net magnetic moments of uranium atoms in UFe_2 have a tenth of Bohr magneton [3.2.2.14]. Ruby et al.

reported the ^{238}U Mössbauer spectrum of UFe_2 at 4.2 K and analyzed the spectrum in consideration for the existence of the hyperfine magnetic field. The magnitude of its magnetic splitting at this temperature was 16 $\pm$ 12 mm s^{-1} [3.2.2.25]. This value was equal to 70 $\pm$ 20 T, using g_{ex} = 0.254. However, the FWHM at 82 K under the ferromagnetic ordering state was nearly equal to the natural line-width, 31.8 $\pm$ 3.4 mm s^{-1}. The hyperfine magnetic field at ^{57}Fe nucleus in UFe_2 has been observed from the ^{57}Fe Mössbauer study of UFe_2 as shown in Fig. 3.2.2.2. The hyperfine field of UFe_2 was almost saturated in the range of these temperatures. These results suggest that the hyperfine magnetic field at ^{238}U is saturated at 82 K and 5.5 K if the hyperfine magnetic field exists.

The FWHM at 5.5 K was larger than that at 82 K. The temperature dependence of FWHM can be discussed, using the temperature dependence of the recoil-free fraction, whether the hyperfine magnetic field exists or not. Generally speaking, the contribution of spin and orbital moments to the hyperfine magnetic field is different. Therefore, if uranium atoms have the magnetic moments and its spin and orbital moments were coupled antiparallelly, the hyperfine magnetic field is expected to be observed at ^{238}U nucleus. Since the FWHM at 82 K was equal to the natural line width of the ^{238}U Mössbauer effect, the result at 82 K shows that no hyperfine magnetic field exist at uranium nucleus. These results indicate that the magnetic moment of uranium atoms in UFe_2 was not canceled out, but that the uranium atoms in UFe_2 have no magnetic moment even in the ferrromagnetic ordered state.

In the ^{57}Fe Mössbauer measurement, the Mössbauer effect of the sample in the longitudinally applied magnetic field was also investigated. Figure. 3.2.2.10 shows the ^{57}Fe Mössbauer spectra at 4.5 K under the applied field up to 7 T. The obtained spectra up to 4 T were narrower as an increase of the magnitude of the applied field. The spectra obtained under the applied field above 4 T were broadened as an increase of the magnitude of the applied field. Generally, the sign of the hyperfine magnetic field due to the magnetic ordering of the probe atoms themselves is minus because of the dominant contribution of the core-polarization. On the contrary, the sign of the hyperfine magnetic field due to the applied field is plus from the definition of the field direction. These results indicate that the sign of the hyperfine magnetic field obtained in 0 T is minus. Therefore, the observed hyperfine magnetic field at ^{57}Fe nucleus is

mainly caused by the magnetic ordering of iron atoms, and not by transferred hyperfine field from the uranium atoms.

Finally, the result of the conversion electron Mossbauer spectroscopy (CEMS) of UFe_2 is shown in Fig. 3.2.2.11. In CEMS, the spectra are obtained by counting the conversion electron during the de-excitation of the Mössbauer resonance. According to the results from the transmission Mössbauer spectra as shown in Fig. 3.2.2.2, the principal axes of the electric field gradient at ^{57}Fe nucleus are in the direction of [111]. The CEMS of UFe_2 has been performed with the single crystal sample which is cut perpendicularly to the <111> direction.

The obtained spectrum seems to be a symmetric doublet. The Mössbauer spectrum of the single crystal is generally expected to be observed as an asymmetric pattern whose intensity-ratio is 1:3 when the principal axis and incident Mössbauer gamma-ray are parallel. In UFe_2, the analyses of the spectra below Curie temperature revealed that the sign of the electric field gradient was minus. In addition, the angles between the incident Mössbauer gamma-ray and the principal axis of the electric field gradient are parallel in Fe(1) site and magic angle in Fe(2) site, respectively. The components of Fe(2) are expected to show the symmetric doublet as shown in Fig. 3.2.2.2 of the spectrum of the powdered UFe_2 at room temperature. The only component of Fe(1) is expected to show the asymmetric doublet when the incident Mössbauer gamma-ray is parallel to the principal axis. The expected intensity-ratio is thus 9:7 as velocity increases. However, the obtained spectrum is symmetric so that the existence of the other component was considered in the spectrum-analysis.

U-Fe intermetallic compounds are easy to be oxidized. Generally speaking, CEMS is sensitive to the surface of the samples because the maximum struggling range of the conversion electron is about 100 nm. In uranium compounds, this range should be shorter than 100 nm because the atomic number of the uranium atom is quite large. Accordingly, the obtained spectrum was analyzed with two components; one is the component of pure UFe_2, and the other is thought to be that of oxidized UFe_2 whose isomer shift value is near 0 mm s^{-1} that has a broad FWHM. When the component of oxidized one was taken into account of, the other components of CEMS correspond to that of the transmission spectra in the ferromagnetic state in the view-point of the sign of the quadrupole splitting.

3. 2. 2. 4. Conclusion

The isomer shift value at room temperature, - 0.21 mm s^{-1} indicates that the 3*d*-electrons of the ion atoms and 5*f*-electrons of the uranium atoms are hybridized very well with each other. The results from the Mössbauer thermal scan method by using the ^{57}Fe Mössbauer effect shows that the Curie temperature is 167 K. The spectra blow the Curie temperature consists of two components. The magnitudes of the hyperfine magnetic field are 3.1 T at Fe(1) and 4.1 T at Fe(2), respectively. The obtained hyperfine coupling constants are 5.3 T / μ_B at Fe(1) and 6.9 T / μ_B at Fe(2), and smaller than that of α-Fe, 15 T / μ_B. These values also indicate that the 3*d*-electrons and 5*f*-electrons are hybridized. The results from the ^{238}U Mössbauer measurement indicate that the uranium atoms in UFe_2 have no magnetic moments because no hyperfine magnetic field exists at the ^{238}U nucleus.

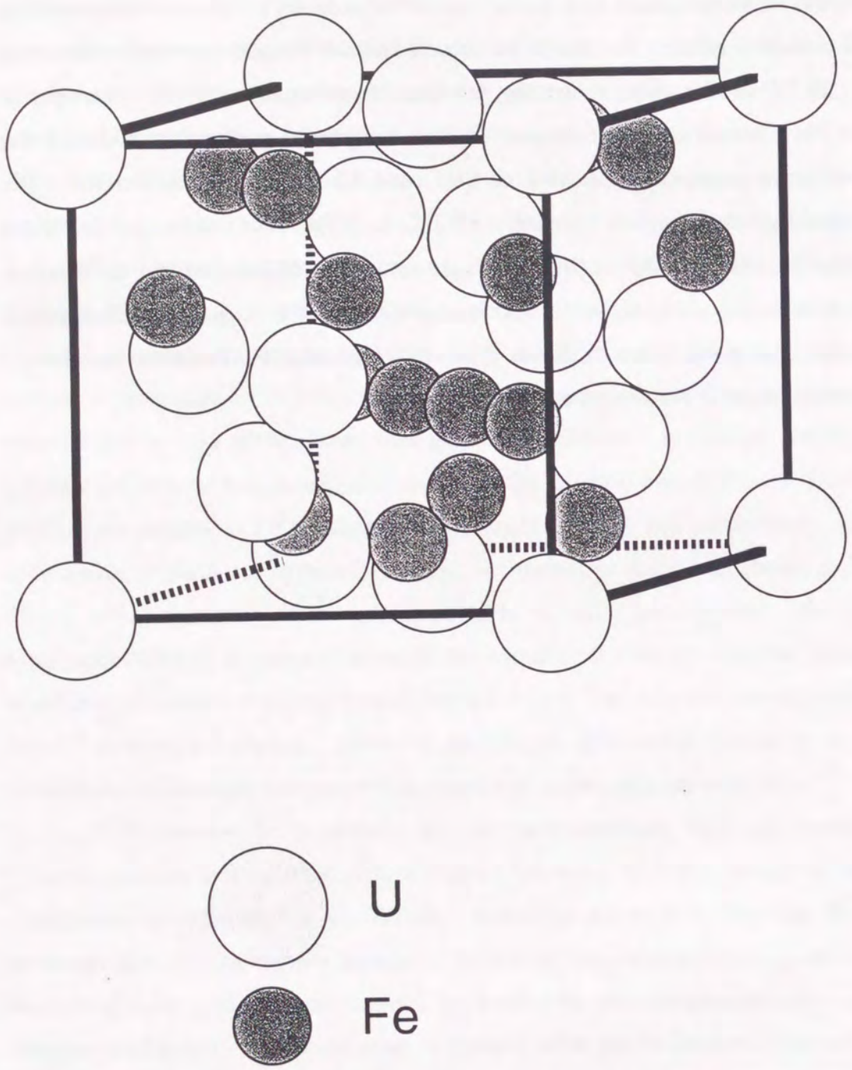

Fig. 3.2.2.1. Crystal structure of UFe_2.

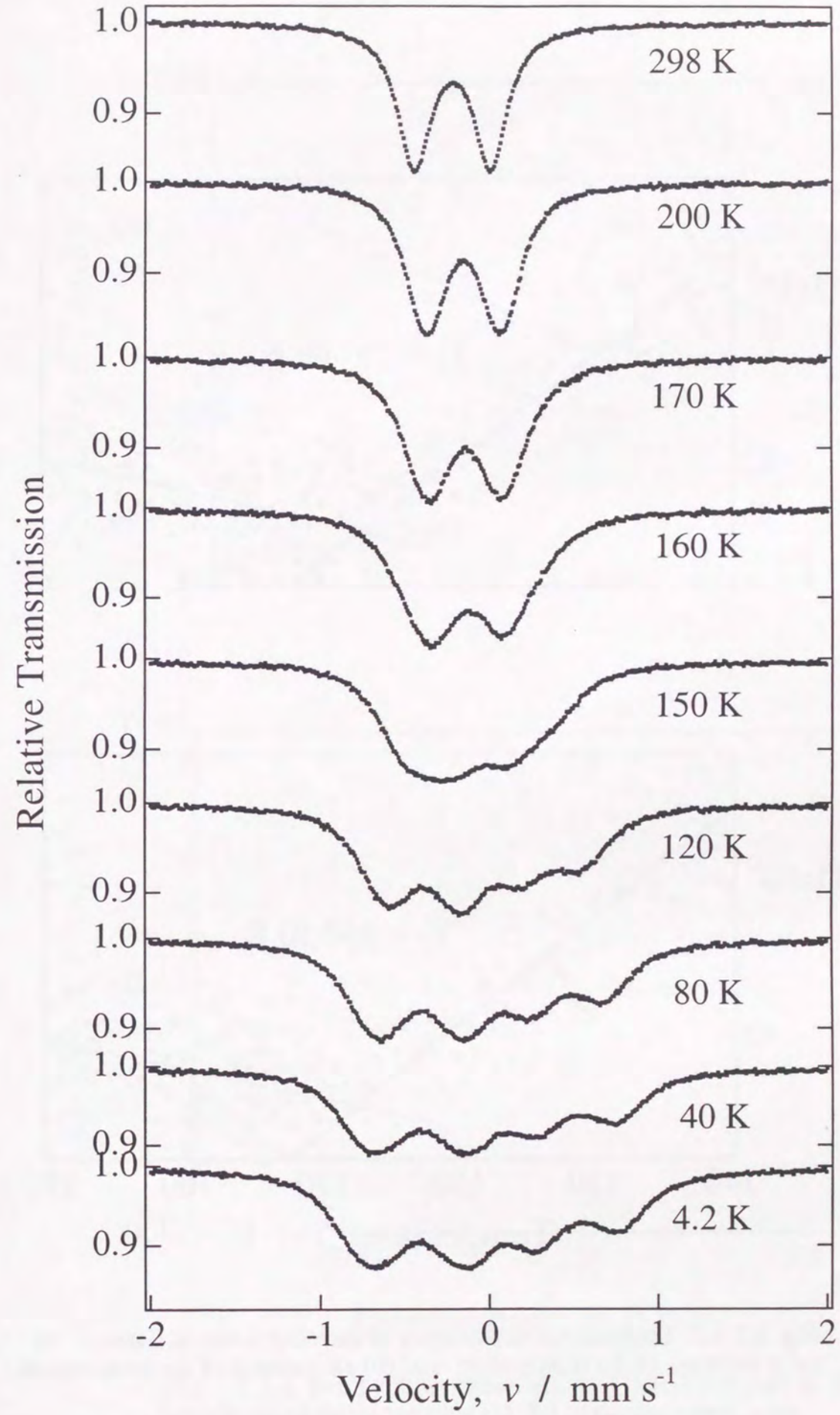

Fig. 3.2.2.2. ^{57}Fe Mössbauer spectra of UFe_2 at various temperatures.

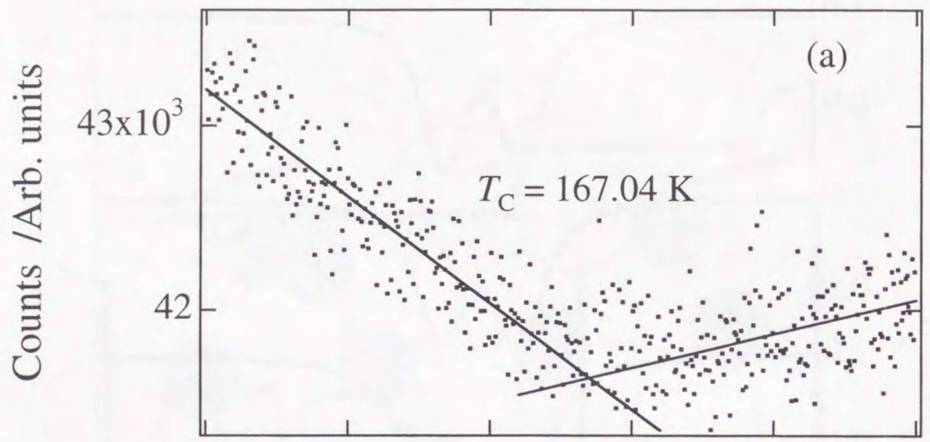

Fig. 3.2.2.3. Temperature dependence of the counts rate at 0 mm s^{-1} as (a) a decrease of the temperature and (b) an increase of the temperature .

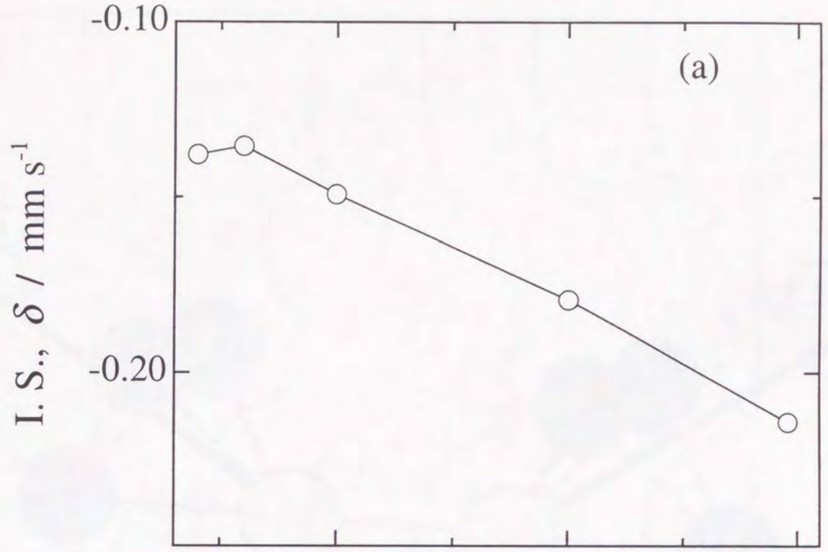

Fig. 3.2.2.4. Temperature dependence of (a) isomer shift (I. S.) and (b) quadrupole splitting (Q. S.) in paramagnetic state.

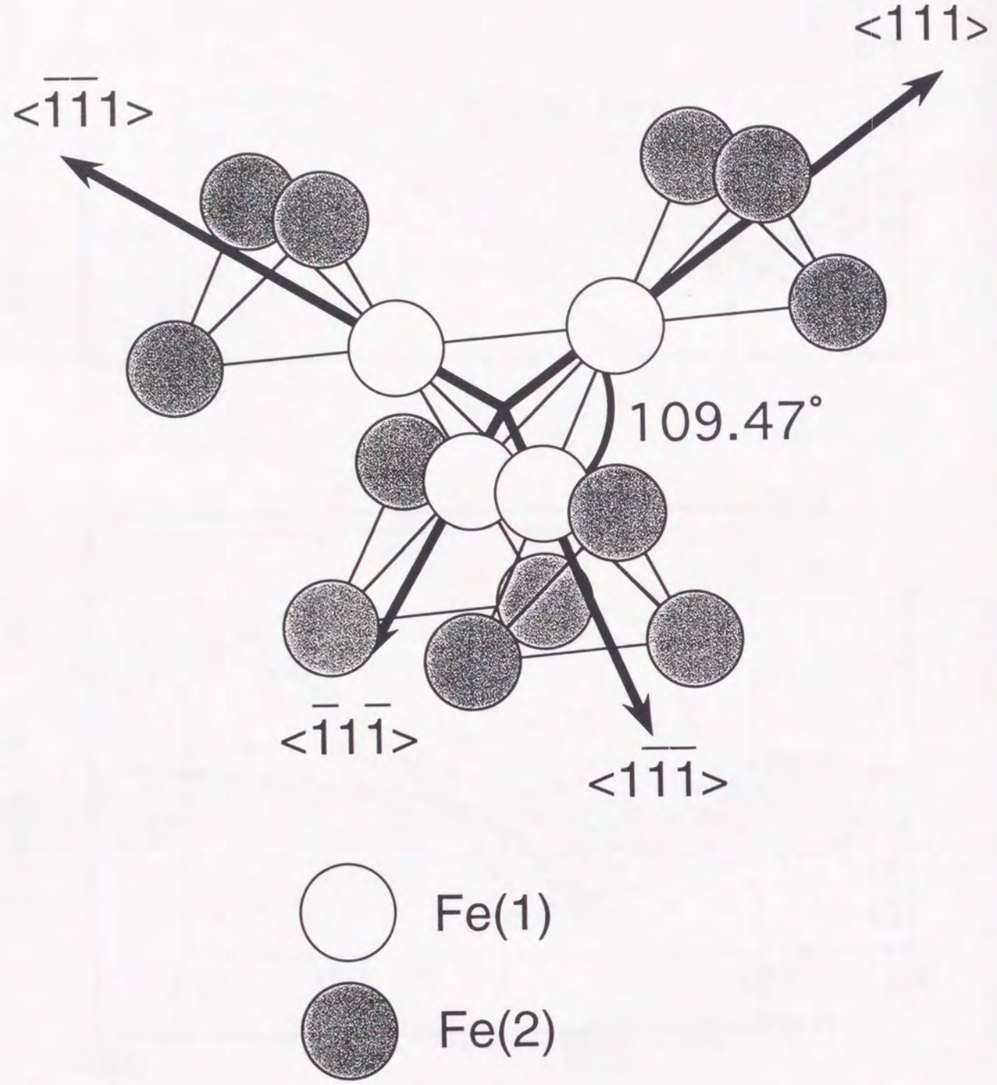

Fig. 3.2.2.5. The atomic arrangement of iron sites in UFe_2.

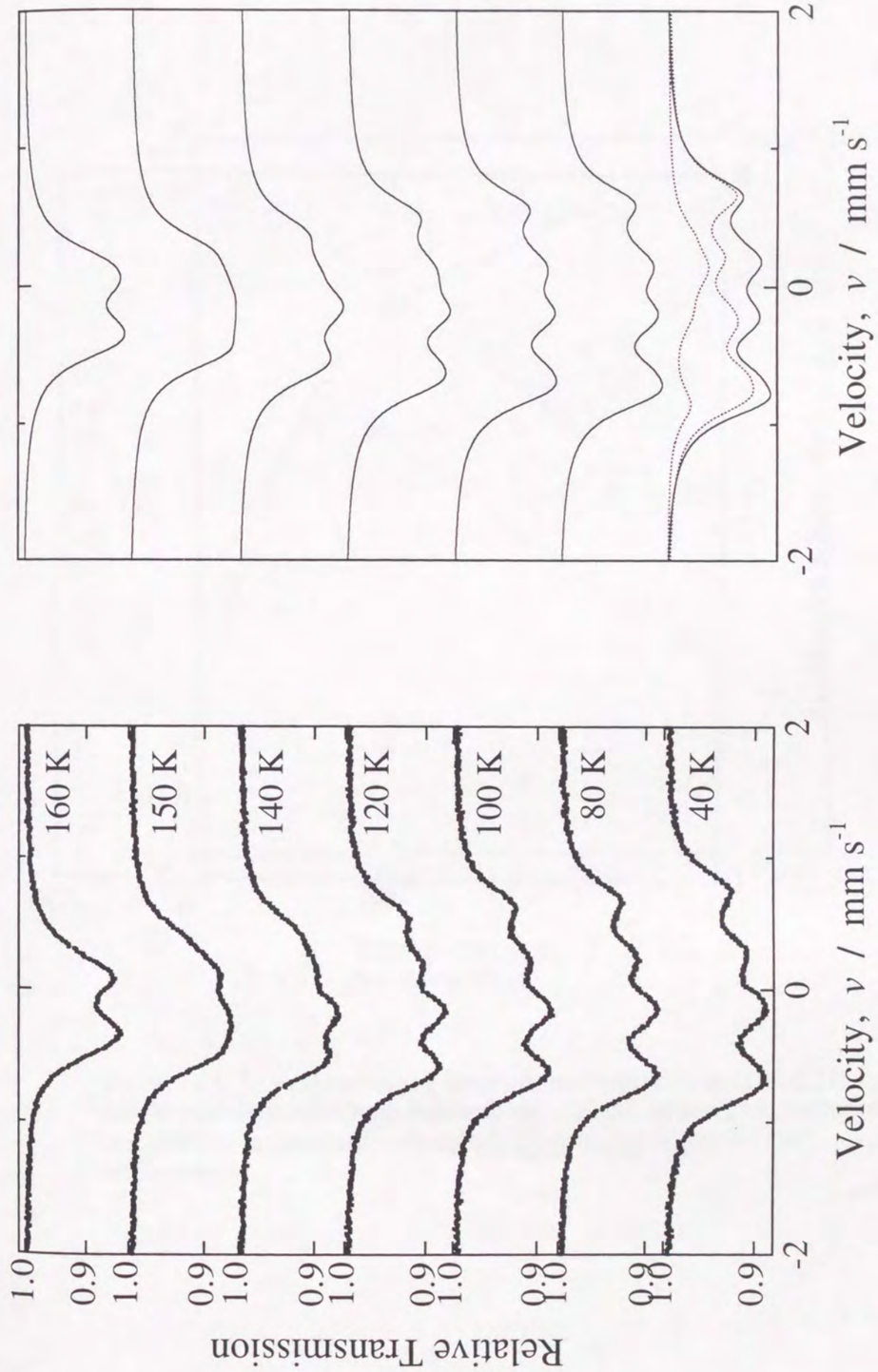

Fig. 3.2.2.6. The obtained and calculated spectra of UFe_2 below Curie temperature.

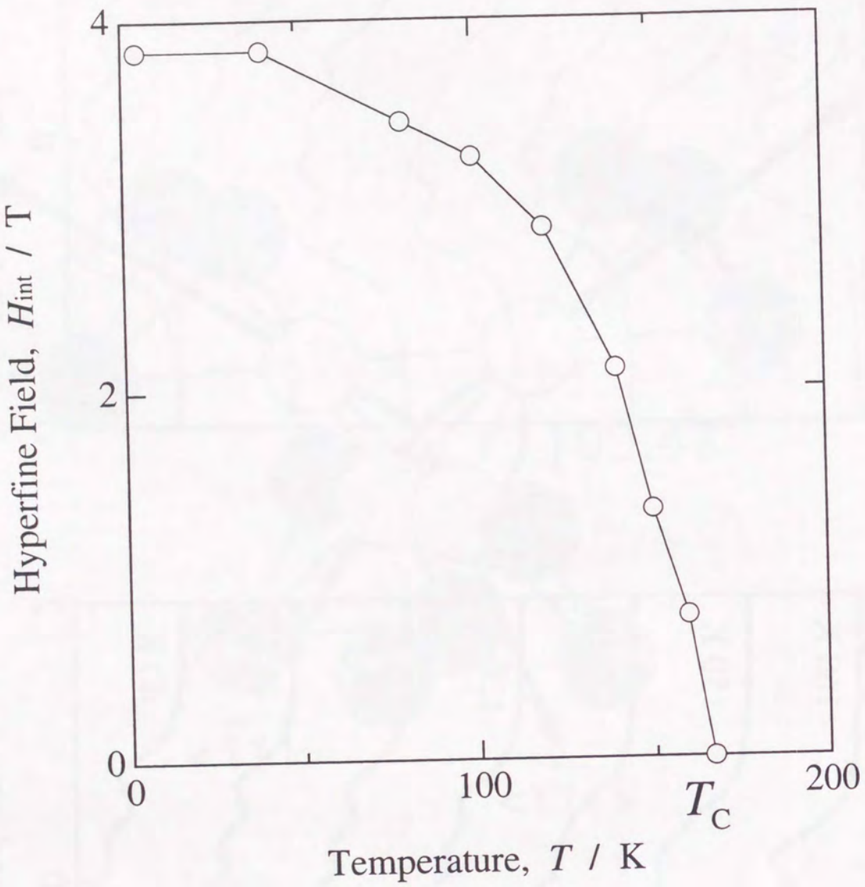

Fig. 3.2.2.7. Temperature dependence of the averaged hyperfine magnetic field at ^{57}Fe nucleus in UFe_2.

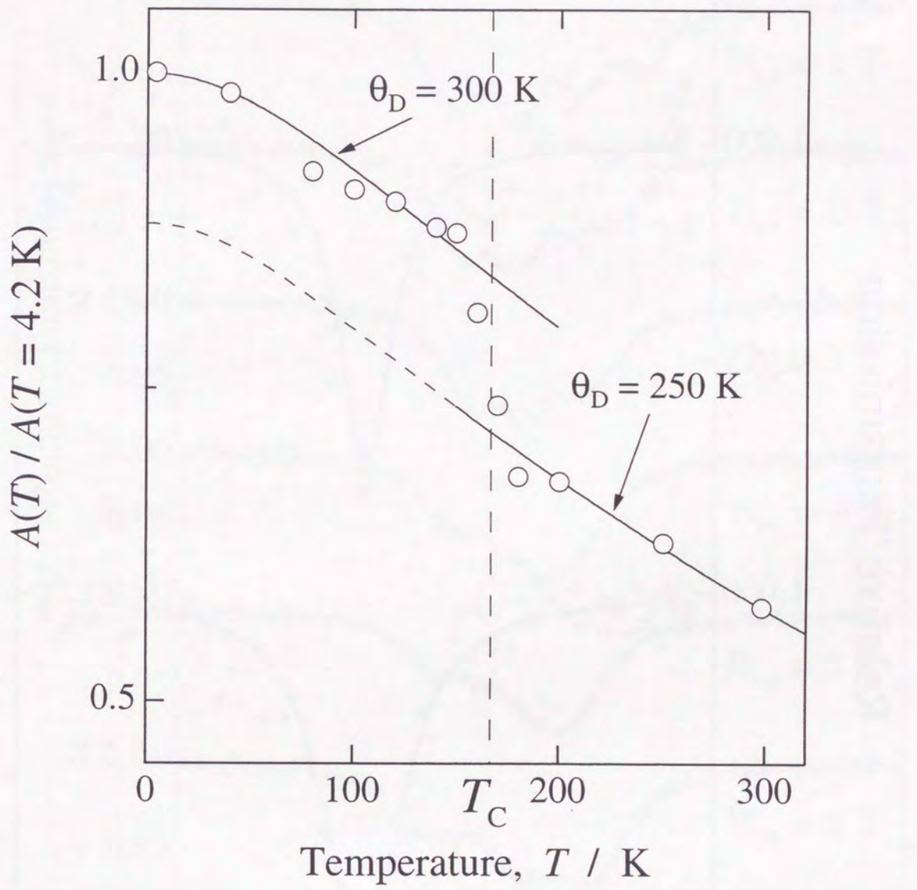

Fig. 3.2.2.8. Temperatre dependence of the absorption area. Solid lines are the theoretical curves using the Debye model whose Debye temperatures are 250 K at paramagnetic state and 300 K at ferromagnetic state, respectively.

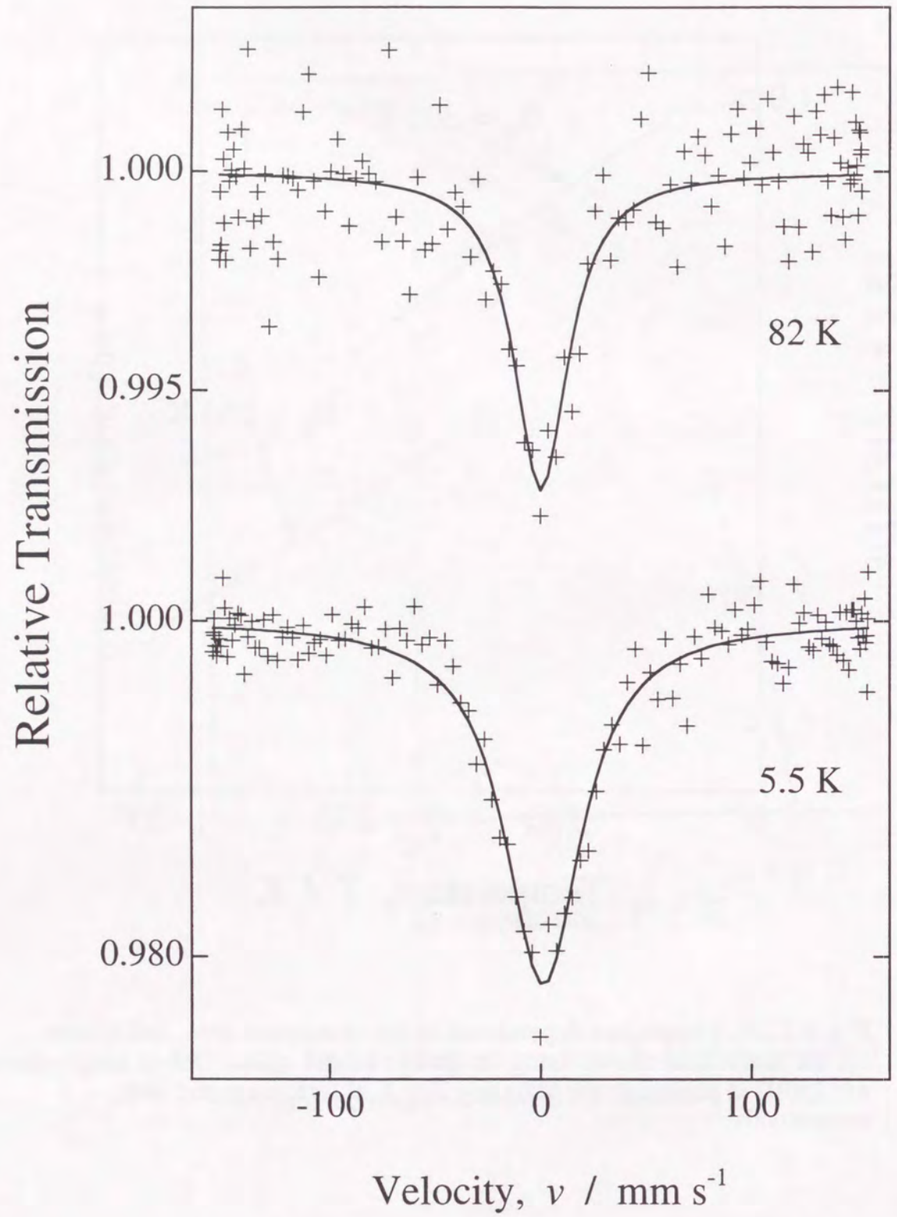

Fig. 3.2.2.9. ^{238}U Mössbauer spectra of UFe_2 at 82 K and 5.5 K.

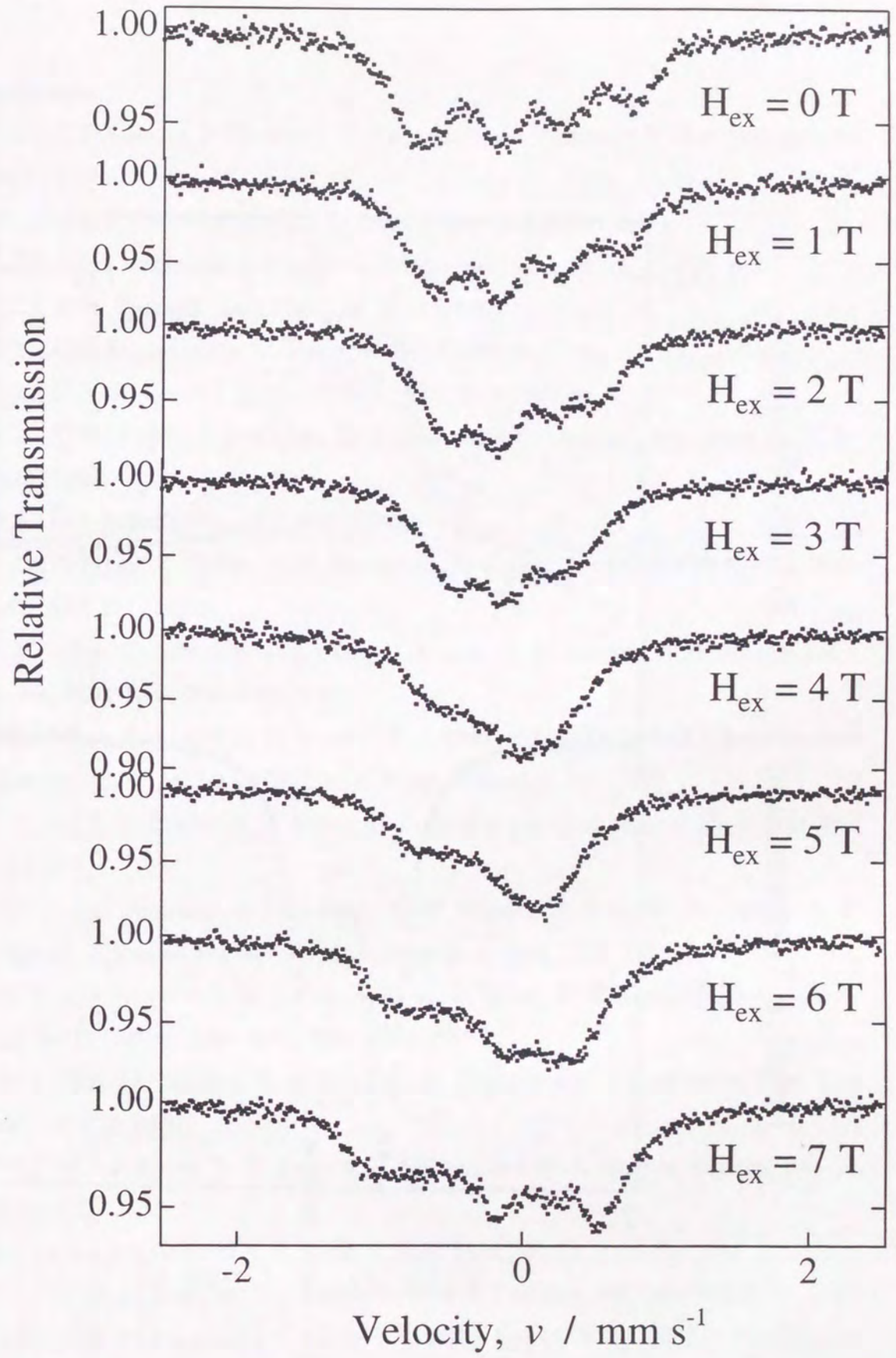

Fig. 3.2.2.10. ^{57}Fe Mössbauer spectra of UFe_2 at 4.5 K under the longitudinally applied field up to 7 T.

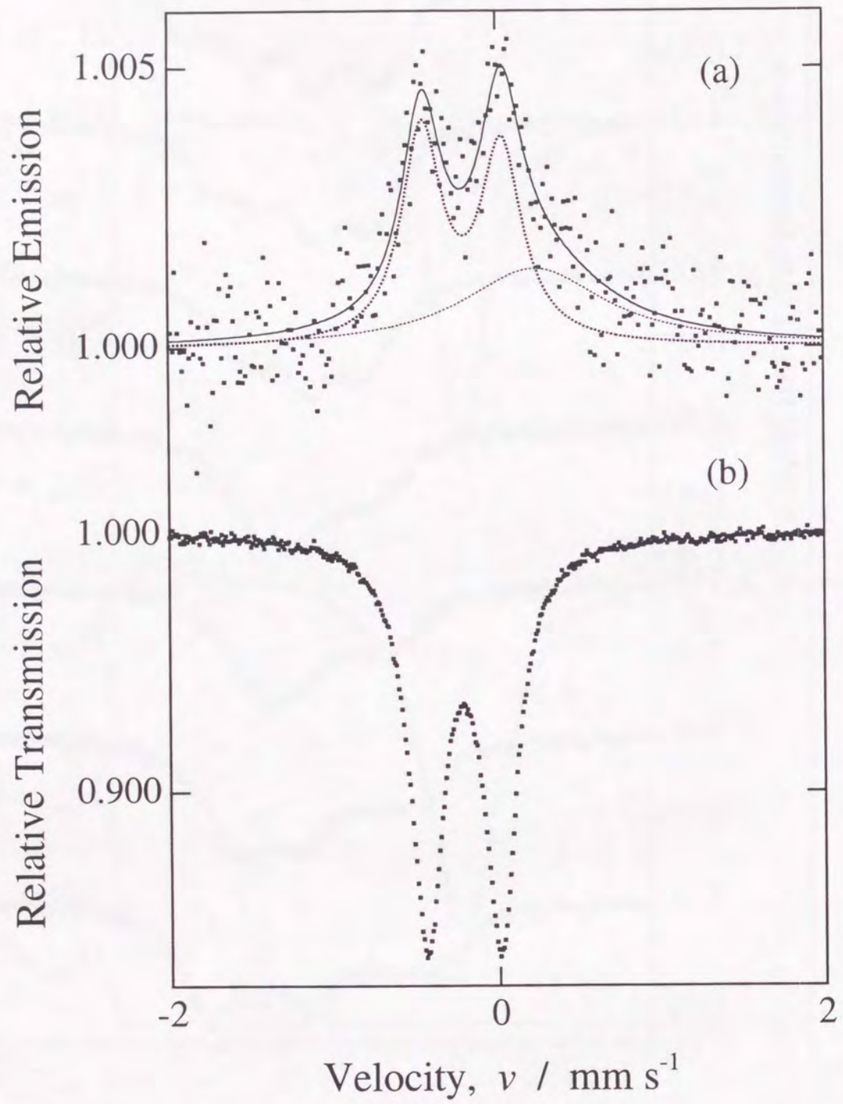

Fig. 3.3.2.11. (a) ^{57}Fe conversion electron Mössbauer spectrum of UFe_2 at room temperature.
(b) ^{57}Fe transmission Mössbauer spectrum of UFe_2 at room temperature.

References

[3.2.2.1] S. Komura, N. Kunitomi, Y. Hamaguchi and Sakamoto, J. Phys. Soc. Jpn., **16**, 1486 (1961).

[3.2.2.2] S. T. Lin and R. E. Ogilvie, J. Appl. Phys., **34**, 1372 (1963).

[3.2.2.3] S. Komura and N. Shikazono, J. Phys. Soc. Jpn., **18**, 323 (1963).

[3.2.2.4] M. Yessik, J. Appl. Phys., **40**, 1133 (1969).

[3.2.2.5] D. J. Lam and A. T. Aldred, A. I. P. Conference Proc., **24**, 349 (1974).

[3.2.2.6] A. T. Aldred, J. Magn. Magn. Mater., **10**, 42 (1979).

[3.2.2.7] Yu. Popov, R. Z. Levitin, M. Zeleny and A. V. Andreev, Sov. Phys. JETP, **51**, 1223 (1980).

[3.2.2.8] S. Blow, J. Phys., **C3**, 835 (1970).

[3.2.2.9] J. Gal, Z. Hadari, E. R. Bauminger, I. Nowik, S. Ofer and M. Perkel, Phys. Lett., **A31**, 511 (1970).

[3.2.2.10] A. T. Aldred, B. D. Dunlap, D. J. Lam, G. H. Lander, M. H. Mueller and I. Nowik, Phys. Rev., **B11**, 530 (1975).

[3.2.2.11] A. T. Aldred, B. D. Dunlap, D. J. Lam, and G. K. Shenoy, *Transplutonium Elements*, ed. W. Müller and R. Linder, North-Holland, p. 191, 1976.

[3.2.2.12] G. H. Lander, A. T. Aldred, B. D. Dunlap and G. K. Shenoy, Physica, **86-88B**, 152 (1977).

[3.2.2.13] L. Paolasini, G. H. Lander, S. M. Shapiro, R. Caciuffo, B. Lebech, L.-P. Regnault, B. Roessli and J-M. Fournier, Phys. Rev., **B54**, 7222 (1996).

[3.2.2.14] P. K. Lawson, M. J. Cooper, M. A. G. Dixon, D. N. Timms, E. Zukowski, F. Itoh and H. Sakurai, Phys. Rev., **B56**, 3239 (1997).

[3.2.2.15] R. M. Nicklow, N. C. Koon, C. M. Williams and J. B. Milstein, Phys. Rev. Lett., **36**, 532 (1976).

[3.2.2.16] J. J. Rhyne, N. C. Koon, J. B. Milstein and H. A. Alperin, Physica, **B86-88**, 149 (1977).

[3.2.2.17] J. J. Rhyne and N. C. Koon, J. Appl. Phys., **49**, 2133 (1978).

[3.2.2.18] N. C. Koon, and J. J. Rhyne, Solid State Commun., **26**, 540 (1978).

[3.2.2.19] N. C. Koon and J. J. Rhyne, *Crystalline Electric Field and Structural Effects in f-Electron Systems*, ed. J. E. Crow, R. P. Guertin and T. W. Mihalisin, Plenum, p125, 1980.

[3.2.2.20] K. Clausen, J. J. Rhyne, B. Lebech and N. C. Koon, J. Phys., **C15**, 3587 (1987).

[3.2.2.21] J. Rhyne, J. Magn. Magn. Mater., **70**, 88 (1987).

[3.2.2.22] A. E. Clark, *Ferromagnetic Materials*, ed. E. P. Wohlfarth, North-Holland, vol. 1, p397, 1980.

[3.2.2.23] H. H. Hill, Nucl. Metall., **17**, 2 (1970).

[3.2.2.24] J. Gal, Z. Hadari, E. R. Bauminger, I. Nowik, S. Offer and M. Perkal, Phys. Lett., **31A**, 511 (1970).

[3.2.2.25] T. K. McGuire and R. H. Herber, Solid State Commun., **48**, 393 (1983).

[3.2.2.26] S. L. Ruby, G. M. Kalvius, B. D. Dunlap, G. K. Shenoy, D. Cohen, M. D. Bodsky and D. J. Lam, Phys. Rev., **184**, 374 (1969).

3. 2. 3. ^{57}Fe Mössbauer Spectroscopy of U_6Fe

3. 2. 3. 1. Introduction

U_6X (X = Mn, Fe, Co and Ni) compounds are superconductors. Their transition temperatures, T_C, are in the range from 3.8 K in U_6Fe to 0.5 K in U_6Ni. The X dependence of T_C is similar to that of Slater-Pauling curve for saturation magnetization of the 3*d*-metal alloys [3.2.3.1]. However, every U_6X compounds does not have the magnetic moment but are Pauli-paramagnetic. U_6Fe has higher upper critical field, H_{C2}, than the other uranium-based superconductor whose superconductivity and magnetic properties are anisotropic [3.2.3.2]. It is 13.1 T along the [001] direction and 10.4 T along [110]. The electronic specific heat coefficient is 150 mJ / K^2. This result indicates the 5*f*-electrons of uranium atoms are well hybridized with the 3*d*-electrons of iron atoms. The crystal structure of U_6Fe is shown in Fig. 3.2.3.1. The arrangement of uranium atoms is a layered-like structure, whereas that of iron atoms is a dimmer-like structure.

The ^{57}Fe Mössbauer studies of U_6Fe were performed previously by Blow [3.2.3.3] and Kimball et al.[3.2.3.4]. In the previous experiments, the spectra obtained were doublet pattern with quadrupole splitting above 4.3 K which is observed in the paramagnetic state. However, the sign of the electric field gradient have not been determined yet. In this work, the ^{57}Fe Mössbauer spectroscopy under the applied field up to 7 T has been performed in order to determine the sign of the electric field gradient of the spectra. The conversion electron Mössbauer spectroscopy (CEMS) of U_6Fe has also been performed by using a single crystal.

3.2.3.2. Experimental Procedure

The sample is a single crystal grown by the Czochralski pulling method [3.2.3.2]. It was powdered in argon gas atmosphere and sealed into the polyethylene-covered sample holder for the transmission measurement. Since the mass absorption coefficient of uranium atoms is large and the natural abundance of ^{57}Fe is only 2 %, the sample used is enriched by ^{57}Fe up to 50 %. The measurement under the longitudinally applied field has been performed by using a cryostat with a superconducting magnet as shown in Fig. 2.3.3. The CEMS has been performed at

room temperature, using a single crystal sample.

The gamma-ray source used is ^{57}Co in Rh. The Doppler velocity calibration is referred to α-Fe spectrum at room temperature.

3. 2. 3. 3. Results and Discussion

Figure 3.2.3.2 shows the ^{57}Fe Mössbauer spectra at various temperatures. All the spectra obtained are symmetric doublets. The isomer shift value and the magnitude of the quadrupole splitting at room temperature are - 0.36 mm s^{-1} and 0.76 mm s^{-1}, respectively. These results agree with the previous results within the experimental error [3.2.3.3-4]. The isomer shift value obtained shows hybridization between 5*f*-electrons of uranium atoms and 3*d*-electrons of iron atoms.

The magnitude of the quadrupole splitting is bigger than that of UFe_2 which is the same as the intermetallics in the U-Fe system. In crystal structure of U_6Fe as shown in Fig. 3.2.3.1, the atomic arrangement around iron site is not a cubic symmetry. Since the strong hybridization between 5*f*- and 3*d*-electrons are well-known in this compound from the specific heat measurements, the 3*d*-electrons are thought to be occupied with the conduction bands of this intermetallic compound [3.2.3.5-7]. The origin of the electric field gradient is thought to be based on its crystal structure. However, the isomer shift value suggests the iron atoms are not *S*-state ion like an high spin state of Fe^{3+}, so that the electric field gradient can result from the 3*d*-electrons themselves at iron sites. The isomer shift value of - 0.36 mm s^{-1} at room temperature is also suggested that the 3*d*-electrons of iron atoms in U_6Fe are well hybridized with the 5*f*-electrons of the uranium atoms like UFe_2. Therefore, the electric field gradient is caused by the 3*d*-orbital which has the existence probability near the Fermi surface..

The electric field gradient based on the orbital of the probe atoms themselves is proportionate to the expectation values of r^{-3}, $\langle r^{-3} \rangle$. In a consideration for the hybridization between 5*f*- and 3*d*-electrons, the orbital of the 3*d*-electrons is thought to be wide-spread. The value of $\langle r^{-3} \rangle$ is thus thought to be smaller in this case than in the other case such as the alloys of iron and another element. These results show the larger quadrupole splitting was based on the specified configuration of 3*d*-electrons. In order to determine the configuration of 3*d* orbital, both of the sign of the quadrupole

splitting and the anisotropy parameter, η, which is defined as $\eta = (V_{xx} - V_{yy})/V_{zz}$ are necessary. Determination of the configuration is discussed below.

The temperature dependence of the Mössbauer parameters is discussed. Figure 3.2.3.3 shows the temperature dependence of the isomer shift, quadrupole splitting and the full-width at half maximum (FWHM). Temperature dependence of the isomer shift increases with a decrease of the temperature. It tends to be saturated at lower temperature and changes continuously. These results can be intersted by the temperature dependence of the second order Doppler shift.

Kimball et al. reported that the temperature dependence of the second order Doppler shift obeys the Debye model where the Debye temperature of U_6Fe is 451 K above 100 K. They insisted a deviation from Debye model below 100 K indicated either a softening in the iron vibrational modes, or a decrease in *s* character in the conduction electron concentration due to the increased occupation of *d* state in iron. The results obtained in this work did not have the anomaly around 100 K.

Moreover, temperature dependence of the absorption area has been obtained, which can be discussed with the Debye model. Figure 3.2.3.4 shows the temperature dependence of the absorption area of the ^{57}Fe Mössbauer spectra obtained from U_6Fe. Temperature dependence of the absorption area was fitted by a theoretical curve where the Debye temperature is 300 K. In this work, no anomalies can be observed.

The magnitudes of quadrupole splitting increases slightly as a decrease of the temperature. Temperature dependence of FWHM has a broad peak around 150 K. Kimball et al. reported the obtained spectra of U_6Fe are asymmetric doublet patterns with the line at higher energy having larger intensity [3.2.3.4]. The spectra obtained in this work are symmetric doublet patterns. As written below, the difference of the intensities between higher and lower energy is thought to be caused by the impurity component because U-Fe intermetallic compounds are easy to be oxidized. Temperature dependence of the quadrupole splitting does not seem to have any anomalies in this work as Kimball et al reported.

In order to determine the 3*d*-electrons from which the electric field gradient results in U_6Fe, the ^{57}Fe Mössbauer spectroscopy under the applied field up to 7 T has been performed at 4.5 K. The Mössbauer spectroscopy has been performed under the

transmission geometry. The applied magnetic field is parallel to the Mössbauer gamma-ray, using a cryostat with superconducting magnet as shown in Fig. 2.3.3.

Figure 3.2.3.5 shows the ^{57}Fe Mössbauer spectra obtained from U_6Fe under the applied magnetic field. The magnitude of the hyperfine field is equal to the applied magnetic field for all of the spectra obtained. These results indicate no induced magnetic field exists at ^{57}Fe nuclei and U_6Fe is a Pauli-paramagnetic substance. The obtained sign of the quadrupole splitting is determined to be minus and the asymetry parameter is $\eta = 0$. Table 2.2.1 shows the relationships between the 3*d* orbital and the sign of the electric field gradient and the asymmetry parameter at ^{57}Fe nuclei. The appropriate orbital is only $3d_{3z^2-r^2}$ which corresponds to both the sign of the field gradient and the asymmetry parameter that agreed with the experimental results. These results show that 3*d*-electron near the Fermi surface has a $3d_{3z^2-r^2}$ symmetry. These results imply that the 3d-electrons at $3d_{3z^2-r^2}$ orbital have an appreciable density at the Fermi surface.

It is also possible to determine the sign of the electric field gradient and asymmtry parameter using a single crystal sample. In this work, the conversion electron Mössbauer spectroscopy of U_6Fe single crystal has been performed in order to verify the results under the applied field. Figure 3.2.3.6 shows the conversion electron Mössbauer spectrum of U_6Fe at room temperature. As written above, the sign of the quadrupole splitting is minus and the asymmetry parameter is nearly equal to zero. The results expected ideally which are consistent to the results obtained under the applied field were the ratio of the doublet peak intensity at lower to higher velocity is 3:1. The spectrum obtained seems to be asymmetric doublet with the line at higher energy having broad FWHM and the greater intensity. These results agreed with the one reported by Kimball et al. within the experimental error [3.2.3.4]. The obtained spectrum is more unclear and weaker than the transmission spectra at room temperature, so that it is difficult to determine the exact Mössbauer parameters. Generally speaking, conversion electron Mössbauer spectroscopy is sensitive to the physical and chemical properties of the surface in the samples because of the short struggling range of the conversion electrons. U-Fe intermetallic compounds are also easy to be oxidized. When the component at 0 mm s^{-1} with broad single line exists, the results of the

spectrum-analysis of CEMS agreed with the results obtained under the applied field. This broad component is thought to be that of the oxidized surface of U_6Fe single crystal.

3.2.3.4. Conclusion

The obtained isomer shift and the quadrupole splitting at room temperature are - 0.36 mm s^{-1} and 0.76 mm s^{-1}, respectively. The isomer shift value shows the 3*d*-electrons of iron atoms are hybridized with 5*f*-electrons of uranium atoms. The larger quadrupole splitting is thought to be mainly based on the orbital of 3*d*-electrons themselves. From the results obtained under the applied magnetic field, the sign of the electric field gradient is minus and the asymmetry parameter is zero. These results show the orbital of $3d_{3z^2-r^2}$ has the density near the Fermi surface.

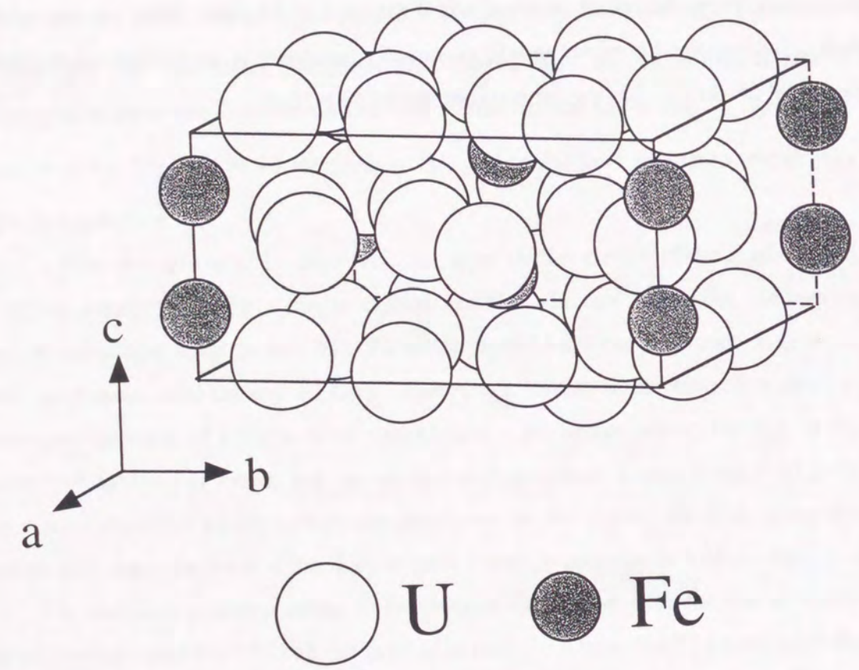

Fig. 3.2.3.1. Crystal structure of U_6Fe.

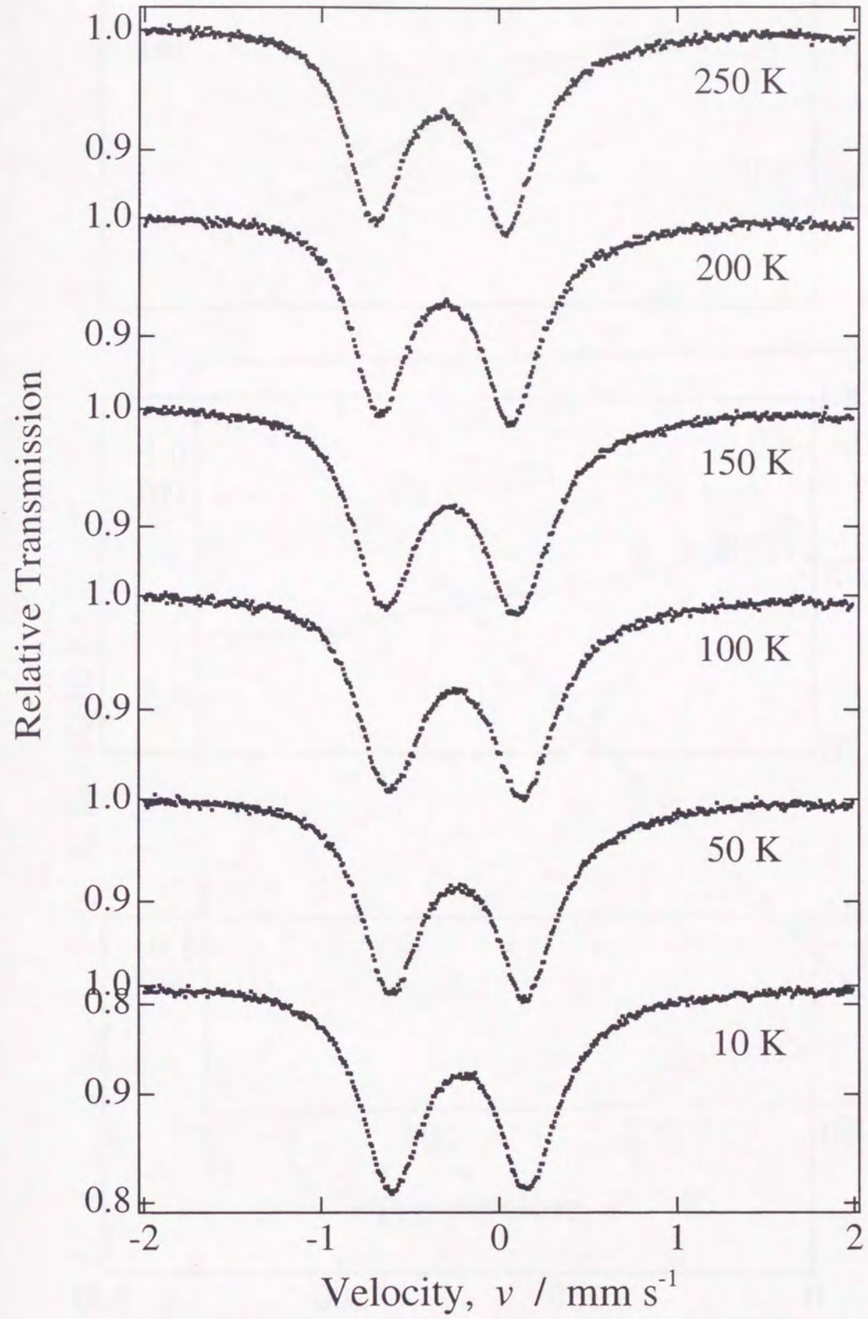

Fig. 3.2.3.2. ^{57}Fe Mössbauer spectra of U_6Fe at varios temperatures.

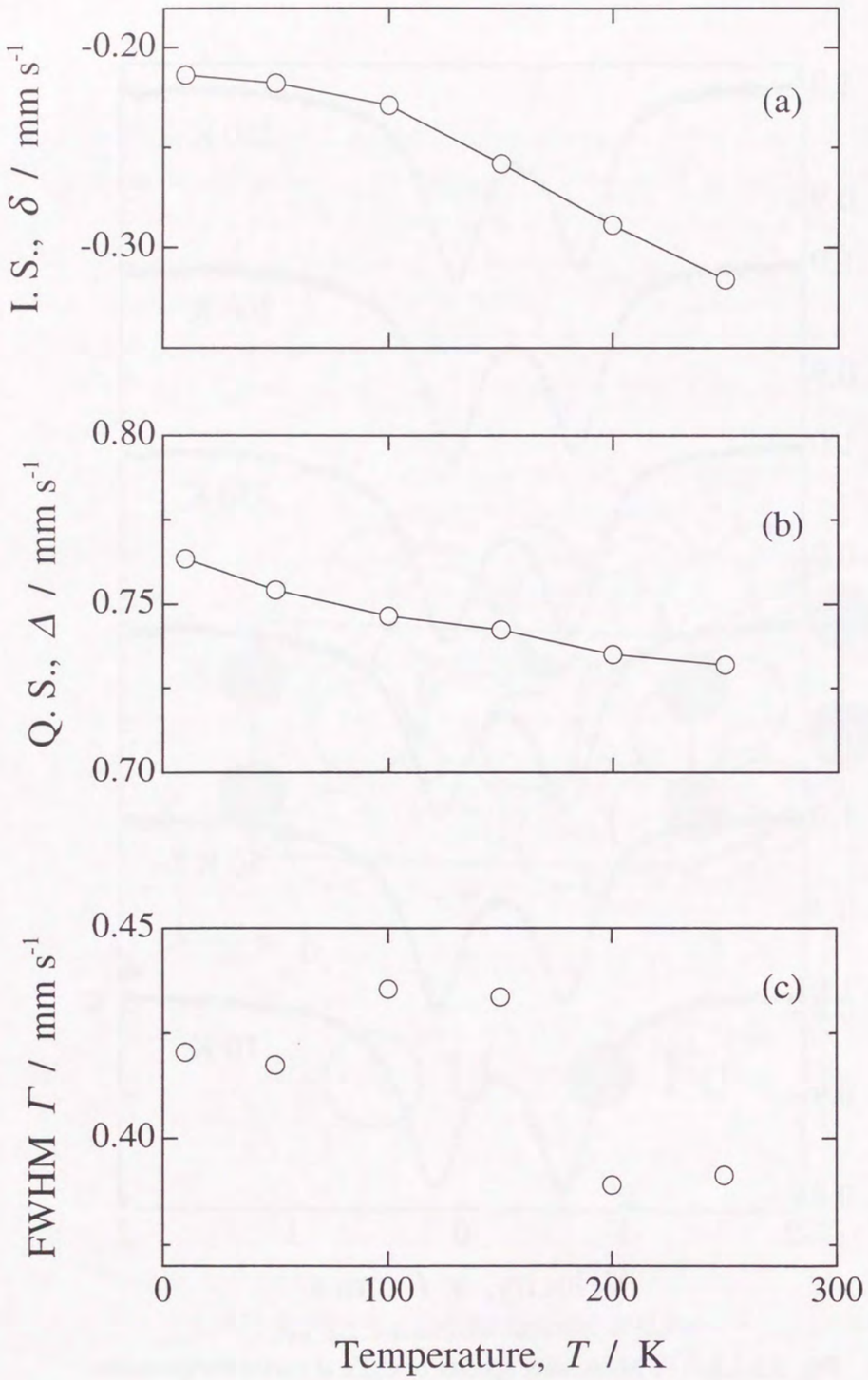

Fig. 3.2.3.3. Temperature dependence of (a) isomer shift, (b) quadrupole splitting and (c) full-width at half maximum.

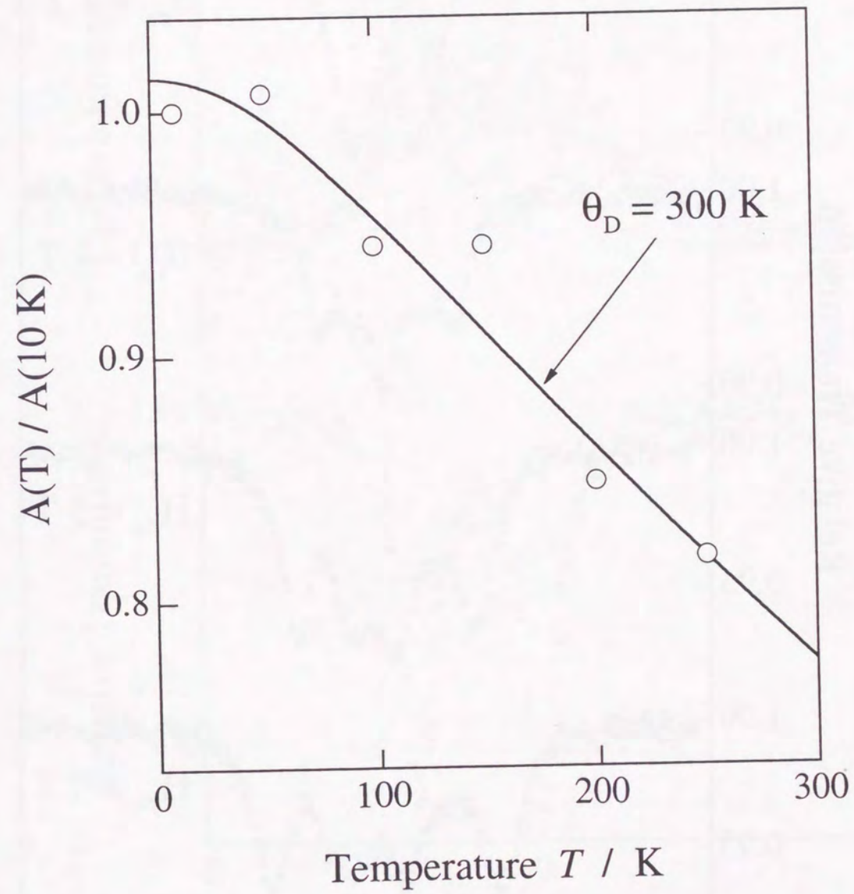

Fig. 3.2.3.4. Temperature dependence of the absorption area of ^{57}Fe Mössbauer spectra of U_6Fe. The solid line is theoretical curve using Debye model where the Debye temperature of U_6Fe is 300 K.

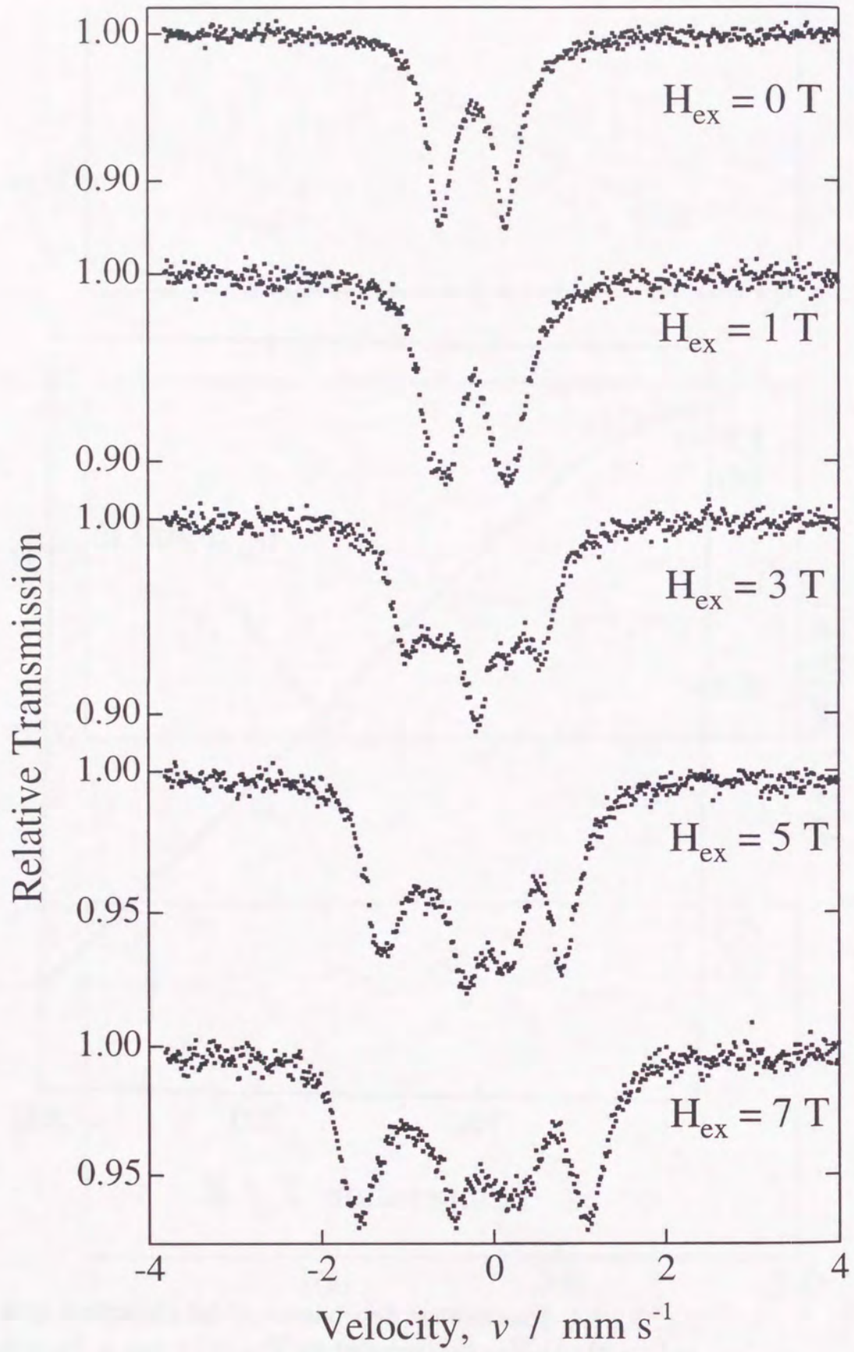

Fig. 3.2.3.5. ^{57}Fe Mössbauer spectra of U_6Fe at 4.5 K under the longitudinally applied field.

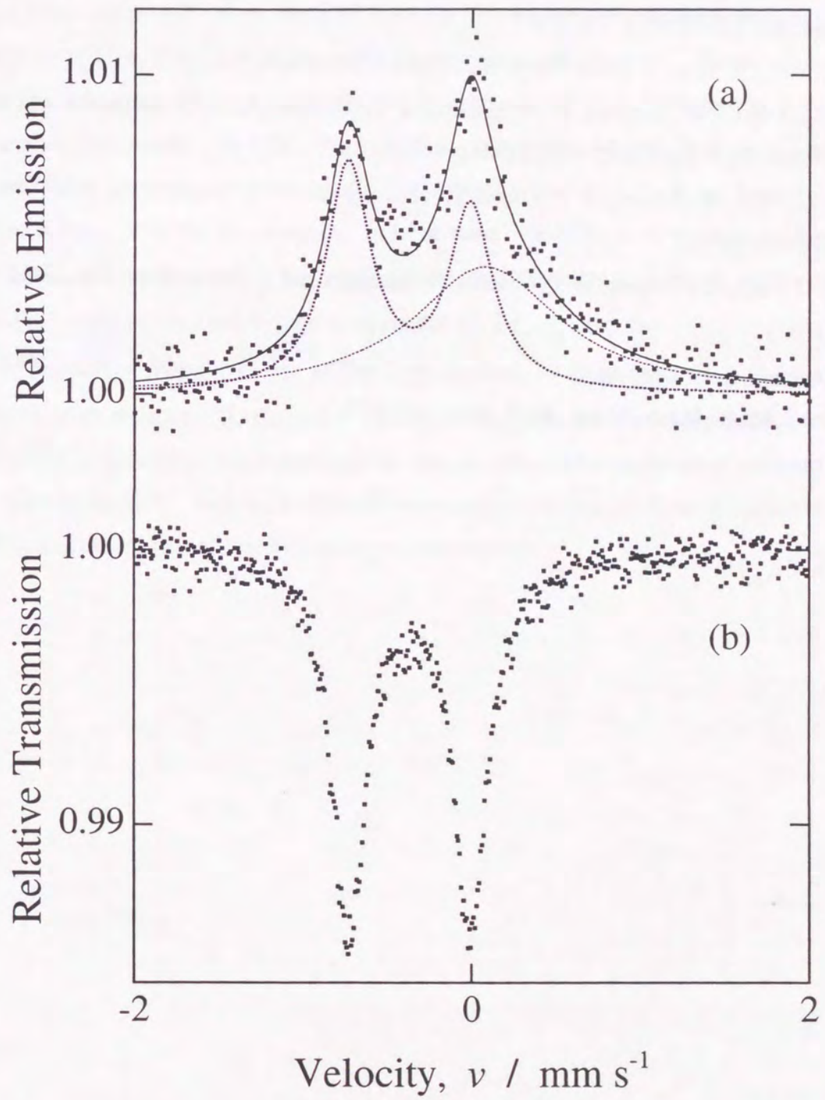

Fig. 3.2.3.6. (a) ^{57}Fe conversion electron Mössbauer spectrum of U_6Fe at room temperature.
(b) ^{57}Fe transmission Mössbauer spectrum of U_6Fe at room temperature.

References

[3.2.3.1] B. S. Chandrasekhar and J. K. Hulm, J. Phys. Chem. Solids, **7**, 259 (1958).

[3.2.3.2] E. Yamamoto, M. Hedo, Y. Inada, T. Ishida, Y. Haga, Y. Ōnuki, J. Phys. Soc. Jpn., **65**, 1034 (1996).

[3.2.3.3] S. Blow, J. Phys. Chem. Solids, **30**, 1549 (1969).

[3.2.3.4] C. W. Kimball, P. P. Vaishnava, A. E. Dwight, J. D. Jorgensen and F. Y. Fradin, Phys. Rev., **B32**, 4419 (1985).

[3.2.3.5] L. E. DeLong, J. G. Huber, K. N. Yang and M. B. Maple, Phys. Rev. Lett., **51**, 312 (1983).

[3.2.3.6] L. E. DeLong, R. P. Guertin, S. Hasanain and T. Fariss, Phys. Rev., **B31**, 7059 (1985).

[3.2.3.7] L. E. DeLong, L. N. Hall, G. W. Crabtree, W. Kwok and K. A. Gschneidner, Jr., J. Magn. Magn. Mater., **63 & 64**, 478 (1987).

3. 2. 4. Conclusion

By means of the ^{57}Fe and the ^{238}U Mössbauer spectroscopy, the physical properties of U-Fe intermetallic compounds have been investigated.

The isomer shift values obtained from the ^{57}Fe Mössbauer measurements are - 0.21 mm s^{-1} of UFe_2 and - 0.36 mm s^{-1} of U_6Fe relative to metallic iron. These values indicate the 3*d*-electrons of iron atoms are well hybridized with the 5*f*-electrons in U-Fe intermetallic compounds. In UFe_2, the hybridization between 3*d*- and 5*f*-elecrons are suggested from the small hyperfine coupling constants whose magnitude are from 5.3 μ_B / T to 6.9 μ_B / T in the ferromagnetic ordered state. In U_6Fe, it is revealed by the ^{57}Fe Mössbauer spectroscopy in the applied field that the large quadrupole splitting obtained is caused by the electric field gradient due to $3d_{3z^2-r^2}$ electrons.

The results of the ^{238}U Mössbauer measurements of UFe_2 show no hyperfine magneticfield exists at the ^{238}U nucleus. This result suggests that the uranium atoms in UFe_2 have no magnetic moments although the spin and the orbital moments of uranium atoms were proposed to have an antiparallel coupling by the results from the neutron scattering and the magnetic Compton scattering experiments.

3.3. Itinerant Ferromagnetic Compound UGe_2

3. 3. 1. Intoroduction

In the U-Ge system, several intermetallic compounds have been formed such as UGe_2, U_3Ge_4, U_5Ge_3 and U_7Ge [3.3.1]. The ferromagnetic compounds in this system are UGe_2 and U_3Ge_4 [3.3.2, 3]. UGe_2 is known as a heavy fermion compound and shows highly anisotropic ferromagnetism with the Curie temperature of 52 K [3.3.3]. A saturated magnetic moment is 1.43 μ_B / U. The crystal structure has been recently determined to be orthorhombic by means of the X-ray precession and neutron powder diffraction methods [3.3.4].

Experimental studies were extensively performed to clarify magnetic and electrical properties of UGe_2 [3.3.1, 3.3.5-10], although the local electronic state of a uranium atom has not been investigated yet. The ^{238}U Mössbauer spectroscopy is one of the useful tools to investigate the local electronic state of the uranium atom which plays an important role of the magnetic properties in UGe_2. We have performed the ^{238}U Mössbauer spectroscopy of UGe_2 in order to investigate its magnetic property and local electronic state.

3. 3. 2. Experimental Procedure

The ^{238}U Mössbauer spectroscopy was performed in the temperature range of 100 K to 5.3 K, using a powdered sample packed in a sample holder made of aluminum. The area density of the sample is 109.59 mg cm^{-2}, which is identical to 60.91 mg U cm^{-2}. The ^{238}U Mössbauer measurements were performed in the transmission geometry. A disk-shaped $^{242}PuO_2$ source, which contains 99.99 % ^{242}Pu, was used as the gamma-ray source. The Doppler velocity was calibrated by the laser calibrator, and the zero isomer shift was adopted as the isomer shift value of ^{238}U in PuO_2.

3. 3. 3. Results and Discussion

Figure 3.3.1 shows typical ^{238}U Mössbauer spectra measured at various temperatures between 100 K and 5.3 K. All of the spectra can be analyzed by the symmetric absorption pattern. When the electric quadrupole interaction is sufficiently large, an expected ^{238}U Mössbauer spectrum becomes asymmetric as In an absorption spectrum of $UO_2(NO_3)_2$•$6H_2O$ [3.3.11].

Here, the Hamiltonian of the electric quadrupole interaction is represented by

$$H_Q = \frac{e^2qQ}{4I(2I-1)}\left\{3M^2 - I(I+1) + \frac{\eta}{2}\left(\hat{I}_+^2 + \hat{I}_-^2\right)\right\}, \qquad (3.3.1)$$

where q is the maximum component V_{zz} of the electric field gradient at the nucleus, Q the quadrupole moment of the probe nucleus, I the nuclear spin, M the z component of I and η an asymmetry parameter defined by $\eta = (V_{xx} - V_{yy})/V_{zz}$. When the axially symmetric electric field gradient exists at the ^{238}U nucleus, the excited state of the ^{238}U nucleus is split into three levels; $e^2qQ/4$, $-e^2qQ/8$ and, $-e^2qQ/4$ which depends on M^2. The origin of the electric field gradient is generally related to the local electronic state at the probe atom.

Two fundamental mechanisms are well known for the origin of the field gradient. One is the field gradient based on the arrangement around the probe atoms, and the second is that of the electron orbitals of the probe atom, namely, ^{238}U itself in UGe_2. Since the crystal structure of UGe_2 is anisotropic and does not have cubic symmetry around uranium atoms as shown in Fig. 3.3.2, the electric field gradient based on 5f electrons at the ^{238}U nucleus can also be expected to exist in UGe_2.

The quadrupole splitting at the ^{238}U nucleus was, however, not observed within an experimental error even in the paramagnetic state. The reason is as follows. The existence of the quadrupole interaction has been recently confirmed by the ^{235}U NMR measurement for an antiferromagnetic compound UO_2 [3.3.12]. The spin-echo spectrum of ^{235}U NMR shows seven resonance lines with a line-width of about 1 MHz in the antiferromagnetic state and indicates the existence of the electric quadrupole interaction with $|e^2qQ(3\cos^2\theta - 1)/h| = 392 \pm 11$ MHz. The electric field gradient of 5*f* electrons in the Γ_5 triplet state might be an origin of the quadrupole interaction observed in NMR. This magnitude of the quadrupole interaction corresponds to 1.70 ± 0.04 mm s^{-1} in the ^{238}U Mössbauer spectrum. The quadrupole splitting of ^{238}U in UO_2 is too small to be detected in the Mössbauer spectrum because the natural line-width of the ^{238}U Mössbauer spectrum is 27 mm s^{-1}, which is a few 10 times larger than the observed electric field gradient.

In the magnetically ordered state, the effects of the quadrupole interaction on the Mössbauer spectrum are a little bit complicated. When the hyperfine magnetic field

is sufficiently large, the axially symmetric field gradient causes shifts of the magnetically split absorption lines by an amount of $e^2qQ(3\cos^2\theta-1)/8$, where θ is the angle between the principle axis of the field gradient and the direction of the hyperfine magnetic field which is antiparallel to the direction of the atomic magnetic moment. A maximum value of the shift, which is expected at $\theta = 0$ or π, is $e^2qQ/4$, which is just half of the splitting observed in the paramagnetic state.

When the quadrupole interaction is comparable or large enough to the magnetic interactions, each nuclear energy levels are no more in the pure state and the expected Mössbauer spectrum shows a broad one based on the mixed hyperfine interaction. However, one can expect an asymmetric spectrum depending on the sign of field gradient, except for the case of $\eta = 1$ where the symmetric spectrum can be expected.

For the present ^{238}U Mössbauer measurements, the line-width is too large to resolve the small shifts of the absorption lines due to the small quadrupole interaction. However, the existence of the quadrupole interaction can be judged from the asymmetry of the absorption spectrum. Nevertheless, the spectrum observed in the paramagnetic state, for example, at 100 K is symmetric, as shown in Fig. 3.3.1. This result claims that the quadrupole splitting does not exist or its magnitude is smaller than the experimental error.

Moreover, we have to consider the contribution of the electron orbitals to the electric field gradient at the nucleus. The electric field gradient is proportional to the expectation value of $1/r^3$, $\langle r^{-3} \rangle$. The value of $\langle r^{-3} \rangle$ in UGe_2 is expected to be smaller than the one in UO_2 whose 5*f* electrons are well-known to be localized. The reason is as follows. The temperature dependence of the magnetic susceptibility of UGe_2 follows the Curie-Weiss law above the Curie temperature [3.3.1]. The effective magnetic moment is 3.1 μ_B / U in the paramagnetic state. On the other hand, a saturated moment of 1.43 μ_B / U is much smaller than the effective moment. From the experimental results of de Haas-van Alphen effect, photoemission and bremsstrahlung isochromat spectra and the temperature dependence of the electrical resistivity, the 5*f* electrons in UGe_2 are considered to be itinerant [3.3.5-7, 3.3.13]. Consequently, the quadrupole splitting in UGe_2 is more difficult to observe than in UO_2.

With decreasing the temperature, especially below the Curie temperature of 52 K, a line broadening is clearly observed in the spectrum, as shown in Fig. 3.3.1. The temperature dependence of full-width at half maximum (FWHM) is shown in Fig. 3.3.3, where the spectra are analyzed by a single Lorentz function. The FWHM values increase steeply below 52 K. Since the Curie temperature of UGe_2 is 52 K, the increase of FWHM is due to the appearance of the hyperfine magnetic field at the uranium nucleus in the ferromagnetic state. The Hamiltonian of the magnetic dipole interaction or the Zeeman effect for the nuclear spin is represented by

$$H_Z = g_{ex}\mu_N HM, \qquad (3.3.2)$$

where g_{ex} is the *g*-factor of the first excited state of ^{238}U, μ_N the nuclear magneton, *H* the local magnetic field or hyperfine magnetic field at the ^{238}U nucleus and *M* the z component of the nuclear spin, *I*. The excited state of the ^{238}U nucleus has $I = 2^+$ and is split into five levels *M* by the hyperfine field at the ^{238}U nucleus, as shown schematically in Fig. 3.3.1. The ^{238}U Mössbauer effect is thus observed in the E2 transition from $I = 2^+$ to $I = 0^+$ of the ^{238}U nucleus. The magnetic pattern of the ^{238}U Mössbauer spectroscopy is, however, observed as a broad single peak which is an unresolved superposition of the Zeeman-split five lines, as discussed previously [3.3.11].

The line-width is related to the recoil-free fraction which depends on the temperature. In the case of the superposed spectrum such as in UGe_2 at 5.3 K, the usual method of least-square fitting using non-constrained FWHM is known not to give the magnitude of the 'true' hyperfine interaction parameters, as discussed by Shenoy and Ruby [3.3.14]. Namely, the obtained line-width generally tends to be smaller than the true one.

In the present case, the spectra in the ferromagnetic state were analyzed by using the value of the line-width obtained at 82 K where UGe_2 is paramagnetic. The obtained magnetic splitting is 57.0 ± 3.1 mm s^{-1} at 5.3 K. The magnitude of the Zeeman splitting is $4g_{ex}\mu_N H = 8.53\times10^{-6}$ eV. By using g_{ex} = 0.254 ± 0.015 μ_N determined from the ^{235}U NMR and the ^{238}U Mössbauer measurements of UO_2 in the antiferromagnetic state, the magnitude of the hyperfine field at the ^{238}U nucleus is determined as 240 ± 10 T at 5.3 K.

We will discuss the present results, comparing with those of UO_2. The saturated moments of UGe_2 and UO_2 are known to be 1.43 μ_B / U and 1.78 μ_B / U, respectively [3.3.1, 3.3.15]. The hyperfine field at the ^{238}U nucleus in UO_2 is 252.3 ± 1 T at 5.4 K [3.3.12]. The hyperfine coupling constants of UGe_2 and UO_2 are thus determined as 160 ± 10 T / μ_B and 142 ± 1 T / μ_B, respectively. The contribution to the hyperfine field is due to the total angular momentum $\boldsymbol{J}$ which contains the orbital and spin moments as well as the core polarization. The hyperfine field due to the former is represented by

$$H_{orb} = a_{hf} \langle J \| N \| J \rangle \langle r^{-3} \rangle m_J , \qquad (3.3.4)$$

and to the latter by

$$\boldsymbol{H}_{core} = \frac{8}{3} \pi \mu_B \boldsymbol{g} \sum_n \left[\rho_{ns}^{\uparrow}(0) - \rho_{ns}^{\downarrow}(0) \right] , \qquad (3.3.5)$$

respectively, where a_{hf} is a hyperfine coupling constant per atomic units, $\langle J \| N \| J \rangle$ a reduced matrix element, $\boldsymbol{N} = \sum \{ \boldsymbol{l}_i - \boldsymbol{s}_i + 3(\boldsymbol{r}_i \cdot \boldsymbol{s}_i)\boldsymbol{r}_i / \boldsymbol{r}_i^2 \}$, $\boldsymbol{l}_i$ the angular momentum, $\boldsymbol{s}_i$ the spin momentum, m_J the azimuthal number connected with J_z, $\langle r^{-3} \rangle$ the expectation value of $1 / r^3$ for the wave functions of the open shell electrons [3.3.16]. $\rho_{ns}^{\uparrow}(0)$ and $\rho_{ns}^{\downarrow}(0)$ are the contact density of s-electrons of the n-th shell having spin up and spin down states. The contribution due to the orbital current is thought to be nearly proportional to the magnetic moment at uranium atoms. Moreover, since the 5f electrons of UGe_2 is thought to be itinerant, $\langle r^{-3} \rangle$ of UGe_2 is most likely smaller than that of UO_2 as mentioned above. The contribution of the orbital current to the hyperfine field of UGe_2 might be smaller than that of UO_2. Therefore, the difference of the hyperfine coupling constants between UO_2 and UGe_2 is mainly due to the difference of the contribution of both the orbital current and the core polarization.

The temperature dependence of the hyperfine magnetic field of UGe_2 is shown in Fig. 3.3.4. Its temperature dependence is the same as the one of the static magnetization shown by squares. This result indicates that the hyperfine coupling constant of ^{238}U in UGe_2 does not depend on the temperature.

3.3.4. Conclusion

The hyperfine field at ^{238}U nucleus in UGe_2 has been observed below the Curie temperature of 52 K. The magnitude of the hyperfine field is determined as 240 ± 10 T at 5.3 K, which is proportional to the magnetization below the Curie temperature. Therefore, the hyperfine coupling constant of 160 T / μ_B does not depend on the temperature.

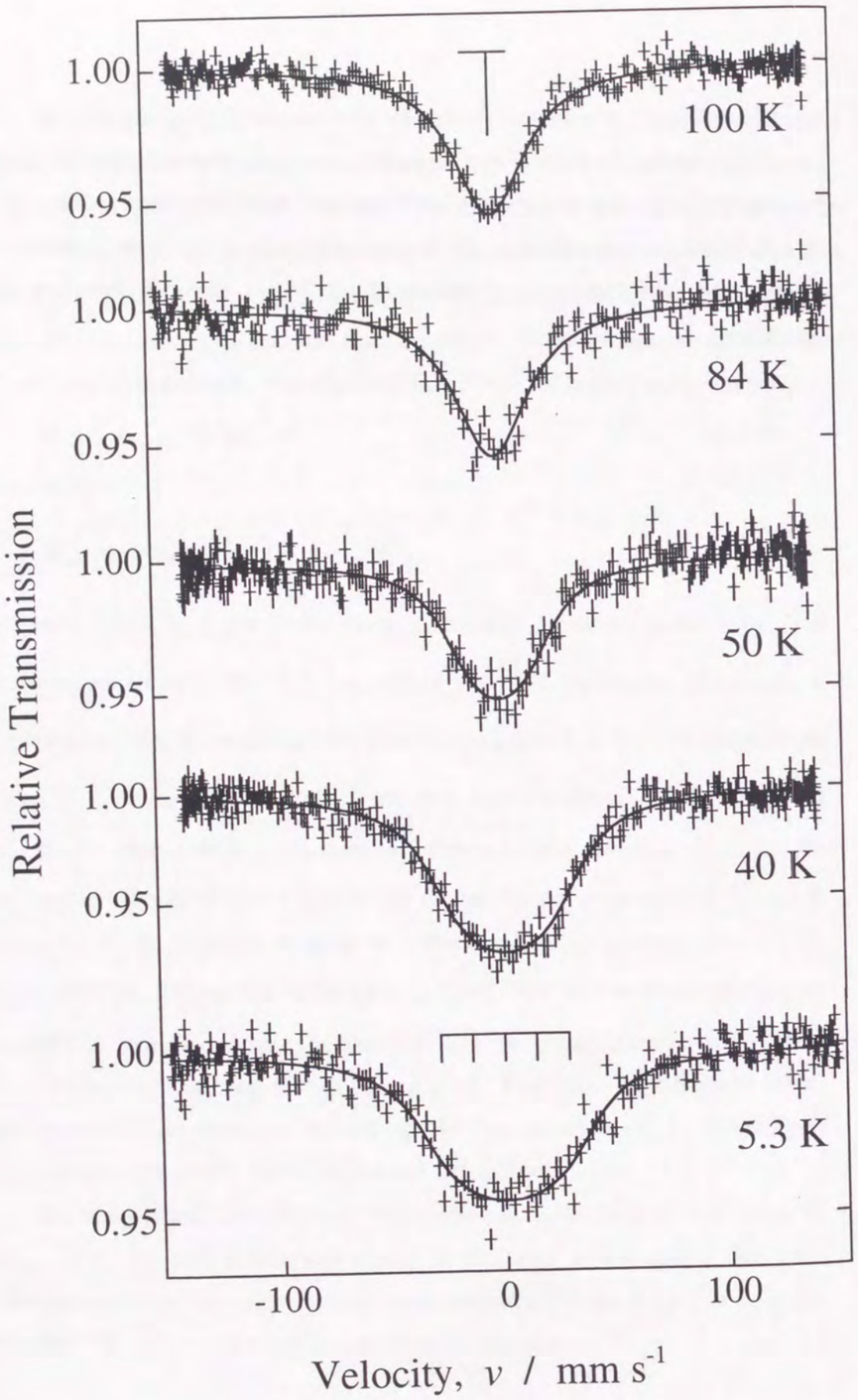

Fig. 3.3.1. ^{238}U Mössbauer spectra of UGe_2 at various temperatures.

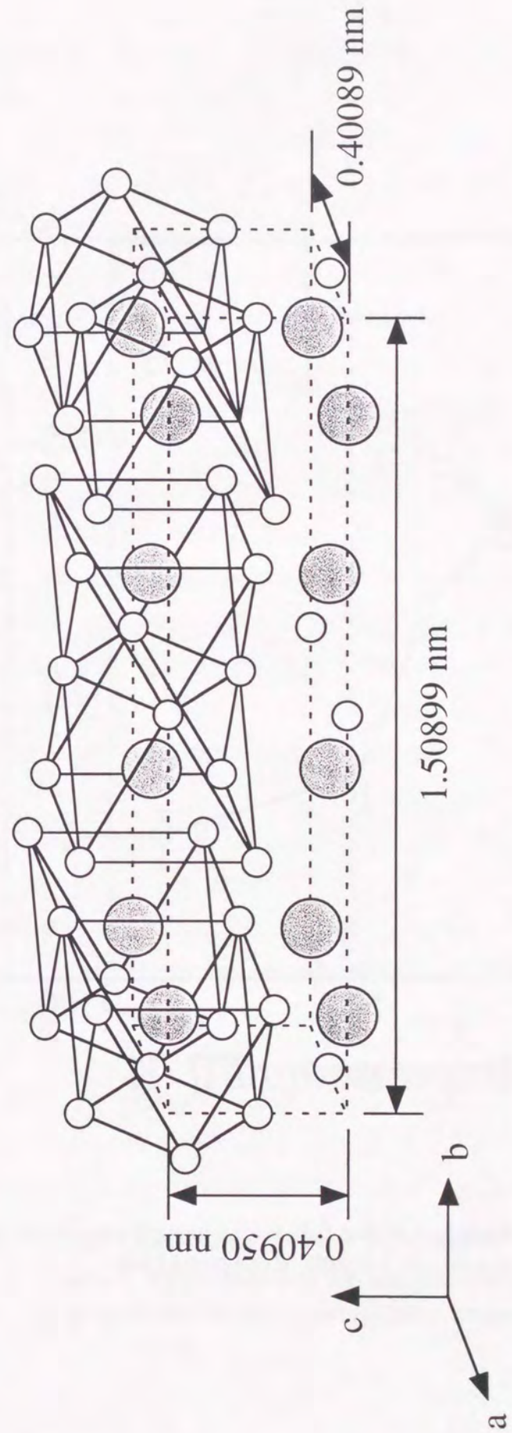

Fig. 3.3.2. Crystal structure of UGe_2 [3.3.4].

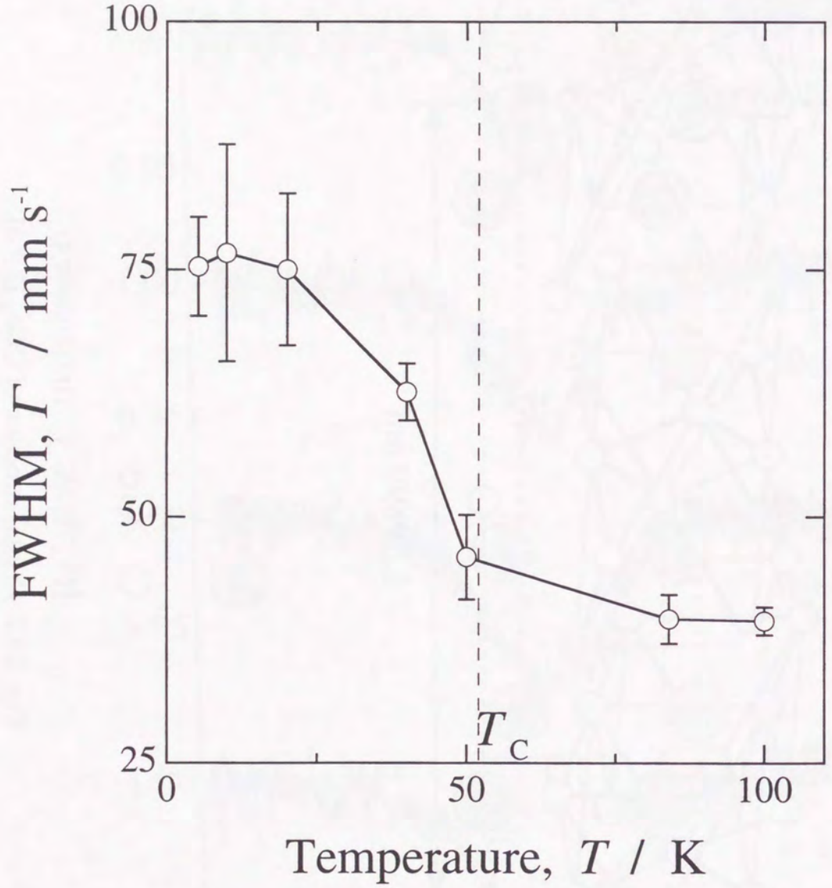

Fig. 3.3.3. Temperature dependence of the full-width at half maximum (FWHM) which was obtained by using a single Lorentz absorption line.

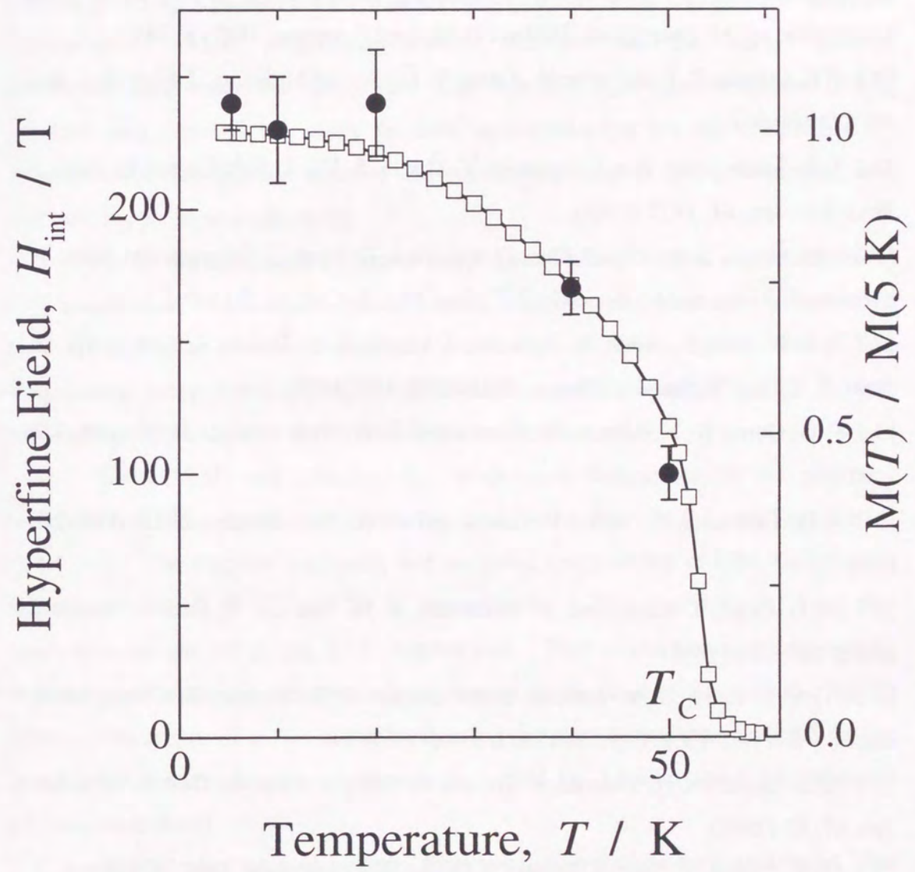

Fig. 3.3.4. Temperature dependence of the hyperfine field atthe ^{238}U nucleus and the magnetization of UGe_2, shown by solid circles and open squares, respectively.

References

[3.3.1] Y. Ōnuki, I. Ukon, S. W. Yun, I. Umehara, K. Satoh, T. Fukuhara, H. Sato, S. Takayanagi, M. Shikama and A. Ochiai: J. Phys. Soc. Jpn. **61**, 293 (1992).

[3.3.2] . Trzebiatwski and A. Misiuk: Roczniki Chemii **42**, 161 (1968).

[3.3.3] Menovsky, F. R. de Boer, P. H. Frings and J. J. M. Franse: *High Field Magnetism*, ed. M. Date (North-Holland Publishing Company, 1983) p. 189.

[3.3.4] K. Oikawa, T. Kamiyama, H. Asano, Y. Ōnuki and M. Kohgi: J. Phys. Soc. Jpn. **65**, 3229 (1996).

[3.3.5] K. Satoh, S. W. Yun, I. Umehara, Y. Ōnuki, S. Uji, T. Shimizu and H. Aoki: J. Phys. Soc. Jpn. **61**, 1827 (1992).

[3.3.6] Y. Ōnuki, S. W. Yun, I. Ukon, I. Umehara, K. Satoh, I. Sakamoto, M. Hunt, P. Meeson, P. Probst and M. Springford: J. Phys. Soc. Jpn. **60**, 2127 (1991).

[3.3.7] S. W. Yun, K. Satoh, Y. Fujimaki, I. Umehara, Y. Ōnuki, S. Takayanagi, H. Aoki, S. Uji and T. Shimizu: Physica B **186-188**, 129 (1993).

[3.3.8] G. Oomi, K. Nishimura, Y. Ōnuki and S. W. Yun: Physica B **186-188**, 758 (1993).

[3.3.9] H. Takahashi, N. Môri, Y. Ōnuki and S. W. Yun: Physica B **186-188**, 772 (1993).

[3.3.10] G. Oomi, T. Kagayama, K. Nishimura, S. W. Yun and Y. Ōnuki: Physica B **206 & 207**, 515 (1995).

[3.3.11] S. L. Ruby, G. M. Kalvius, B. D. Dunlap, G. K. Shenoy, D. Cohen, M. B. Brodsky and D. J. Lam: Phys. Rev. **184**, 374 (1969).

[3.3.12] K. Ikushima, H. Yasuoka, S. Tsutsui, M. Saeki, S. Nasu, M. Date: J. Phys. Soc. Jpn. **67**, 65 (1998).

[3.3.13] T. Eijima, S. Sato, S. Suzuki, Y. Saito, S. Fujimori, N. Sato, M. Kasaya, T. Komatsubara, T. Kasuya, Y. Ōnuki and T. Ishii: Phys. Rev. B **53**, 1806 (1996).

[3.3.14] G. K. Shenoy and S. L. Ruby: *Mössbauer Methodology*, Ed. I. J. Gruverman (Prenum Press, New York, 1974), Vol. 9 p.227.

[3.3.15] B. C. Frazer, G. Shirane, D. E. Cox and C. E. Olsen: Phys. Rev. **140**, A1448 (1965)

[3.3.16] R. Elliott and K. W. H. Stevens: Proc. Roy. Soc., **A218**, 553 (1953).

3. 4. Heavy Fermion Superconductors, UPd_2Al_3 and URu_2Si_2

3. 4. 1. Introduction

Since a heavy fermion superconductor $CeCu_2Si_2$ was discovered by F. Steglich et al. [3.4.1.1], the other heavy fermion superconductors, UBe_{13} [3.4.1.2], UPt_3 [3.4.1.3], URu_2Si_2 [3.4.1.4], UNi_2Al_3 [3.4.1.5] and UPd_2Al_3 [3.4.1.6], were discovered in uranium intermetallics. The progressive studies clarified that the heavy fermion superconductors were the anisotropic and non-BCS-type superconductor. The common characters of the heavy fermion superconductors are the coexistence or competition of the magnetic ordering and superconductivity in their ground state, and their anisotropic superconductivity.

As for the macroscopic physical properties of heavy fermion superconductors, their temperature dependence of the electrical resistivity and magnetic susceptibility have a broad peak at the characteristic temperature of Kondo effect. Below this temperature, every electrical resistivity shows a metallic behavior. And then, it become zero at the superconducting transition temperature.

For UPd_2Al_3 and URu_2Si_2, the temperature dependence of the electrical resistivity and the magnetic susceptibility is shown in Fig. 3.4.1.1 and Fig. 3.4.1.2 [3.4.1.6-8]. The electrical resistivity and magnetic susceptibility of UPd_2Al_3 have the maximums around 80 K and 30 K, respectively. Those of URu_2Si_2 have the maximums around 100 K and 50 K, respectively. Both of the maximums of electric resistivity and magnetic susceptibility is thought to be characteristics of the Kondo effect. The origins of the difference in those temperature dependence observed for the uranium-based heavy fermion superconductors, UPd_2Al_3, URu_2Si_2 and so on, have not yet been understood.

On the other hand, the results from microscopic studies are as follows: The NMR studies revealed $CeCu_2Si_2$ [3.4.1.9] and UPd_2Al_3 [3.4.1.10-15] were an even parity and *d*-wave type superconductors, and that UPt_3 was an odd parity superconductor [3.4.1.16]. The neutron studies clarified the interplay between their magnetic ordering and superconductivity from the anomalies of the magnetic reflection in the elastic scattering at the superconducting transition temperature [3.4.1.17-24].

Although the ^{238}U Mössbauer measurement is also the microscopic experiments,

it has never been performed since the discovery of its Mössbauer effect because of the reason as written in Chapter 1. The motivation of this work is mainly to investigate their magnetic properties by using the ^{238}U Mössbauer spectroscopy. The ^{238}U Mössbauer spectroscopy might clarified the local electronic states of 5*f*-electrons of uranium atoms which attribute to the physical properties of the uranium-based heavy fermion superconductor. In this work, ^{238}U Mössbauer measurements of UPd_2Al_3 and URu_2Si_2 have been performed in order to investigate their magnetic properties and the origin of the appearance of a heavy fermion which plays an important role for the superconductivity.

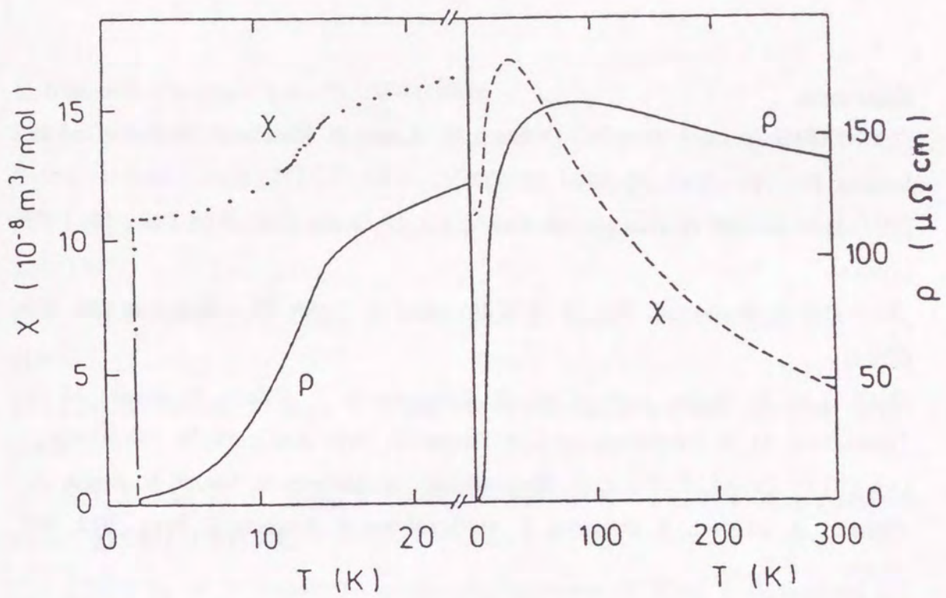

Fig. 3.4.1.1. Temperature dependence of the magnetic susceptibility, χ, and electrical resistivity, ρ, of UPd_2Al_3 [3.4.1.6].

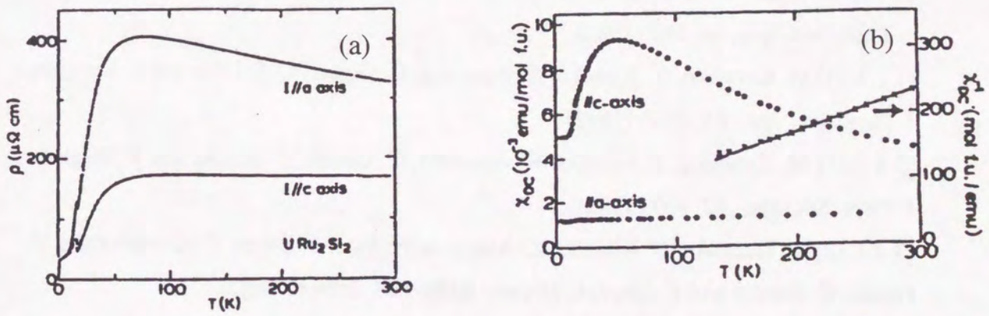

Fig. 3.4.1.2. Temperature dependence of (a) the electrical resistivity, ρ, and (b) magnetic susceptibility, χ, of URu_2Si_2 [3.4.1.6-8].

References

[3.4.1.1] F. Steglich, J. Aarts, C. D. Bredl, W. Lieke, D. Meschede, W. Franz and H. Schafer, Phys. Rev. Lett., **43**, 1892 (1979).

[3.4.1.2] H. R. Ott, H. Rudigier, Z. Fisk and J. L. Smith, Phys. Rev. Lett., **50**, 1595 (1983).

[3.4.1.3] G. R. Stewart, Z. Fisk, J. O. Willis and J. L. Smith, Phys. Rev. Lett., **52**, 679 (1984).

[3.4.1.4] M. B. Maple, J. W. Chen, Y. Dalichaouch, T. Kohara, C. Rossel, M. S. Torikachvili, M. W. McElfresh and J. D. Thompson, Phys. Rev. Lett., **56**, 185 (1986).

[3.4.1.5] C. Geibel, S. Theis, D. Kaczorowski, A. Mehner, A. Gauel, B. Seidel, U. Ahlheim, R. Helfrich, K. Petersen, C. D. Bredl and F. Steglich, Z. Phys., **B83**, 305 (1991)

[3.4.1.6] C. Geibel, C. Schank, S. Thies, H. Kitazawa, C. D. Bredl, A. Bohm, M. Rau, A. Grauel, R. Caspary, R. Helfrich, U. Ahlheim, G. Weber and F. Steglich, Z. Phys., **B84**, 1 (1991)

[3.4.1.7] T. T. M. Palstra, A. A. Menovski, J. van den Berg, A. J. Dirkmaat, P. H. Kes, G. J. Nieuwenhuys and J. A. Mydosh, Phys. Rev. Lett., **55**, 2727 (1985).

[3.4.1.8] T. T. M. Palstra, A. A. Menovski and J. A. Mydosh, Phys. Rev., **B33**, 6527 (1986).

[3.4.9] K. Ueda, Y. Kitaoka, H. Yamada, Y. Kohori, T. Kohara and K. Asayama, J. Phys. Soc. Jpn., **56**, 867 (1987).

[3.4.1.10] M. Kyogaku, Y. Kitaoka, K. Asayama, C. Geibel, C. Schank and F. Steglich, J. Phys. Soc. Jpn., **61**, 2660 (1992).

[3.4.1.11] M. Kyogaku, Y. Kitaoka, K. Asayama, C. Geibel, C. Schank and F. Steglich, J. Phys. Soc. Jpn., **62**, 867 (1992).

[3.4.1.12] M. Kyogaku, Y. Kitaoka, K. Asayama, N. Sato, T. Sakon, T. Komatsubara, C. Geibel, C. Schank and F. Steglich, Physica **B186-188**, 2660 (1992).

[3.4.1.13] H. Tou, Y. Kitaoka, K. Asayama, C. Geibel, C. Schank and F. Steglich, J. Phys. Soc. Jpn., **64**, 725 (1995).

[3.4.1.14] Y. Kohori, K. Matsuda and T. Kohara, Physica **B206-207**, 622 (1995).

[3.4.1.15] Y. Kohori, K. Matsuda and T. Kohara, Solid State Commun., **95**, 121 (1995).

[3.4.1.16] H. Tou, Y. Kitaoka, K. Asayama, N. Kimura, Y. Ō nuki, E. Yamamoto and K. Maezawa, Phys. Rev. Lett. **77**, 1374 (1996).

[3.4.1.17] N. Sato, N. Aso, B. Roessli, G. H. Lander, T. Komatsubara, Y. Endo and O. Sakai, J. Alloys Compd., **271-273**, 4336 (1998).

[3.4.1.18] Y. Koike, N. Metoki, Y. Haga, Y. Morii and Y. Ō nuki, Physica **B241-243**, 823 (1997).

[3.4.1.19] N. Metoki, Y. Haga, Y. Koike and Y. Ō nuki, Physica **B241-243**, 845 (1997).

[3.4.1.20] N. Metoki, Y. Haga, Y. Koike and Y. Ō nuki, Phys. Rev. Lett., **80**, 5417 (1998).

[3.4.1.21] N. Metoki, Y. Haga, Y. Koike, N. Aso and Y. Ō nuki, J. Magn. Magn. Mater., **177-181**, 449 (1998).

[3.4.1.22] Y. Koike, N. Metoki, N. Kimura, E. Yamamoto, Y. Haga, Y. Ō nuki and K. Maezawa, J. Phys. Soc. Jpn., **67**, 1142 (1998).

[3.4.1.23] N. Sato, N. Aso, N. Tateiwa, N. Koga, T. Komatsubara and N. Metoki, Physica **B230-232**, 367 (1997).

[3.4.1.24] T. Honma, Y. Haga, E. Yamamoto, N. Metoki, Y. Koike, H. Ohkuni and Y. Ō nuki, unpublished.

3. 4. 2. ^{238}U Mössbauer Spectroscopy of UPd_2Al_3

3. 4. 2. 1. Introduction

A heavy fermion superconductor UPd_2Al_3 has the Néel temperature of 14 K and shows the superconducting ordered state below 2 K [3.4.2.1]. The saturated magnetic moment is 0.85 μ_B / U. The electronic specific-heat coefficient is 145 mJ / K^2. This compound is a typical heavy fermion superconductor whose magnetic ordering coexists with superconductivity. Figure 3.4.2.1. shows the crystal and magnetic structure of UPd_2Al_3. The results of NMR spectroscopy suggest the parity of its superconducting is the *d*-wave type [3.4.2.2-7]. From the report of the results for neutron scattering experiments, the magnetic peak has an anomaly at the onset temperature of its superconducting transition [3.4.2.8-12]. This phenomenon was observed in the other heavy fermion superconductor, UPt_3 [3.4.2.13], URu_2Si_2 [3.4.2.14] and UNi_2Al_3 [3.4.2.15]. In the neutron inelastic spectrum of UPd_2Al_3, a scattering excitation appears below the transition temperature which is due to the energy gap of its superconductivity. These results suggest that their superconductivity has the relation to their magnetic properties.

On the other hand, the electronic resistivity and magnetic susceptibility measurements have the broader peak at 80 K and 30 K, respectively [3.4.2.1]. The magnetic susceptibility obeyed the Curie-Weiss law above 100 K. The Weiss temperature and magnitude of the effective moment are - 47 K and 3.2 μ_B / U. The metamagnetic transition was observed at 18 T below the Néel temperature [3.4.2.16]. Even above Néel temperature, the metamagnetic transition was observed. It was observed up to the temperature where the magnetic susceptibility has a maximum value [3.4.2.17].

The Mössbauer spectroscopy has been performed in order to investigate the physical properties, mainly magnetic properties of UPd_2Al_3.

3. 4. 2. 2. Experimental Procedure

A single crystal of UPd_2Al_3 was grown by the Czochralski pulling method in a tetra-arc farce and annealed using the solid-state electrotransport method under vacuum of 10^{-10} torr [3.4.2.18]. It was powdered in argon gas atmosphere and sealed into the

sample holder made of aluminum. The gamma-ray source used for the ^{238}U Mössbauer spectroscopy was a PuO_2 source which contains 99.99 % ^{242}Pu. The ^{238}U Mössbauer measurement was performed in a transmission geometry. The Doppler velocity of the gamma-ray source was given with the sinusoidal motion. The Doppler velocity was calibrated with a laser calibrator. The isomer shift of ^{238}U in PuO_2 was adopted to the zero isomer shift value.

3. 4. 2. 3. Results and Discussion

Figure 3.4.2.2 shows the ^{238}U Mössbauer spectra obtained from the UPd_2Al_3 specimen at various temperatures. The line-width observed is obviously broad below 10 K and all of the spectra obtained are symmetric. These results show the obtained spectra do not include the quadrupole interaction or its magnitude is too small to be detected by ^{238}U Mössbauer spectroscopy, as discussed in Section 3.3. Since the Néel temperature of UPd_2Al_3 is 14 K, this line broadening is thought to be due to the appearence of the hyperfine magnetic field with the magnetic ordering. In order to determine the temperature dependence of the Mössbauer parameters in more detail, the results from the analysis of the spectra with a single peak is discussed.

Figure 3.4.2.3 shows the temperature dependence of the full width at half maximum (FWHM) and resonance absorption area of the ^{238}U Mössbauer spectra where the spectra are analyzed with a single Lorentzian function. The absorption area increases monotonously with decreasing the temperature. The results obtained are fitted by the Debye model as shown in Fig. 3.4.2.3.

The values of FWHM do not show simple temperature dependence. As written above, the obvious broadening below Néel temperature is thought to be caused by the appearance of the hyperfine magnetic field. Moreover, the temperature dependence of FWHM seems to have the maximum around 50 K. Firstly, the temperature dependence around 50 K is discussed.

The thickness of the used source was about 50 μm and the fractional abundance of ^{238}U was adequately small because of the very long half-life of ^{242}Pu, 3.76 $\times 10^5$ years. Since the effective thickness of ^{238}U Mössbauer resonance is small, the self-absorption in the source can be neglected. As shown in Eq.(2.1.17), transmission spectrum by the combination of gamma-ray source and the absorber is thus expressed

by

$$p(v) = N_0 + \int_{-\infty}^{+\infty} \frac{f_S \Gamma_S}{2\pi} \frac{1}{(E-E_0)+(\Gamma_S/2)^2} \exp\left[-\frac{t_{eff}(\Gamma_A/2)^2}{(E-E_0)^2+(\Gamma_A/2)^2} \right] dE . \tag{3.4.2.1}$$

Since the recoil-free fraction f depends on the temperature and is proportionate to the strength of the resonant absorption, the temperature dependence of the observed FWHM in the single peak spectrum, which include neither magnetic splitting nor quadrupole splitting, depends on the change in recoil-free fraction [3.4.2.19]. FWHM is thus related to the absorption area if the spectra above Néel temperature consist of single peak without any hyperfine interactions. In this case, the temperature dependence of the FWHM observed above Néel temperature must increase monotonously as a decrease of temperature such as that of absorption area from Eq. (3.4.2.1). In fact, temperature dependence of FWHM seems to possess a maximum around 30 K. Therefore, it is not appropriate to analyze each spectrum with a single Lorentazian, but with a magnetic splitting or quadrupole splitting pattern. However, all the spectra observed in UPd_2Al_3 are symmetric patterns so that the quadrupole splitting is treated as the negligibly small contribution to the line broadening as discussed in Section 3.3.

The recoil-free fraction is related to the absorption area. When the effective thickness t_{eff} ($= f_a n_a a_a \sigma_0 t_a$) is small, Eq. (2.1.18) can be abbreviated and the absorption area is given by

$$A = \int \{N_0 - p(v)\} dv \approx A' f_S \times f_A , \tag{3.4.2.2}$$

where N_0 is the background. The recoil-free fraction is the probability of zero-phonon emission and absorption of the gamma-ray from the lattice and is given by

$$f = \exp\left[\frac{-6E_R}{k\theta_D} \left\{ \frac{1}{4} + \left(\frac{T}{\theta_D} \right)^2 \int_0^{\frac{\theta_D}{T}} \frac{x dx}{e^x - 1} \right\} \right], \tag{3.4.2.3}$$

as written above Eq. (2.1.13). The Debye temperature of ^{238}U in PuO_2 is determined as 250 K as discussed in Section 3.1. By using this Debye temperature of PuO_2, we determined the Debye temperature of UPd_2Al_3 as 200 ± 25 K by fitting the data of the absorption area with Eq. (3.4.2.3) and the results obtained is shown by the solid line in

Fig. 3.4.2.3.

Since the Néel temperature of UPd_2Al_3 is 14 K, it is difficult to consider the hyperfine magnetic field due to the magnetic ordering exists above Néel temperature. As discussed above, the line-broadening around 30 K must be thought to be caused by some hyperfine interactions.

Since the spectra obtained are symmetric patterns as written above, the line-broadening results from the magnetic hyperfine interaction. Above the Néel temperature of 14 K, UPd_2Al_3 is paramagnetic. Therefore, the hyperfine magnetic field observed around 30 K is thought to be caused by the paramagnetic relaxation phenomenon.

The temperature of 30 K where the magnitude of FWHM has a maximum above Néel temperature, corresponds to the one that the temperature dependence of the magnetic susceptibility has a peak [3.4.2.20]. In the elastic neutron scattering, however, the magnetic ordering was not observed in this temperature range. These results might be explained as follows: A Mössbauer effect can detect phenomena in the time scale more than the life-time of the excited state in the Mössbauer transition. In the ^{238}U Mössbauer effect, the life-time of the excited state is very short one, 0.21 ns, so that the change of the state can be detected as a static state in several times more than the life time. The temperature with the maximum value of the magnetic susceptibility might mean the line-broadening observed around 30 K is due to paramagnetic relaxation phenomenon. The line broadening observed might be caused by the appearance of the hyperfine magnetic field. The observation of the hyperfine magnetic field around 30 K suggests some magnetic fluctuation exists and the static magnetic ordering does not.

The reason why the observation phenomenon is due to a paramagnetic relaxation is as follows: The Mössbauer spectra observed as relaxation spectra, which are reported in the case of many ^{237}Np Mössbauer spectra in actinide [3.4.2.21], cannot determine both the relaxation time and the magnitude of the hyperfine magnetic field in this case [3.4.2.22]. It is the reason the exchange energy due to the magnetic interaction and relaxation time between each state have the uncertainty relation each other [3.4.2.23-24]. Moreover, the poor energy resolution of ^{238}U Mössbauer spectroscopy is prevented from detection of the exact physical value. These results are

thought to indicate the fluctuation of the magnetic interaction in this temperature range, but cannot give the exact relaxation time and magnitude of the hyperfine magnetic fields.

The origin of the line broadening above Néel temperature is discussed. The temperature dependence of the apparent FWHM is the same as that of the magnetic susceptibility, as written above. In the 4*f*-electron systems such as cerium compounds, the maximum of the magnetic susceptibility is explained with the relation to the Kondo effect. In the case of uranium compounds, the maximum of the magnetic susceptibility does not necessarily indicate the direct relation to the Kondo effect, but this phenomenon is characteristic of the Kondo effect. Namely, the temperature where the temperature dependence of the magnetic susceptibility has maximum value is related to the one of the appearance of the heavy fermion which plays an important role of the superconductivity. In another approach, the temperature of this line-broadening corresponds to the upper-limit temperature of the observation of the metamagnetic transition [3.4.2.17]. The temperature where the metamagnetic transition vanishes and the temperature dependence of the magnetic susceptibility has maximum is thought to be related to appearance of the heavy fermion. Therefore, the temperature of 30 K might be related to the appearance of the heavy fermion.

Secondary, the hyperfine magnetic field below the Néel temperature is discussed. Since the magnitude of the magnetic splitting obtained by the spectrum-analysis with the non-constrained FWHM is larger than that of the 'true' magnetic splitting, as written in Section 3.3. The FWHM are related to the absorption area. The temperature dependence of the area ratio does not almost change below 20 K. These results mean that the recoil-free fraction does not change below 20 K. In this temperature, UPd_2Al_3 is paramagnetic. The spectra obtained at 20 K is a single peak spectrum because the apparent FWHM does not almost change between 15 K and 20 K within the experimental error. The spectra below the Néel temperature were thus analyzed with the least-square fit using the value of FWHM at 20 K, 50.0 ± 2.8 mm s^{-1}. The magnitude of the hyperfine magnetic field at 5.1 K is 140 ± 10 T obtained with the spectrum analysis of the constrained FWHM using that of 20 K. Figure 3.4.2.3 shows the temperature dependence of the hyperfine magnetic field of UPd_2Al_3 below the Néel temperature. The magnitude of the hyperfine magnetic field increases steeply with

decreasing temperature. This temperature dependence of the hyperfine magnetic field is same as that of the magnetic moment obtained by the neutron elastic scattering [3.4.2.25]. These results show the hyperfine coupling constant of ^{238}U nucleus might be constant in UPd_2Al_3. Since the magnitude of the saturated magnetic moment of UPd_2Al_3 at uranium atoms is 0.85 μ_B, that of the hyperfine coupling constant is 160 ± 10 T / μ_B. This result obtained in UPd_2Al_3 is nearly equal to in UGe_2.

3.4.2.4. Conclusion

The results from the ^{238}U Mössbauer spectroscopy of UPd_2Al_3 indicate the broadened spectra have the magnetic splitting around 50 K and below 14 K. The magnetic splitting around 50 K is thought to be the appearance of the magnetic fluctuation. The temperature where the temperature dependence of FWHM has maximum almost corresponds to the maximum of the magnetic susceptibility and the upper limit temperature of the observation of the metamagnetic transition of UPd_2Al_3. These phenomena are thought to be related to the appearance of the heavy fermion.

The magnetic splitting below 14 K was due to the antiferromagnetic ordered state whose the Néel temperature is 14 K. The magnitude of the hyperfine magnetic field at ^{238}U in UPd_2Al_3 at 5.1 K is 140 ± 10 T. The hyperfine coupling constant of UPd_2Al_3 is 160 ± 10 T / μ_B and nearly equal to that of UGe_2.

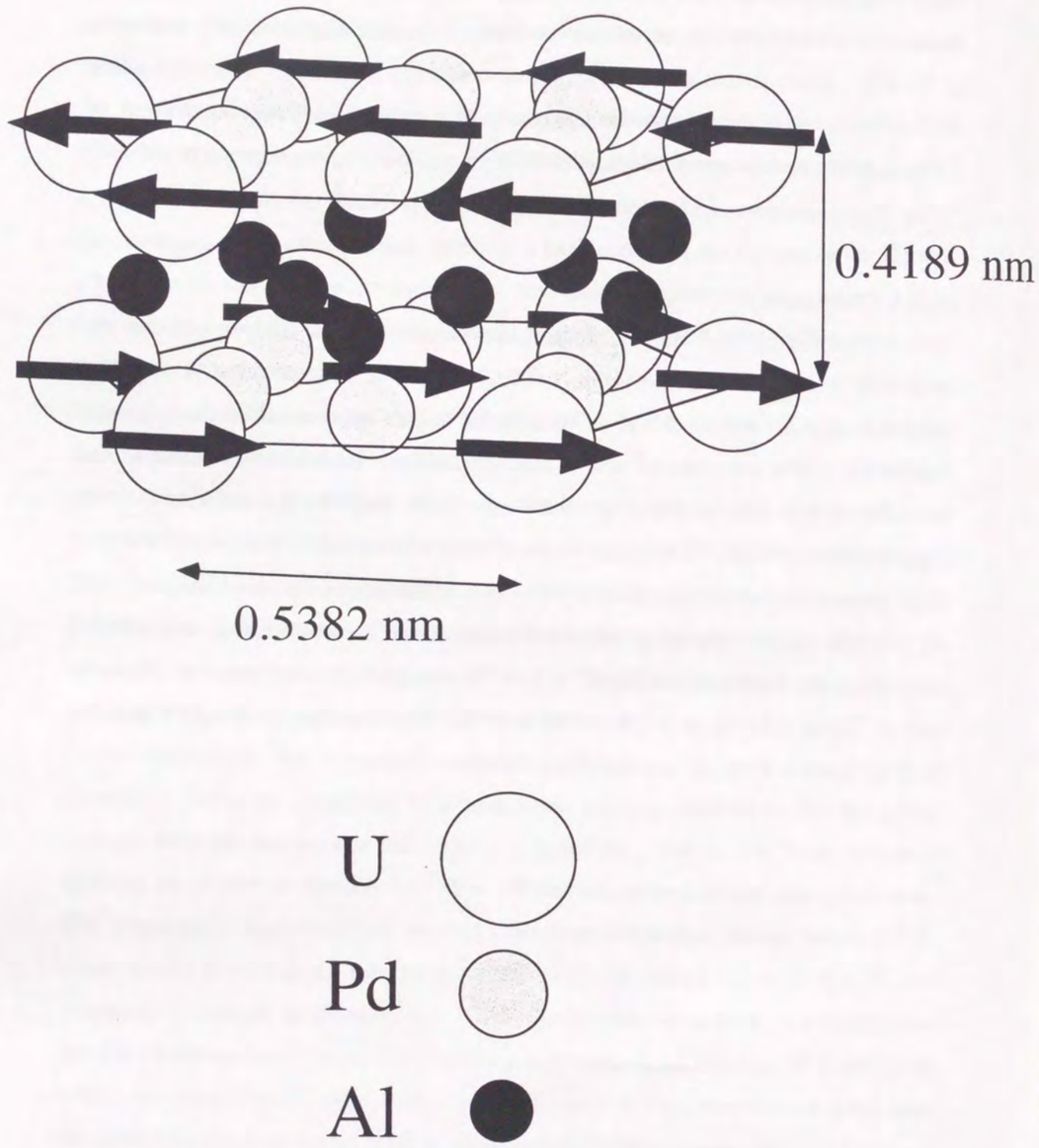

Fig. 3.4.2.1. Crystal and Magnetic Structure of UPd_2Al_3.

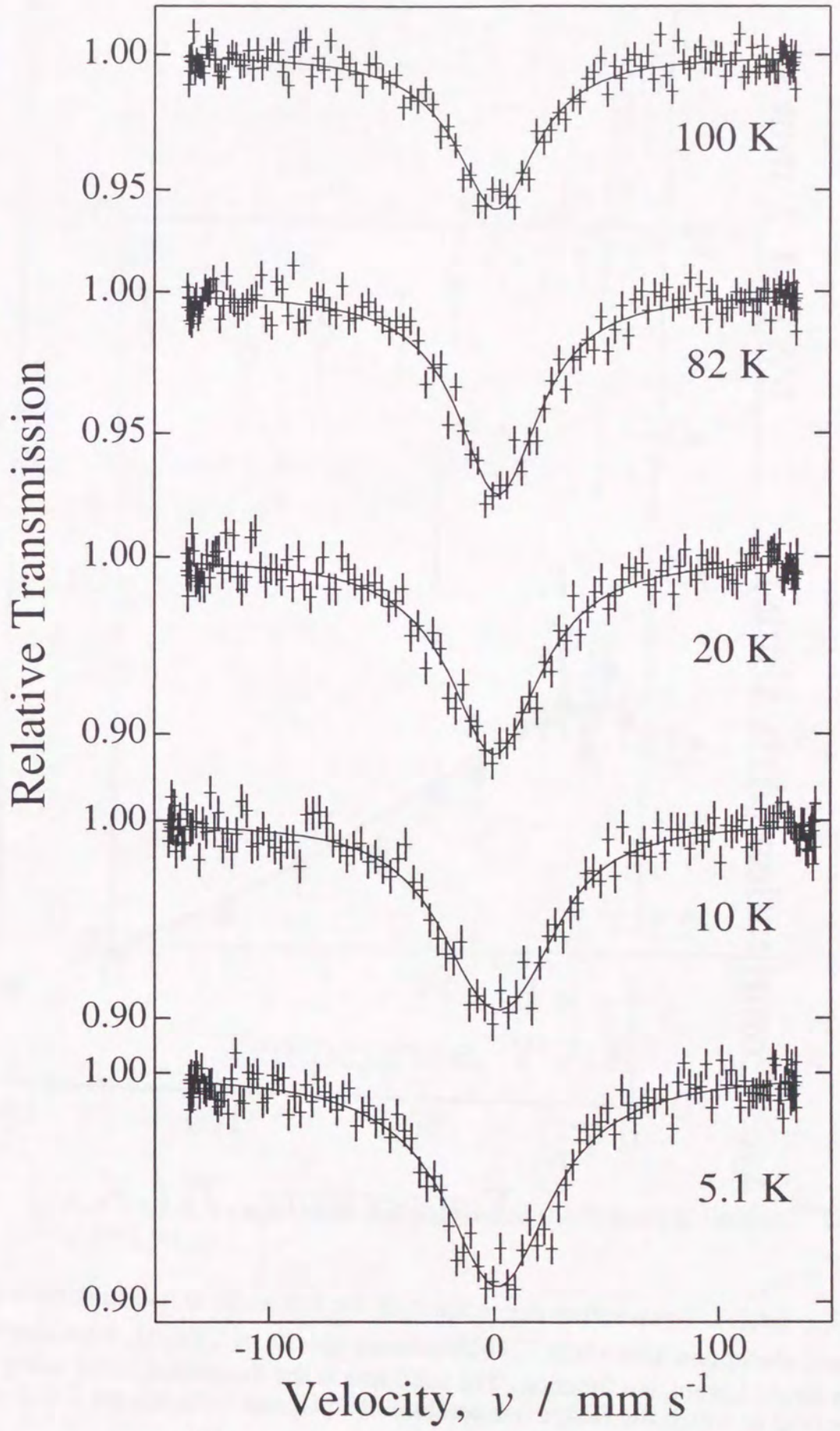

Fig. 3.4.2.2. ^{238}U Mössbauer spectra of UPd_2Al_3 at various temperatures.

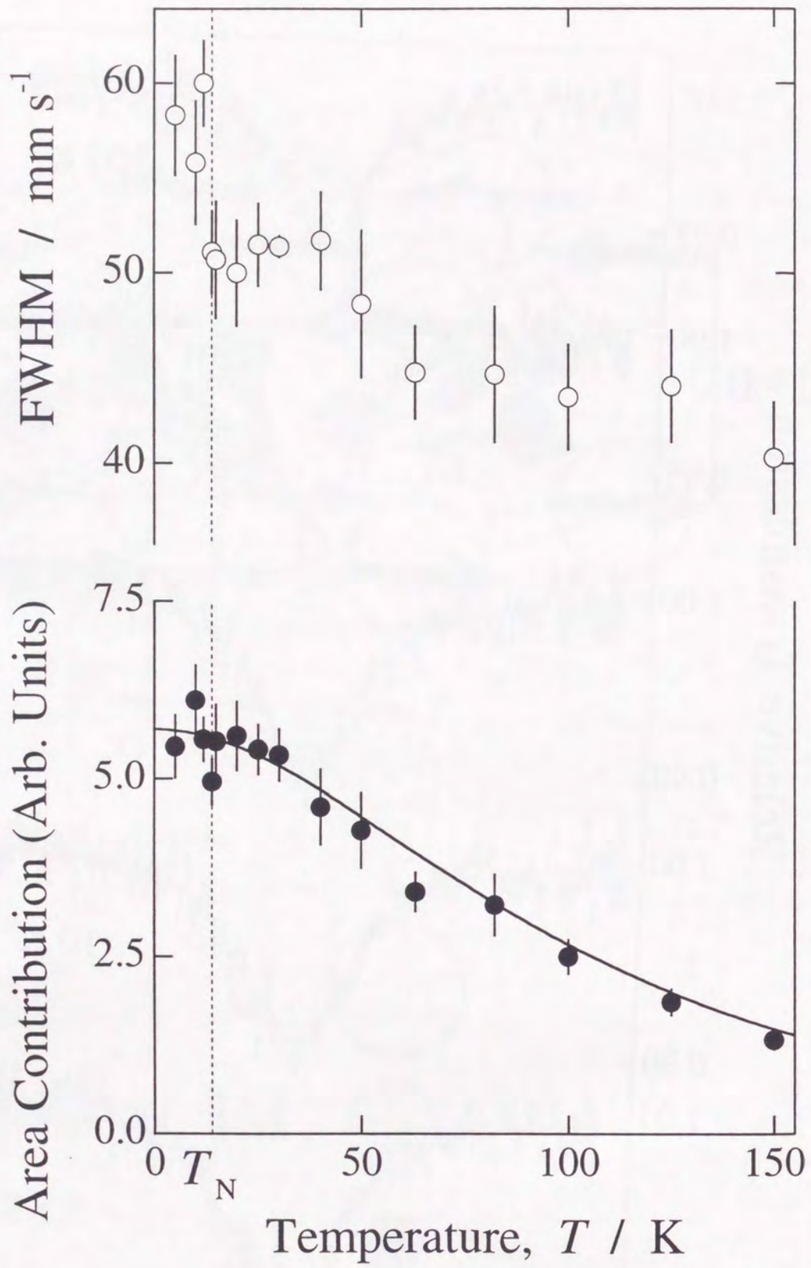

Fig. 3.4.2.3. Temperature dependence of the full width at half maximum (FWHM) and absorption area when ^{238}U Mössbauer spectra of UPd_2Al_3 were analyzed with a single Lorentzian function. The solid line is the theoretical curve using Debye model in which the Debye temperature of PuO_2 and UPd_2Al_3 are 250 K and 225 K, respectively.

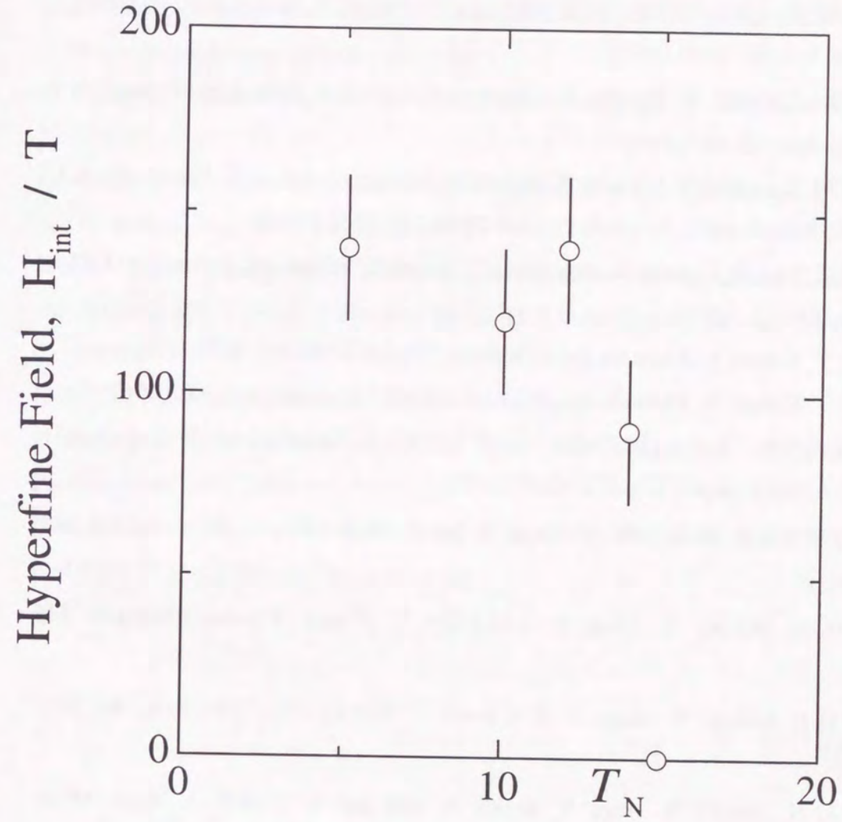

Fig. 3.4.2.4. Temperature dependence of the hyperfine field at ^{238}U in UPd_2Al_3.

References

[3.4.2.1] C. Geibel, C. Schank, S. Thies, H. Kitazawa, C. D. Bredl, A. Bohm, M. Rau, A. Grauel, R. Caspary, U. Helfrich, G. Weber and F. Steglich, Z. Phys. **B84**, 1 (1991).

[3.4.2.2] M. Kyogaku, Y. Kitaoka, K. Asayama, C. Geibel, C. Schank and F. Steglich, J. Phys. Soc. Jpn., **61**, 2660 (1992).

[3.4.2.3] M. Kyogaku, Y. Kitaoka, K. Asayama, C. Geibel, C. Schank and F. Steglich, J. Phys. Soc. Jpn., **62**, 867 (1992).

[3.4.2.4] M. Kyogaku, Y. Kitaoka, K. Asayama, N. Sato, T. Sakon, T. Komatsubara, C. Geibel, C. Schank and F. Steglich, Physica **B186-188**, 2660 (1992).

[3.4.2.5] H. Tou, Y. Kitaoka, K. Asayama, C. Geibel, C. Schank and F. Steglich, J. Phys. Soc. Jpn., **64**, 725 (1995).

[3.4.2.6] Y. Kohori, K. Matsuda and T. Kohara, Physica **B206-207**, 622 (1995).

[3.4.2.7] Y. Kohori, K. Matsuda and T. Kohara, Solid State Commun., **95**, 121 (1995).

[3.4.2.8] N. Sato, N. Aso, B. Roessli, G. H. Lander, T. Komatsubara, Y. Endo and O. Sakai, J. Alloys Compd., **271-273**, 4336 (1998).

[3.4.2.9] Y. Koike, N. Metoki, Y. Haga, Y. Morii and Y. Ō nuki, Physica **B241-243**, 823 (1997).

[3.4.2.10] N. Metoki, Y. Haga, Y. Koike and Y. Ō nuki, Physica **B241-243**, 845 (1997).

[3.4.2.11] N. Metoki, Y. Haga, Y. Koike and Y. Ō nuki, Phys. Rev. Lett., **80**, 5417 (1998).

[3.4.2.12] N. Metoki, Y. Haga, Y. Koike, N. Aso and Y. Ō nuki, J. Magn. Magn. Mater., **177-181**, 449 (1998).

[3.4.2.13] Y. Koike, N. Metoki, N. Kimura, E. Yamamoto, Y. Haga, Y. Ō nuki and K. Maezawa, J. Phys. Soc. Jpn., **67**, 1142 (1998).

[3.4.2.14] N. Sato, N. Aso, N. Tateiwa, N. Koga, T. Komatsubara and N. Metoki, Physica **B230-232**, 367 (1997).

[3.4.2.15] T. Honma, Y. Haga, E. Yamamoto, N. Metoki, Y. Koike, H. Ohkuni and Y. Ō nuki, unpublished.

[3.4.2.16] K. Sugiyama, T. Inoue, T. Ikeda, N. Sato, T. Komatsubara, A. Yamagishi amd M. Date, Physica **B186-188**, 723 (1993).

[3.4.2.17] K. Sugiyama, M. Nakashima, H. Ohkuni, K. Oda, K. Kindo, N. K. Sato, N. Kimura, T. Komatsubara, E. Yamamoto, Y. Haga, T. Honma, R. Settai and Y. Ō nuki, J. Jpn. Appl. Phys., in press

[3.4.2.18] Y. Haga, E. Yamamoto, N. Kimura, M. Hedo, H. Ohkuni and Y. Ō nuki, J. Magn. Magn. Mater., **177-181**, 437 (1998).

[3.4.2.19] H. Frauenfelder, *The Mössbauer Spectroscopy*, W. A. Benjamin, Inc., New York, 1962.

[3.4.2.20] A. Grauel, A. Bohm, H. Fisher, C. Geibel, R. Kohler, C. Schank, F. Steglich and G. Weber, Phys. Rev. **B46**, 5818 (1992).

[3.4.2.21] B. D. Dunlap and G. K. Kalvius, Handbook on the Physics and Chemistry of the Actinide, vol. 2, ed. A. J. Freeman and G. H. Lander,Elsevier Science Publishers B. V., 1985.

[3.4.2.22] T. Nakamoto, KURRI, KR, **22**, 19 (1998).

[3.4.2.23] H. H. Wickmann, *Mössbauer Effect Methodology*, ed. I. J. Gruverman, Plenum, New York, 1966.

[3.4.2.24] H. H. Wickman, M. P. Klein and D. A. Shirley, Phys. Rev., **152**, 345 (1966).

[3.4.2.25] Y. Haga, Private Communication.

3. 4. 3. ^{238}U Mössbauer Spectroscopy of URu_2Si_2

3. 4. 3. 1. Introduction

URu_2Si_2 is known as a heavy fermion superconductor which has the antiferromagnetic order below T_N = 17.5 K and show the superconductivity below T_C = 1.3 K. Its electric specific-heat coefficient and the Debye temperature were determined previously and reported to be 180 mJ / K^2 mol and 312 K , respectively [3.4.3.2.1]. At the transition temperature of 17.5 K, some anomalies were obviously observed in the electrical resistivity and specific heat measurements, claiming that a spin density wave is formed below T_N like as in Cr [3.4.3.1-4]. The magnetic moment of URu_2Si_2 in the antiferromagnetic state is very small and is reported to be 0.03 μ_B / U [3.4.3.5]. In order to explain this small magnetic moment in the antiferromagnetic state, it has been discussed whether this transition is due to the antiferromagnetic ordering or quadrupole ordering transition which induces the antiferromagnetic ordered state. The crystal and magnetic structures have been determined as shown in Fig. 3.4.3.1.

The uranium atoms in an itinerant ferromagnet UFe_2 have also been reported to have a small magnetic moment of 0.01 μ_B / U in its magnetic ordered state as written in Section 3.2 [3.4.3.6]. In the case of UFe_2, it has been proposed that uranium atom's spin and orbital moments cancel each other [3.4.3.6-8]. However, there is no direct evidence to explain the origin of the small moment experimentally. For example, the hyperfine magnetic field at U nuclei in UFe_2 has not been observed in the ferromagnetic ordered state by using the ^{238}U Mössbauer spectroscopy as discussed in Section 3.2, although the contribution to the hyperfine magnetic field are different for the orbital current and the core polarization.

The ^{238}U Mössbauer spectroscopy may enable to know whether the small magnetic moment of URu_2Si_2 is intrinsically small or not, by considering the hyperfine coupling constants for the core polarization and for the orbital current. In this work, the ^{238}U Mössbauer spectroscopy of URu_2Si_2 has been performed for the first time in order to investigate its magnetic properties and local electronic state of uranium atoms.

3. 4. 3. 2. Experimental Procedure

The sample preparation and ^{238}U Mössbauer measurements of URu_2Si_2 have been performed in the same way of UPd_2Al_3 as follows. A single crystal of URu_2Si_2 was grown by the Czochralski pulling method in a tetra arc furnace and was annealed using a solid-state electrotransport method under the high vacuum of 10^{-10} Torr [3.4.3.9-10]. It was powdered in argon gas atmosphere and sealed into the sample holder made of aluminum. The gamma-ray source used for the ^{238}U Mössbauer spectroscopy was a PuO_2 source which contains 99.99 % ^{242}Pu. The gamma-ray source was driven with sinusoidal motion. The Doppler velocity was calibrated with a laser calibrator. The zero isomer shift value is adopted to that of ^{238}U in PuO_2.

3. 4. 3. 3. Results and Discussion

Figure 3.4.3.2 shows ^{238}U Mössbauer spectra at various temperatures. Each spectrum seems to be a single and symmetric peak pattern. The observation of the symmetric spectra indicates the quadrupole splitting is small enough to be neglected, as discussed in previous sections. The obtained spectra seem to be independent on the temperature. In order to investigate the temperature dependence of the spectra in detail, the spectrum-analysis has been performed in the same way of UPd_2Al_3 as follows.

Figure 3.4.3.3 shows the temperature dependence of the full-width at half maximum (FWHM) and the absorption area of the ^{238}U Mossbauer spectra where all the spectra were analyzed with a single Lorentzian function. The absorption area increases monotonously with a decrease of the temperature. On the other hand, FWHM does not show the simple temperature dependence like that of the absorption area. The temperature dependence of FWHM has the maximum around 50 K.

As discussed in previous section, the thickness of the source used was thin enough to neglect the self-absorption in the source; in this case, the transmission absorption spectrum is expressed by

$$p(v) = N_0 + \int_{-\infty}^{\infty} \frac{f_S \Gamma_S}{2\pi} \frac{1}{(E - E_0) + (\Gamma_S / 2)^2} \exp\left[- \frac{t_{eff} (\Gamma_A / 2)^2}{(E - E_0)^2 + (\Gamma_A / 2)^2} \right] dE \,. \qquad (3.4.3.1)$$

The recoil-free fraction f_S, depends on the temperature, and the effective thickness of the absorber, t_{eff} ($= f_a n_a a_a \sigma_0 t_a$) also depends on the temperature because of its including the recoil free fraction of absorber. The observed FWHM thus depends on the recoil-free fraction, that is, the strength of the resonance absorption. Therefore, the temperature dependence of FWHM without any hyperfine interaction may have proportionality to the temperature dependence of the absorption area. Since the observed FWHM's does not show monotonous the increase of FWHM might be due to the temperature induced hyperfine interaction like a slow relaxation of the magnetic fluctuation with a decrease of the temperature, the spectra obtained include the paramagnetic relaxation phenomena. Moreover, since all of the observed spectra are the symmetric pattern, the hyperfine interaction detected by ^{238}U Mössbauer spectroscopy is mainly the magnetic one as discussed in Section 3.3 and 3.4.2. The temperature dependence of FWHM has a maximum around 50 K and increase a little below 10 K. Therefore, the spectra around 50 K and below 10 K were analyzed with a magnetically split pattern.

The recoil-free fraction is related to the absorption area. When the effective thickness t_{eff} is small, Eq. (2.1.18) can be abbreviated and the absorption area is given by

$$A = \int \{N_0 - p(v)\} dv \approx A' f_S \times f_A , \qquad (3.4.3.2)$$

where N_0 is background. The recoil-free fraction is the probability of zero-phonon emission and absorption in the lattice and given by

$$f = \exp\left[\frac{-6E_R}{k\theta_D}\left\{\frac{1}{4} + \left(\frac{T}{\theta_D}\right)^2 \int_0^{\frac{\theta_D}{T}} \frac{x dx}{e^x - 1}\right\}\right], \qquad (3.4.3.3)$$

as written previously as Eq. (2.1.13). The Debye temperature of ^{238}U in PuO_2 is determined to be 250 K as discussed in Section 3.1. By using this Debye temperature of PuO_2, we determined the Debye temperature of ^{238}U in URu_2Si_2 as 225 ± 25 K from fit with Eq. (3.4.2.3) to the data of the absorption area, as shown in Fig. 3.4.2.3. The Debye temperature obtained with the Mössbauer measurements is smaller than the one by the specific heat measurement [3.4.3.1]. The former is the local Debye temperature at uranium atoms, and the latter is the whole lattice of a URu_2Si_2 bulk. The difference

between them is thought to depend on whether the Debye temperature was obtained in the local site or not.

Anyhow, the temperature dependence of the absorption area can be interpreted by using a single value of the Debye temperature. This result indicates that the phonon spectrum of URu_2Si_2 does not change in the temperature range between 5.1 K and 200 K. If the quadrupole ordering exist in this temperature range, the softening of the elastic constant can be observed. The elastic constant is generally related to the recoil-free fraction. This phenomenon can thus be observed in the change of the strength of the absorption area. However, since the temperature dependence of the absorption area was described as the only Debye temperature, the quadrupole ordering is not thought to exist in the temperature range where ^{238}U Mössbauer spectroscopy has been performed.

Since the temperature dependence of the absorption area changes continuously, the behaviors of FWHM around 50 K and below 10 K are thought to be caused by the appearance of the hyperfine magnetic field due to the paramagnetic relaxation. Firstly, the behavior of FWHM around 50 K is discussed.

As written above, the Néel temperature of URu_2Si_2 is 17.5 K. The observed hyperfine magnetic field is thus not related to the magnetic ordering. On the other hand, the temperature dependence of the magnetic susceptibility has a maximum around this temperature [3.4.3.1], the same as UPd_2Al_3 [3.4.3.11]. Its metamagnetic transition was also observed up to this temperature [3.4.3.12]. As discussed above, this phenomenon is the same as the one observed in UPd_2Al_3 around 30 K. Therefore, its behavior around 50 K is also thought to be related to the appearance of the heavy fermion, and to be the common phenomenon for the heavy fermion superconductor.

Secondary, the behavior of FWHM below 10 K is discussed. The results from the temperature dependence of the recoil-free fraction in URu_2Si_2 suggest the quadrupole ordering does not induce antiferromagnetic ordering. The FWHM and absorption area do not change between 10 K and 30 K exceeding the experimental error, but the FWHM increases and the absorption area decreases slightly below 10 K. These results indicate FWHM is broadened intrinsically, and that the decrease of the absorption area might be caused by the spectrum analysis with the substitution of a single Lorentzian function from the magnetic pattern. Since the obtained spectra were

symmetric ones, the line broadening below 10 K are thought to be the well overlapped magnetic pattern.

Since the magnetic pattern below 10 K consists of superposed five resonance lines, in spectrum analysis of these spectra the least-square fitting could not be available using non-constrained FWHM [3.4.3.13]. We analyzed the spectra below the Néel temperature, 17.5 K, with the magnetic pattern although the obvious broadened spectra were not observed at 10 K and 15 K. The recoil-free fraction is nearly equal at 10 K and 25 K. URu_2Si_2 is a paramagnetic at 25 K. The spectrum at 25 K is thought to be a single line one because of its symmetry. The spectra below the Néel temperature were thus analyzed by the least-square fit using the value of FWHM at 25 K, 50.6 ± 1.8 mm s^{-1}. The spectrum at 5.2 K has the magnitude of the hyperfine field at ^{238}U are 90 ± 20 T, using $g_{ex} = 0.25$ determined in this work.

Figure 4 shows the temperature dependence of the hyperfine fields obtained for URu_2Si_2. The magnitudes of the hyperfine field at 10 K and 15 K were thought to be comparable to the lower limit of the hyperfine field detected by ^{238}U Mössbauer spectroscopy, because the lower limited value of the hyperfine field in ^{238}U Mössbauer spectroscopy is about 30 T [3.4.3.14]. The magnitude of the saturated hyperfine field at 0 K is estimated at about 100 ± 30 T.

The obtained values of the hyperfine magnetic field below Néel temperature was extremely large compared with the value which was expected from the magnitude of the magnetic moment of URu_2Si_2, 0.03 μ_B. The hyperfine coupling constants of ^{238}U nuclei obtained in his work are 142 ± 1 T / μ_B in UO_2 and 160 ± 10 T / μ_B in UGe_2 and UPd_2Al_3, respectively. If the hyperfine coupling constant of URu_2Si_2 is equal to the other uranium compounds measured in this work, UO_2, UGe_2 and UPd_2Al_3, the magnitude of the expected hyperfine magnetic field is between 4 T and 5 T. The lower limited value of the hyperfine magnetic field is about 30 T in ^{238}U Mössbauer spectroscopy. [3.4.3.13] In the consideration for the lower limited value of the hyperfine field observed with ^{238}U Mössbauer spectroscopy, such small hyperfine field was not detectable. Therefore, the origin of the observed hyperfine field of URu_2Si_2 must be thought to be different from the other uranium compounds.

Generally the contributions to the magnetic hyperfine field from core polarization and orbital current were different. In non-relativistic theory as shown in Chapter II, the contribution of the orbital current, $\boldsymbol{B}_{orb}$, is represented by

$$\boldsymbol{B}_{orb} = \boldsymbol{a}_{hf} \langle \boldsymbol{J} \| \boldsymbol{N} \| \boldsymbol{J} \rangle \langle \boldsymbol{r}^{-3} \rangle \boldsymbol{m}_J , \qquad (3.4.3.4)$$

where $\langle J \| N \| J \rangle$ is a reduced matrix element, $\boldsymbol{N} = \sum_n \{ \boldsymbol{l}_i - \boldsymbol{s}_i + 3(\boldsymbol{r}_i \cdot \boldsymbol{s}_i)\boldsymbol{r}_i / \boldsymbol{r}_i^2 \}$, $\boldsymbol{l}_i$ the angular magnetic momentum, $\boldsymbol{s}_i$ the spin momentum, $\boldsymbol{m}_J$ is the azimuthal number connected with J_z, $\langle r^{-3} \rangle$ the quantum mechanical average of $1 / r^3$ using the wave functions of the open shell electrons. $\boldsymbol{B}_{orb}$ is thus proportionate to $\langle r^{-3} \rangle$ and $\boldsymbol{m}_J$. On the other hand the core polarization field, $\boldsymbol{B}_{core}$, in non-relativistic theory is given by

$$\boldsymbol{B}_{core} = \frac{8}{3} \pi \mu_B \boldsymbol{g} \sum_n \left[\rho_{ns}^{\uparrow}(0) - \rho_{ns}^{\downarrow}(0) \right] , \qquad (3.4.3.5)$$

where $\rho_{ns}^{\uparrow}(0)$ or $\rho_{ns}^{\downarrow}(0)$ are the contact density of s-electrons of the n-th shell having spin up or spin down and S the net spin of the open-shell electrons. Therefore the contribution of the orbital current depends on the quantum number $\boldsymbol{J}$, approximately.

Although the hyperfine coupling constants of UO_2, UGe_2 and UPd_2Al_3 corresponds to each other, that of URu_2Si_2 is extremely different. This result suggest that the configuration of uranium atoms might be different from that of the other compounds whose hyperfine fields are proportionate to their magnetic moment. In this case, it can be proposed that the contribution of the core polarization or Fermi contact interaction to the hyperfine magnetic field is larger than that of the orbital current. Therefore, the results of ^{238}U Mössbauer spectroscopy might indicate that the orbital and spin moments of URu_2Si_2 whose magnitude is large enough cancel each other. This result corresponds to the proposal of the band calculation [3.4.3.15], and can explain the anomaly of the electrical resistivity and specific heat measurement at 17.5 K.

3.4.3.4. Conclusion

The results from ^{238}U Mössbauer spectroscopy of URu_2Si_2 indicate that the obtained broadened spectra have the magnetic splitting around 50 K and below 10 K. The magnetic splitting observed around 100 K might be caused by the appearance of

the heavy fermions, in the consideration for the results of the metamagnetic transition and magnetic susceptibility measurement.

The magnetic splitting observed below 10 K was due to the antiferromagnetic ordering. The magnitude of the hyperfine field of URu_2Si_2 at 5.2 K is 90 ± 20 T. The hyperfine coupling constant of URu_2Si_2 is thus about 20 times lager than the one of UO_2. The origin of the hyperfine field is thought to be different from that of the other compounds in this work, UO_2, UGe_2 and UPd_2Al_3. The temperature dependence of the absorption area between 5.1 K and 200 K is fitted by the Debye model of the only Debye temperature and cannot show the anomaly at 17.5 K. These result suggests the phase transition at 17.5 K is the simple antiferromagnetic ordering temperature, and the anomalies of the electrical resistivity and specific heat measurement at that temperature are related to the adequate large spin and orbital moments.

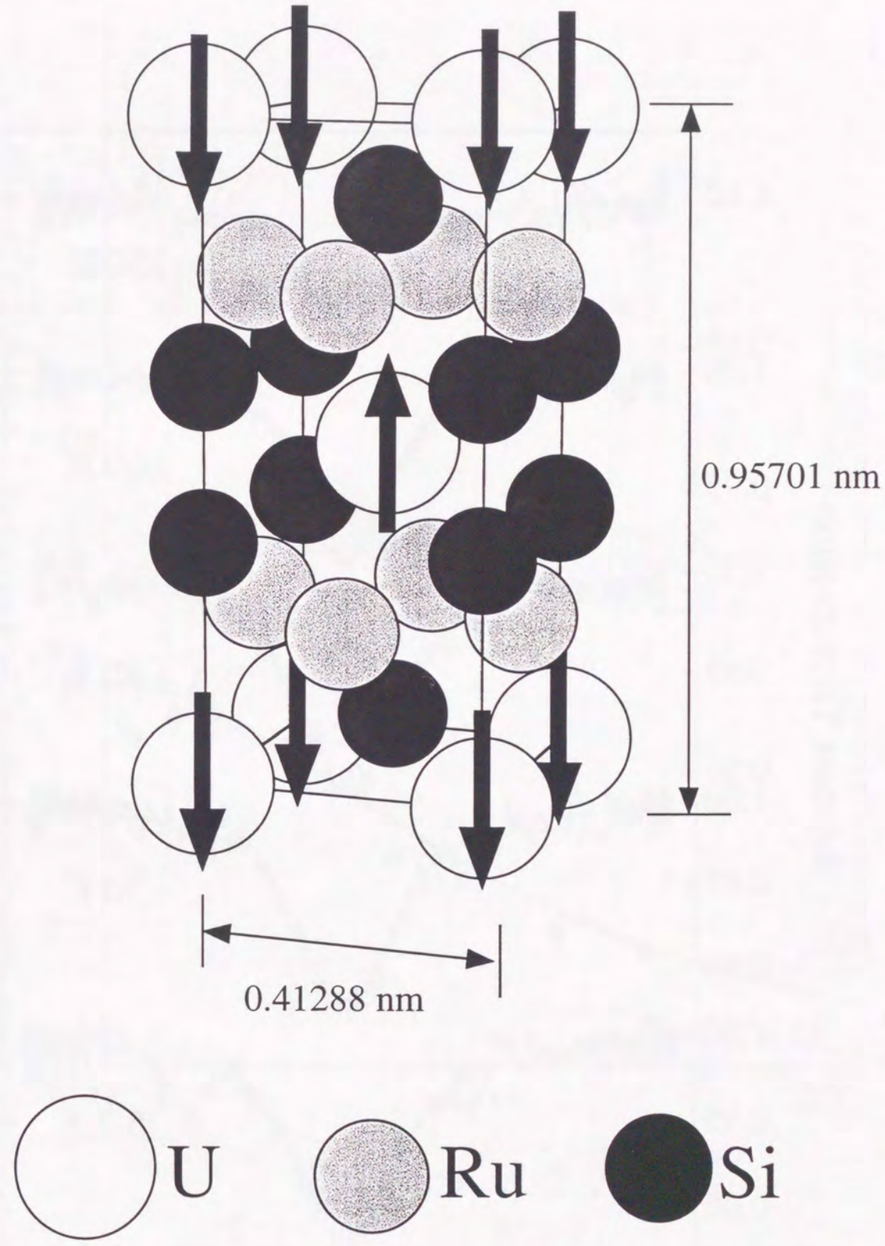

Fig. 3.4.3.1. Crystal and Magnetic Structure of URu_2Si_2.

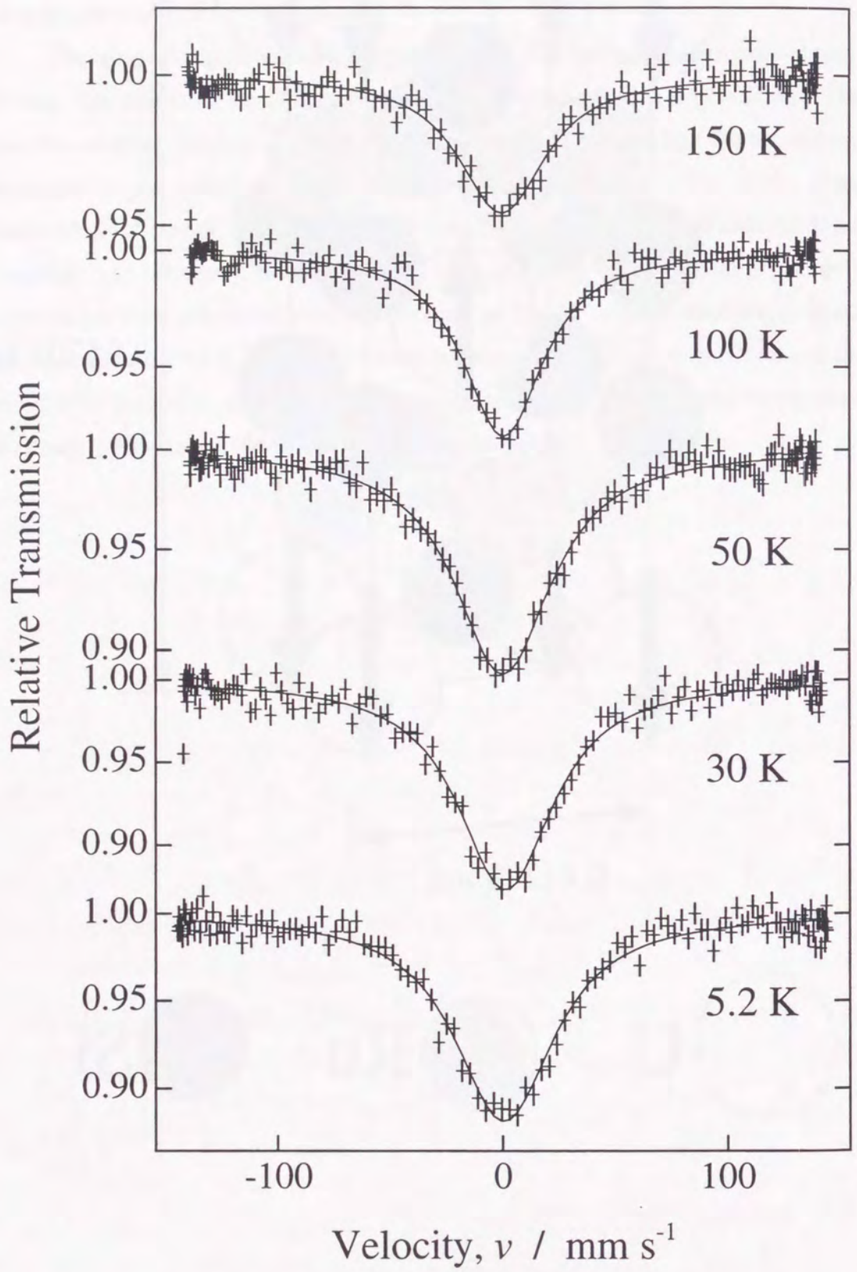

Fig. 3.4.3.2. ^{238}U Mössbauer spectra at various temperatures.

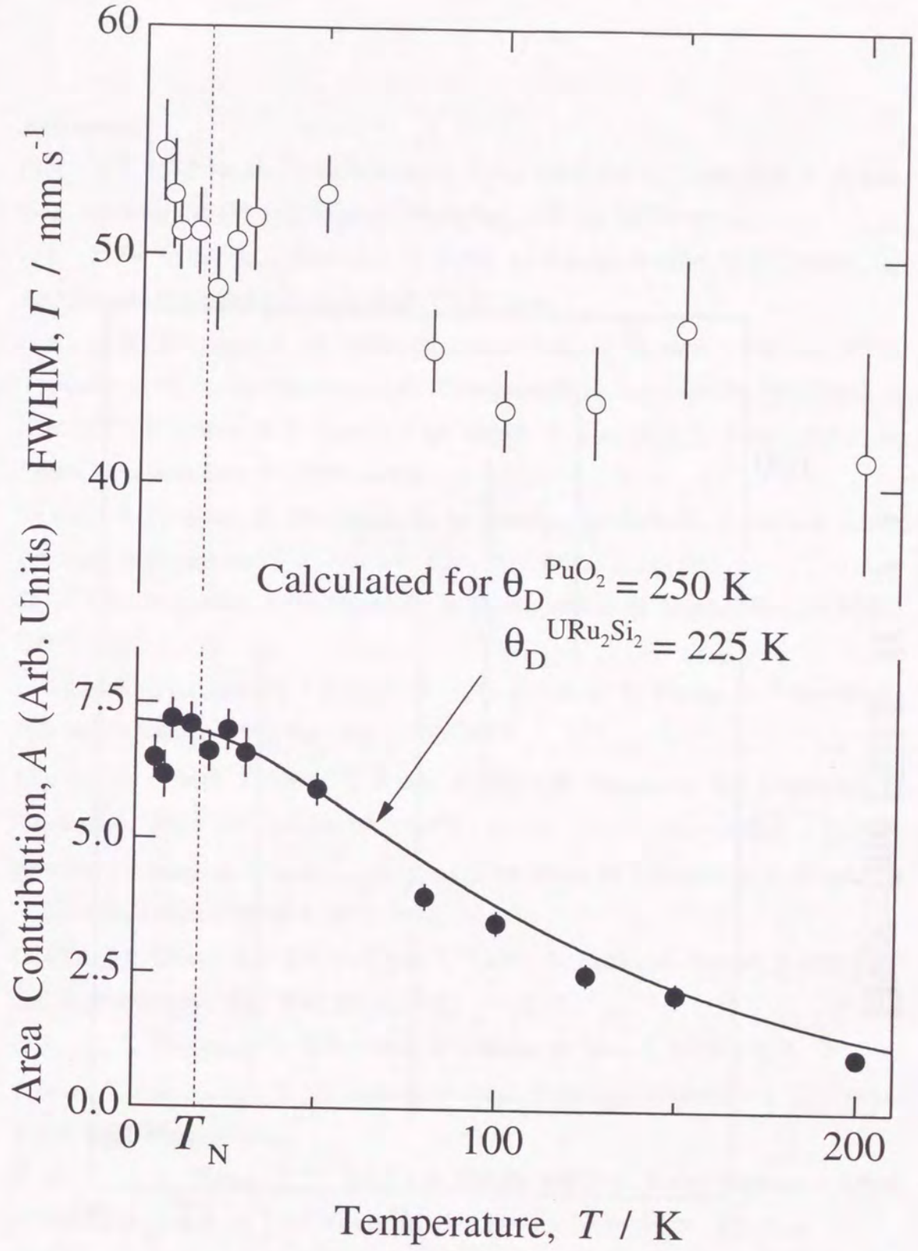

Fig. 3.4.3.3. Temperature dependence of the full width at half maximum (FWHM) and absorption area when ^{238}U Mössbauer spectra were analyzed with a single Lorentzian function. The Solid line is the theoretical curve using Debye model in which the Debye temperature of PuO_2 and URu_2Si_2 are 250 K and 225 K, respectively.

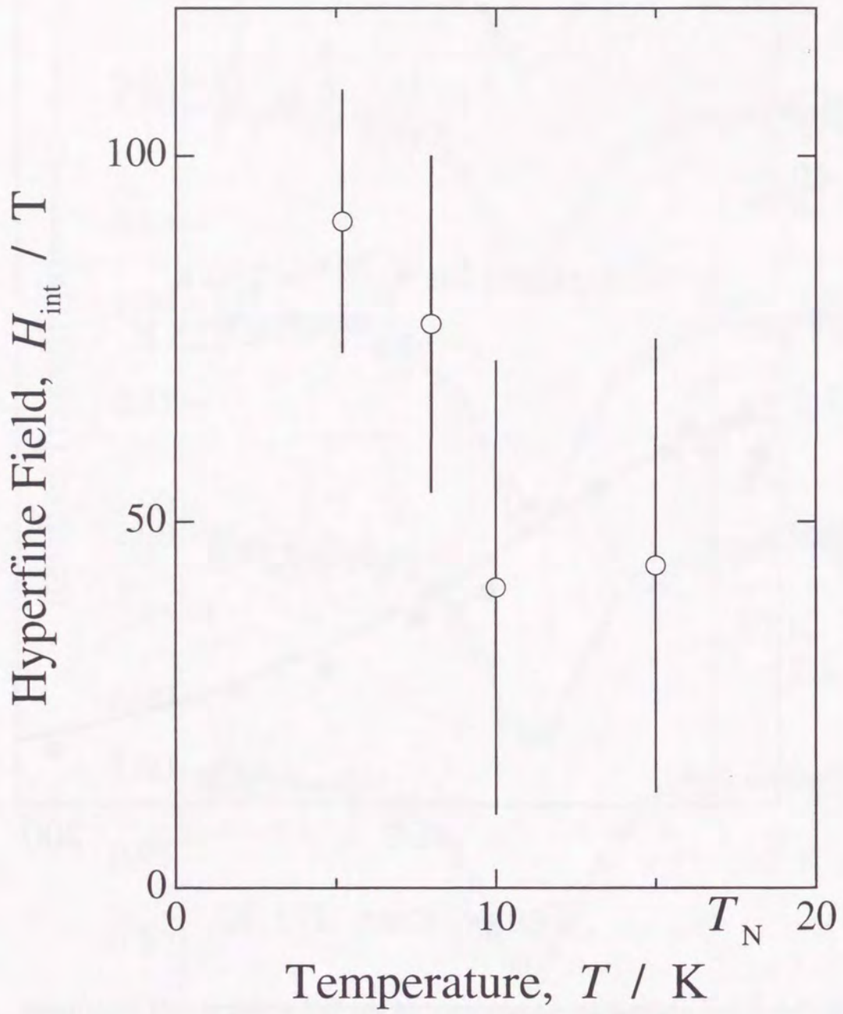

Fig. 3.4.3.4. Temperature dependence of the hyperfine magnetic field at ^{238}U in URu_2Si_2.

References

[3.4.3.1] T. T. M. Palstra, A. A. Menovsky, J, van den Berg, A. J. Dirkmaat, P. H. Kes, G. J. Nieuwenhuys and J. A. Mydosh, Phys. Rev. Lett. **55**, 2727 (1985).

[3.4.3.2] W. Schlabiz, J. Baumann, B. Pollit, U. Rauchschwalbe, H. M. Mayer, U. Ahlheim and C. D. Bredl, Z. Phys. **B62**, 171 (1986).

[3.4.3.3] M. B. Maple, J. W. Chen, Y. Dalichaouch, T. Kohara, C. Rossel, M. S. Torikachvili, M. W. McElfresh and J. D. Thompson, Phys. Rev. Lett. **56**, 185 (1986).

[3.4.3.5] T. E. Mason, B. D. Gaulin, J. D. Garrett, Z. Tun, W. J. L. Buyers and E. D. Isaacs, Phys. Rev. Lett. **65**, 3189 (1990).

[3.4.3.6] T. Paolasini, G. H. Lander, S. M. Shapiro, R. Caciuffo, B. Lebech, L. -P. Regnault, B. Roessli and J. -F. Fournier, Phys. Rev. **B54**, 7222 (1996).

[3.4.3.7] G. H. Lander, A. T. Aldred, B. D. Dunlap and G. K. Shenoy, Physica **86-88**, B152 (1977).

[3.4.3.8] P. K. Lawson, M. J. Cooper, M. A. G. Dixon, D. N. Timms, E. Zukowski, F. Itoh and H. Sakurai, Phys. Rev. **B56**, 3239 (1997).

[3.4.3.9] H. Ohkuni, T. Ishida, Y. Inada, Y. Haga, E. Yamamoto, Y. Ōnuki and S. Takahashi, J. Phys. Soc. Jpn. **66**, 945 (1997).

[3.4.3.10] Y. Haga, E. Yamamoto, N. Kimura, M. Hedo, H. Ohkuni and Y. Ōnuki, J. Magn. Magn. Mater. **177-181**, 437 (1998).

[3.4.3.11] A. Grauel, A. Bohm, H. Fisher, C. Geibel, R. Kohler, C. Schank, F. Steglich and G. Weber, Phys. Rev. **B46**, 5818 (1992).

[3.4.3.12] K. Sugiyama, M. Nakashima, H. Ohkuni, K. Oda, K. Kindo, N. K. Sato, N. Kimura, T. Komatsubara, E. Yamamoto, Y. Haga, T. Honma, R. Settai and Y. Ōnuki, J. Jpn. Appl. Phys., in press

[3.4.3.13] G. K. Shenoy, J. M. Friedt, H. Maletta and S. L. Ruby, *Mössbauer Effect Methodology*, vol. 9, ed. I. J. Gruverman, Plenum, New York, 1966.

[3.4.3.14] S. L. Ruby, G. M. Kalvius, B. D. Dunlap, G. K. Shenoy, D. Cohen, M. B. Brodsky and D. J. Lam, Phys. Rev. **184**, 374 (1969).

[3.4.3.15] H. Yamagami, Private Communication.

3. 4. 4. Conclusion

From the results of the ^{238}U Mössbauer measurements of heavy fermion superconductors, UPd_2Al_3 and URu_2Si_2, their physical properties were revealed as follows.

The hyperfine magnetic fields in a paramagnetic state of both UPd_2Al_3 and URu_2Si_2 were observed. It is suggested that the observed hyperfine field is caused by the paramagnetic relaxation at uranium nucleus. They appeared around the temperature where the magnetic susceptibility has a maximum value each other. These temperatures to show the maximum values are agreed also with the upper-limits temperature to show the metamagnetic transition by the externally applied magnetic field. This common phenomenon observed for UPd_2Al_3 and URu_2Si_2 is thought to be the characteristic property of the heavy fermion superconductor. This phenomenon is related to the appearance of a heavy fermion which plays an important role for their superconductivity.

In UPd_2Al_3, the hyperfine magnetic field is observed below Néel temperature of 14 K. The magnitude of the hyperfine magnetic field is 140 ± 10 T at 5.1 K. The hyperfine coupling constant obtained for UPd_2Al_3 is 160 ± 10 T which agrees with that of UGe_2.

In URu_2Si_2, the hyperfine magnetic field is also observed below Néel temperature of 17.5 K, although the magnitude of the saturated magnetic moment is quite small as 0.03 μ_B. The magnitude of the hyperfine magnetic field obtained at 5.2 K is 90 ± 20 T. The observation of the hyperfine magnetic field is thought to be reflected by the difference of hyperfine coupling constants between the orbital current and the core polarization. This result suggests that the small saturated moment is caused by the antiparallel coupling between the spin and the orbital moments. The spin and the orbital moments are thought to have finite magnitudes, respectively. The obvious anomalies observed in the specific heat and the electrical resistivity measurements of URu_2Si_2 might be explained using this model.

Chapter 4. Conclusion

The ^{238}U and ^{57}Fe Mössbauer measurements have been performed for the uranium intermetallic compounds in order to investigate their local electronic states, mainly their magnetic properties. The materials, which were studied by the Mössbauer effect, are an antiferromagnetic compound of UO_2, itinerant ferromagnetic compounds of UFe_2 and UGe_2, a Pauli-paramagnetic compound showing superconductivity of U_6Fe, and heavy fermion superconductors of UPd_2Al_3 and URu_2Si_2.

In order to determine the g-factor of the first excited state of ^{238}U, ^{238}U Mössbauer and ^{235}U NMR measurements have been performed for UO_2. ^{57}Fe Mössbauer measurements have been performed for U-Fe intermetallic compounds of UFe_2 and U_6Fe. ^{238}U Mössbauer measurements have been performed for itinerant ferromagnetic compounds of UFe_2 and UGe_2, and for heavy fermion superconductors of UPd_2Al_3 and URu_2Si_2.

The nuclear magnetic moment of the first excited state of ^{238}U has been not yet reported except for the theoretical value, which is an important parameter as a coupling constant to determine the hyperfine magnetic field at ^{238}U nucleus. The hyperfine magnetic field is important to discuss the magnetic properties by using the Mössbauer and NMR measurement. In this work, the ^{238}U Mössbauer and the ^{235}U NMR measurements of UO_2 in its antiferromagnetic ordered state have been performed. The magnitude of the hyperfine magnetic field has been already determined as 252.3 ± 0.5 T by the ^{235}U NMR measurements. The magnitude of the nuclear Zeeman splitting of ^{238}U Mössbauer spectrum is determined as $(8.85 \pm 0.58) \times 10^{-6}$ eV. From these results, the nuclear magnetic moment of the first excited state of ^{238}U is determined as $0.254 \pm 0.015\ \mu_N$.

In U-Fe intermetallic compounds, the isomer shift values obtained by the ^{57}Fe Mössbauer spectroscopy are smaller than 0 mm s^{-1} relative to α-Fe at room temperature. These results show the hybridization between 3*d*- and 5*f*-electrons exists in UFe_2 and U_6Fe. The hyperfine coupling constant of UFe_2 is much smaller than that of α-Fe. It shows the strong hybridization exists between 3*d*- and 5*f*-electrons. The origin of the electric field gradient of ^{57}Fe in U_6Fe was determined as the orbital of $3d_{3z^2-r^2}$ electrons from the ^{57}Fe Mössbauer measurements under the externally applied field.

The results from the ^{238}U Mössbauer measurements of UFe_2 show no hyperfine

magnetic field exists at ^{238}U nucleus. This suggests that the uranium atoms in UFe_2 have no magnetic moments although the spin and orbital moments of uranium atoms were proposed to be coupled antiparallel by the neutron scattering and the magnetic Compton scattering experiments.

The hyperfine magnetic field at ^{238}U nucleus in the itinerant ferromagnet UGe_2 has been observed below the Curie temperature. The magnitude of the hyperfine magnetic field is determined as 240 ± 10 T at 5.3 K. Temperature dependence of the hyperfine magnetic field is proportionate to the magnetization below the Curie temperature.

In heavy fermion superconductors of UPd_2Al_3 and URu_2Si_2, spectral broadening due to the magnetic fluctuation was observed even in the paramagnetic states. The observed hyperfine fields in both the compounds are caused by the paramagnetic relaxation at uranium atoms. They appeared around the temperature where the temperature dependence of the magnetic susceptibility has a maximum value. In consideration for the temperature range of the observation of the metamagnetic transition, the common phenomena in UPd_2Al_3 and URu_2Si_2 are thought to be related to the appearance of a heavy fermion which plays an important role for their superconductivity.

In UPd_2Al_3, the hyperfine magnetic field is observed below Néel temperature of 14 K. The magnitude of the hyperfine magnetic field at 5.1 K is 140 ± 10 T. Even in URu_2Si_2, the hyperfine magnetic field is also observed below Néel temperature, 17.5 K, although the magnitude of the saturated magnetic moment is quite small as 0.03 μ_B. The magnitude of the hyperfine magnetic field at 5.2 K is 90 ± 20 T. This result suggests that the small net moment is caused by the antiparallel coupling between the spin and orbital moments whose magnitudes are finite. The obvious anomalies observed in the specific heat and electrical resistivity measurements for URu_2Si_2 might be explained by using this model.

In this work, the obtained hyperfine coupling constants are 142 ± 1 T / μ_B of UO_2 and 160 ± 10 T / μ_B of UGe_2 and UPd_2Al_3. As for these compounds except for UFe_2 and URu_2Si_2, the magnitude of the hyperfine magnetic field at ^{238}U nucleus is proportionate to the magnetic moment at a uranium atom.

Acknowledgment

The author would like to express his great appreciation and gratitude to Professor S. Nasu of Osaka University for his continual encouragement and support in coordinate this thesis. He would also like to appreciate Profs. Y. Ōnuki, Y. Kitaoka and K. Miyake of Osaka University for their kind advice and critical reading of this thesis.

He would like to express his gratitude to Professor M. Date, and Drs. S. Nagai and K. Tanase of Japan Atomic Energy Research Institute for their hearty encouragement and advice.

He especially wishes to thank Dr. M. Saeki, Mr. M. Nakada, Dr. T. Nakamoto and Mr. N. M. Masaki of Japan Atomic Energy Research Institute for their experimental support and fruitful discussion of the Mössbauer spectroscopy experiments. He wishes to thank Drs. A. Nakamura, E. Yamamoto, Y. Haga and T. Honma of Japan Atomic Energy Research Institute and Mr. H. Ohkuni of Osaka University for their preparation of the extremely purified samples and fruitful discussion. He also wishes to thank to Professor H. Yasuoka and Mr. K. Ikushima of University of Tokyo for their experimental support and fruitful discussion of the NMR study, especially in the firstly observation of ^{235}U NMR signals in solid state compounds.

He is grateful to Professor G. M. Kalvius of Thchnische Universität München for his helpful advice based on the previous experiments of the Mössbauer spectroscopy of the uranium isotopes. He is also grateful to Drs. K. Sasaki, T. Yamashita and N. Metoki of Japan Atomic Energy Research Institute, Professor Y. Hinatsu of Hokkaido University, Drs. K. Ishida and Y. Inada of Osaka University for helpful discussion and encouragement. He would like to thank Drs. S. Morimoto, Y. Kobayashi and T. Hinomura for their helpful discussion and cordial encouragement. Other thanks are due to the staffs of Japan Atomic Energy Research Institute and all members of Nasu laboratory of Osaka University for their helpful discussion and continuous encouragement.

Finally, he would like to express his gratitude to his parents for their mental support and his grandmother for her hearty support during his stay in Osaka.

The present works are partially supported by the scholarship and the REIMEI Research Resources of Japan Atomic Energy Research Institute.

List of Publications

[1] M. Tabuchi, C. Masquelier, T. Takeuchi, K. Ado, I. Matsubara, T. Shirane, R. Kanno, S. Tsutsui, S. Nasu, H. Sakaebe and O. Nakamura:
"Li^+/Na^+ Exchange from α-$NaFeO_2$ Using Hydrothermal Reaction",
Solid State Ionics, **90**,129-132 (1996).

[2] M. Tabuchi, S. Tsutsui, C. Masquelier, R. Kanno, K. Ado, I. Matsubara, S. Nasu and H. Kageyama:
"The Effect of Cation Arrangement on the Magnetic Properties of Lithium Ferrites ($LiFeO_2$) Prepared by Hydrothermal Reaction and Post Annealing Method",
J. Solid State Chem., **140**, 159-167 (1998).

[3] S. Tsutsui, M. Nakada, N. M. Masaki, M. Saeki, S. Nasu, A. Nakamura, Y. Haga, E. Yamamoto and Y. Ōnuki:
"^{238}U Mössbauer Study of Uranium Compounds",
Hyperfine Int. C, **3**,225 (1998).

[4] S. Tsutsui, M. Saeki, and S. Nasu:
"^{238}U Mössbauer Spectroscopy and its Application to the Study on Magnetic Properties of Uranium Compounds",
Kotaibutsuri (Solid State Physics) **32**, 821-828 (1997). (in Japanese)

[5] K. Ikushima, H. Yasuoka, S. Tsutsui, M. Saeki, S. Nasu and M. Date:
"Observation of ^{235}U NMR in the Antiferromagnetic State of UO_2",
J. Phys. Soc. Jpn., **67**, 69-70 (1998).

[6] S. Tsutsui, S. Nasu, M. Nakada, N. M. Masaki, M. Saeki, K. Ikushima, H.Yasuoka and A. Nakamura:
"Nuclear Magnetic Moment of the First Excited State ($I = 2^+$) of ^{238}U",
J. Phys. Soc. Jpn., **67**, 2641-2644 (1998).

[7] M. Nakada, M. Saeki, N. M. Masaki and S. Tsutsui :
"Preparation of Sources and Sealed Absorber Holders for ^{237}Np and ^{238}U Mössbauer Measurements"
J. Radioanal. Nucl. Chem., **232**, 201-207 (1998).

[8] S. Tsutsui, M. Nakada, Y. Kobayashi, N. M. Masaki, M. Saeki, S. Nasu, A. Nakamura, Y. Haga, T. Honma, E. Yamamoto, H. Ohkuni and Y. Ōnuki:
"Mössbauer Study of Uranium Compounds",
Jpn. J. Appl. Phys., in press.